Title
Chemical removal of nitrogen oxides from the atmosphere: Impacts on air quality and effects of temperature

Author
Romer, Paul

Publication Date
2018

Peer reviewed|Thesis/dissertation

Chemical removal of nitrogen oxides from the atmosphere: Impacts on air quality and effects of temperature

by

Paul Romer

A dissertation submitted in partial satisfaction of the

requirements for the degree of

Doctor of Philosophy

in

Chemistry

in the

Graduate Division

of the

University of California, Berkeley

Committee in charge:

Professor Ronald C. Cohen, Chair
Professor Kristie A. Boering
Professor Allen H. Goldstein

Summer 2018

Chemical removal of nitrogen oxides from the atmosphere: Impacts on air quality and effects of temperature

Abstract

Chemical removal of nitrogen oxides from the atmosphere:
Impacts on air quality and effects of temperature

by

Paul Romer

Doctor of Philosophy in Chemistry

University of California, Berkeley

Professor Ronald C. Cohen, Chair

The concentration of nitrogen oxides ($NO_x \equiv NO + NO_2$) regulates the concentrations of all major atmospheric oxidants and the formation of secondary air pollutants, with consequences for climate, human health, and ecosystems. The chemical cycling between NO_x and its oxidation products controls the concentration and transport of NO_x and affects the spatial extent of air pollution. Previous studies have shown that permanent loss of NO_x occurs both through production of HNO_3 and through production of alkyl and multifunctional nitrates ($RONO_2$). Despite their importance to atmospheric chemistry, significant uncertainties remain in the relative importance of these pathways and in the fates of $RONO_2$ and HNO_3 in the atmosphere.

I use observations from two intensive field studies, the Southern Oxidant and Aerosol Study (SOAS) in Centreville Alabama and the Korea-United States Air Quality Study (KORUS-AQ) over South Korea, to provide new constraints on the lifetimes and fates of NO_x oxidation products. I show that $RONO_2$ compounds produced from isoprene oxidation have a lifetime under three hours and are lost both by gas-phase chemistry to re-release NO_x to the atmosphere and by aerosol-phase hydrolysis to form HNO_3. In contrast, observations of HNO_3 and NO_x over the Yellow Sea between China and South Korea confirm that HNO_3 is nearly chemically inert in the troposphere. This finding contradicts recent proposals that HNO_3 undergoes photolysis extremely rapidly in the aerosol phase.

I apply these findings to investigate how the chemistry of NO_x oxidation products affects the lifetime of NO_x and the production of O_3 in different environments. I show that, in general, the formation of short-lived NO_x reservoirs extends the lifetime of NO_x by sequestering NO_x in less reactive forms. Furthermore, I show that in areas where the formation of $RONO_2$ is the dominant pathway for NO_x loss, ozone production efficiency no longer increases with temperature, changing the response of air quality to meteorology. Finally, I show that over the past decade, NO_x chemistry has shifted in the United States towards a regime where $RONO_2$ chemistry plays a greater role in the loss of NO_x.

Contents

List of Figures

List of Tables

Acknowledgments

Thanks to my advisor Ron Cohen, who was a source of support and inspiration throughout graduate school, and who let me work on the questions that interested me while trusting that our flights of fancy would end up somewhere interesting. Thanks to Paul Wooldridge, whose experience with field work is unmatched, and is the only person I know who could deduce that there was a dead bug on our optics from 2000 miles away. Thanks to Maria Rodriguez, for keeping the group running and dealing with my propensity to submit expense reports about 4 months after I should have. Best wishes to her in her next adventure.

Thanks to the Cohen Research Team, past, present, and future, for a near-infinite supply of delicious desserts, endless scientific advice, and suffering through my terrible puns for 6 years. Thanks to past group members Sally and Megan for giving me my first experience with our NO_2 and NO instruments, to Kaitlin for doing so much to make our measurements during SOAS a success, and to Lance for patiently teaching me how to align lasers through a multipass cell. Thank you to all my office mates, Tamara, Alexis, Carly, and Kaity for keeping me grounded — days when the office was empty were never quite the same. Thanks and best wishes for success in their studies to the rising students Hannah, Bryan, Erin, Helen, Jinsol, and Qindan. Thank you Josh for helping me with satellite data and encouraging me to be a better programmer, and thank you Azimeh for providing modeling output from WRF.

Thanks to my committee members, Allen Goldstein and Kristie Boering, for providing useful comments on this dissertation and throughout graduate school.

Thanks to everyone who organized SOAS and KORUS-AQ. More work goes into planning and executing a large field campaign than I could ever have imagined before experiencing it first hand. Thank you especially to AnnMarie Carlton and Jim Crawford who worked tirelessly and diplomatically to make the campaigns a success.

Thank you to my undergraduate research advisor, Robert Field, who gave me my first experience with lasers, taught me physical chemistry and statistical mechanics, and encouraged me to attend Berkeley.

Thank you to my very first research mentor Rachel Stanley, who introduced me to environmental chemistry and without whom I would never have ended up studying the atmosphere.

Thank you to my parents David and Christina and my siblings Katie and Matt for being the best of friends and the best of family, for encouraging my love of science and of puzzles, and for always encouraging me to search for ways to make a difference.

Thanks to friends near and far for puzzle hunts, board games, good movie nights, bad movie nights, cookouts, dinner parties, dances, holiday celebrations, hikes in the snow, bike rides, and some of the strangest conversations I'm likely to ever encounter. And thanks to Elaina, for more than I could ever list here and who moved mountains in order for us to be together while I finished graduate school.

Thanks to The Coffee Lab and Ricardo for providing essential fuel to my research and for making sure I saw a friendly face every day I was on campus.

Thanks to innumerable past researchers and scientists who made previous field campaigns possible, and NASA and NOAA for providing freely available and easily accessible archives of past campaigns. Data from ARCTAS, DC3, FRAPPÉ, INTEX-NA, INTEX-B, KORUS-AQ and SEAC4RS are available from `https://www-air.larc.nasa.gov/missions.htm`. Data from ITCT2k2, CALNEX, SOAS, UBWOS, and WINTER are available from `https://www.esrl.noaa.gov/csd/field.html`.

Finally, thanks to all the co-authors or collaborators who shared their data in order to make the large coordinated field campaigns worthwhile. That includes: Hannah M. Allen, Benjamin R. Ayres, Steven S. Brown, William H. Brune, John D. Crounse, Joost de Gouw, Danielle C. Draper, Philip A. Feiner, Juliane L. Fry, Allen H. Goldstein, Abigail Koss, Pawel K. Misztal, Tran B. Nguyen, Kevin Olson, Alex P. Teng, Paul O. Wennberg, Robert J. Wild, and Li Zhang from SOAS; and Alan Fried, Denise D. Montzka, Michelle Kim, Eric Scheuer, Alexander B. Thames, Andrew J. Weinheimer, John D. Crounse, Paul O. Wennberg, Donald R. Blake, David O. Miller, William H. Brune, Jack E. Dibb, Simone Meinardi, Alexandra L. Brosius, Armin Wisthaler, Glenn Diskin, and Samuel Hall from KORUS-AQ.

Chapter 1

Introduction

Trace constituents in the atmosphere affect our health, our climate, and our environment. Globally, indoor and outdoor air pollution are estimated to cause over 6 million deaths each year, making poor air quality one of the leading causes of premature mortality worldwide (Forouzanfar et al., 2015). In the United States, efforts to improve air quality, especially those following the passage of the Clean Air Act of 1970, have led to significant increases in life expectancy and human health (Pope et al., 2009). However, despite these achievements, many places in the United States routinely experience air pollution above the National Ambient Air Quality Standards (NAAQS) for both fine particulate matter ($PM_{2.5}$) and ozone (O_3). Recent studies have suggested that improvements in air quality in major cities across the United States have slowed or stopped after decades of success. (Jiang et al., 2018).

Photochemical air pollution is difficult to control in part because a significant portion of $PM_{2.5}$ and nearly all O_3 is not emitted directly, but is produced in situ from chemical reactions in the atmosphere. When nitrogen oxides (NO_x) and volatile organic compounds (VOCs) are exposed to sunlight, a pair of radical chain reactions is formed (Fig. 1.1A) that rapidly produces O_3 (Seinfeld and Pandis, 2006). This same chemistry, especially in the presence of additional species such as SO_2 and NH_3, also generates low vapor pressure compounds that can condense to form particles. The linked radical chain reactions lead to a strikingly non-linear dependence of ozone production on the concentration of NO_x and the VOC reactivity (VOCR) (e.g., Thornton et al., 2002). At low concentrations, increasing NO_x leads to more efficient radical cycling and increases in the concentration of the hydroxyl radical (OH) and the rate of ozone production (Fig. 1.1B). Eventually, increases in NO_x serve to terminate the radical chain reactions rather than propagate them, leading to a decline in OH concentrations and O_3 production.

More broadly, NO_x controls both the rates and pathways of oxidation in the atmosphere. NO_x not only determines the concentration of OH, the most important atmospheric oxidant, but also the concentration of O_3, an oxidant in addition to being a pollutant, and the concentration of NO_3, often the most important oxidant at night. The concentration of NO_x also controls the fate of organic peroxy radicals (RO_2), determining whether they react with NO to form aldehydes and ketones, or whether they will be sufficiently long-lived to react with

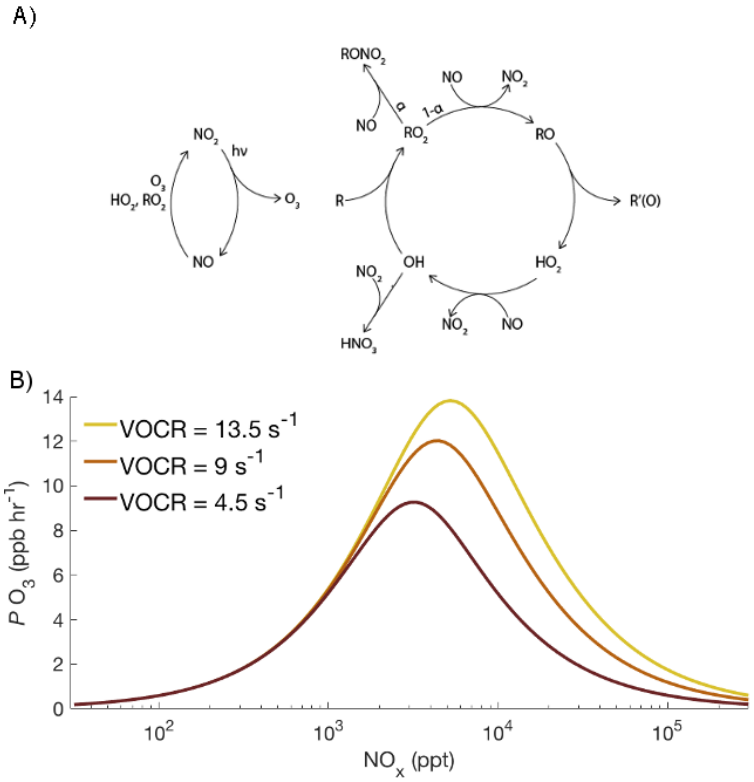

Figure 1.1: The linked radical chain reactions that lead to ozone production and NO_x loss in the troposphere (Panel A) and the non-linear dependence of instantaneous ozone production on NO_x concentration (Panel B).

HO_2 or undergo unimolecular isomerization to eventually form hydroperoxides or epoxides (e.g., Orlando and Tyndall, 2012; Teng et al., 2017). Understanding the chemical factors that control the concentration of NO_x is therefore crucial to understanding atmospheric oxidation.

NO_x is emitted to the atmosphere from a variety of sources, most of which involve high-temperature processes that lead to dissociation of N_2. These sources are both anthropogenic and natural, and include power plants, motor vehicles, and lightning (e.g., Dallmann and Harley, 2010; Nault et al., 2017). Fires emit NO_x as a direct combustion product of nitrogen from proteins and DNA in the fuel (Andreae and Merlet, 2001). Soil microbes also emit NO_x as a by-product of nitrification and de-nitrification (Pilegaard, 2013). Once in the atmosphere, NO_x can undergo a variety of different chemical processes that oxidize it to form higher oxides of nitrogen (NO_z). While there are many classes of NO_z, the two with the largest role in the long-term removal of NO_x from the atmosphere are nitric acid (HNO_3) and alkyl and multifunctional nitrates ($RONO_2$). Understanding the chemical budget of NO_x requires understanding the production and loss of these two classes.

Previous studies combining laboratory experiments, chemical transport models, and field

measurements have helped to greatly constrain the production of these species. Laboratory experiments by Mollner et al. (2010) found that the rate constant for the production of HNO_3 from OH and NO_2 had been overestimated by 10–20% under standard conditions, due to a minor channel that produces a weakly bound isomer of nitric acid that rapidly decomposes back to NO_2. New constraints on the temperature and pressure dependencies of the reaction rate were provided by Henderson et al. (2012) and Nault et al. (2016) using kinetic modeling and direct observations of NO_2 in the upper troposphere.

Recent studies have also greatly constrained the production rate of $RONO_2$. For many years there were substantial disagreements between the concentration and formation rates of total alkyl and multifunctional nitrates ($\Sigma RONO_2$) and the sum of individually measured $RONO_2$ species (Day et al., 2003; Rosen et al., 2004; Perring et al., 2010). Advances in technologies for detecting and quantifying individual multifunctional nitrates have substantially reduced this discrepancy (Beaver et al., 2012; Lee et al., 2016), establishing that field observations of $\Sigma RONO_2$ were likely correct. This convergence in the measured concentrations suggests that discrepancies between the formation rate of alkyl and multifunctional nitrates derived from measurements of $\Sigma RONO_2$ and the rate calculated from individual VOCs is due to uncertainties in laboratory kinetics or model representations.

$RONO_2$ are produced in the daytime through the reaction of RO_2 radicals with NO. While this reaction typically produces NO_2 and an alkoxy radical (RO), a fraction of the time these two compounds will instead associate to form an $RONO_2$. The branching ratio α_i represents the $RONO_2$ yield from the $RO_2 + NO$ reaction. Values of α_i for the production of alkyl nitrates from alkane oxidation have been measured since the 1980s (Atkinson et al., 1982; Carter and Atkinson, 1989). Recently, Teng et al. (2015) reported that values of α_i for alkene oxidation were significantly higher than previously assumed, helping to explain high concentrations of $\Sigma RONO_2$ observed in Houston, TX.

Recent laboratory studies have also substantially reduced the uncertainty in the $RONO_2$ yield from isoprene oxidation. As the most common VOC besides methane, the rate of $RONO_2$ production from isoprene oxidation has been found in modeling studies to have major implications for the response of air pollution to future changes in emissions or the climate (Ito et al., 2009; Paulot et al., 2012; Mao et al., 2013; Zare et al., 2018). For many years, laboratory studies reported wildly varying rates of $RONO_2$ formation from isoprene oxidation, with branching ratios ranging from 0.04–0.15 (Chen et al., 1998; Sprengnether et al., 2002; Paulot et al., 2009; Teng et al., 2015). Within the past decade, laboratory studies have converged on a yield of 0.13 ± 0.02 (Teng et al., 2017), a value matched by field studies estimating α_i for isoprene from the correlation of $\Sigma RONO_2$ and HCHO (Perring et al., 2009).

However, understanding the production of $RONO_2$ and HNO_3 from NO_x oxidation does not fully describe their role in the atmosphere. Completely understanding the effects of these species on NO_x also requires knowledge of their subsequent chemistry and deposition. For example, if $RONO_2$ oxidation efficiently recycled NO_x to the atmosphere, $RONO_2$ would become temporary NO_x reservoirs, transporting NO_x on regional or continental scales but not leading to the permanent loss of NO_x.

Investigating the fate of $RONO_2$ and HNO_3 in the ambient atmosphere requires studying their chemistry over a range of ages (time since emission) or watching the evolution of NO_x and NO_z on time scales of hours to days. Studies focused on the short-term evolution of NO_x within plumes provide key constraints on the oxidation of NO_x, but are not well suited to examining the balance of reactions from the production and the loss of NO_z compounds that occur on longer timescales.

A few studies have been able to investigate the bi-directional cycling between NO_x and NO_z by focusing on environments with little or no fresh emissions of NO_x. Perring et al. (2010) investigated the cycling of NO_z by examining polluted plumes originating from Mexico City that were aged for 1–2 days. They found that NO_z species accounted for a growing fraction of total reactive nitrogen (NO_y) as the plume aged, mostly in the form of HNO_3, and estimated that the chemical loss of $RONO_2$ was always insignificant ($< 10\%$) compared to $RONO_2$ production. Bertram et al. (2013) used measurements over the northern Pacific Ocean to investigate NO_x cycling in highly aged air. They found $\Sigma RONO_2$ to be unimportant, accounting for $< 10\%$ of total NO_y. In contrast, release of NO_x from photolysis and oxidation of gas-phase HNO_3 accounted for over a quarter of total NO_x production in the upper troposphere. Other studies of NO_x chemistry in the remote marine atmosphere have found anomalously high concentrations of NO_x or anomalously low concentrations of HNO_3, suggesting that unknown chemistry was converting HNO_3 into NO_x (e.g., Hauglustaine et al., 1996; Gao et al., 1999; Perkins et al., 2001). However, not all studies have agreed with this assessment. Bertram et al. (2007) suggested that wet deposition (rainout) of HNO_3 could equally explain the observations, and Neuman et al. (2006) found that, if anything, concentrations of HNO_3 were higher than expected based on known chemistry.

Other studies have investigated the cycling of NO_x and NO_z in forested environments. These studies have suggested rapid loss of $RONO_2$ compounds formed from biogenic VOCs, based on comparison of $\Sigma RONO_2$ with HCHO (Perring et al., 2009), $\Sigma RONO_2$ with HNO_3 (Browne et al., 2013), and isoprene nitrates with methyl vinyl ketone (Grossenbacher et al., 2004). Comparison between measurements and models further suggested the need for rapid chemical loss of these species (Giacopelli et al., 2005; Horowitz et al., 2007). However, none of these studies were able to strictly constrain the products of $RONO_2$ loss. Laboratory experiments suggested that oxidation to form secondary nitrates, recycling of NO_x, and heterogeneous conversion to nitric acid could potentially all play an important role (Darer et al., 2011; Liu et al., 2012; Lee et al., 2014a; Müller et al., 2014).

The relatively small number of studies that have been able to study the bi-directional cycling of NO_x and the significant variation in their results highlight the need for additional field measurements to better constrain the fate of NO_z in the atmosphere. Here, I investigate the chemistry of both $\Sigma RONO_2$ and HNO_3 using observations from two field intensives: the Southern Oxidant and Aerosol Study (SOAS, June – July 2013) in Centreville, Alabama, and the Korea-United States Air Quality Study (KORUS-AQ, May – June 2016) over South Korea. The contrasting chemistry in these two locations, moving from a forested environment dominated by biogenic VOC emissions to a highly polluted megacity makes it possible to isolate the chemistry of different NO_z molecules and to examine how NO_x chemistry varies

between different environments.

While intensive field deployments are excellent tools for investigating specific chemical mechanisms, they give little information about the trends in chemical mechanisms over time. Doing so requires more context than obtainable from a single 6 week field deployment and more detailed information than typically reported from long-term monitoring stations. Overcoming this barrier requires synthesizing multiple sources of information to better understand mechanistic trends over time. For example, Pusede et al. (2014) combined measurements from a short-term field deployment with long-term monitoring at the same location to understand how ozone production was changing in the San Joaquin Valley, CA. The combination of short- and long-term measurements was crucial to understanding how the chemistry of ozone production was affected by changing emissions and fluctuating temperatures in this polluted region. Similarly, Edwards et al. (2017) combined measurements from two short-term field campaigns near Atlanta, GA in 1999 and 2013 to understand how the mechanisms of nighttime VOC oxidation are changing in the southeast United States.

In the first half of this dissertation, I present new constraints on the fate and lifetime of $\Sigma RONO_2$ and HNO_3 using results from both the SOAS and KORUS-AQ field campaigns.

In Chapter 2, I demonstrate the need for multiphase chemistry to act as a sink of $\Sigma RONO_2$ and a source of HNO_3 in an isoprene-dominated forest. By examining the behavior of $\Sigma RONO_2$ and HNO_3 during SOAS, I show that known gas-phase chemical production and loss processes cannot explain their evolution and infer that a significant portion of $\Sigma RONO_2$ must rapidly undergo heterogeneous hydrolysis to form HNO_3. I find that during the SOAS campaign, approximately half of the $\Sigma RONO_2$ produced permanently removed NO_x from the atmosphere and the other half recycled NO_x to the atmosphere within a few hours of being formed.

In Chapter 3, I investigate the recent proposal that HNO_3 in aerosols undergoes photolysis between 10 and 300 times more rapidly than in the gas phase. Using a chemical box model and airborne observations of NO_x and HNO_3 over the Yellow Sea during KORUS-AQ, I show that rapid aerosol nitrate photolysis is inconsistent with other NO_x chemistry. This result confirms that HNO_3 has a long (> 50 hr) lifetime to chemical loss and is predominantly removed by wet and dry deposition.

In the second half of this dissertation, I study how the chemistry of NO_x and O_3 is changing over time by merging the results of the previous two chapters with long-term chemical monitoring and archived measurements from NASA and NOAA. By combining results from multiple sources, I am able to provide a more comprehensive look at how NO_x chemistry will be affected by changes to emissions or to the climate.

In Chapter 4, I investigate ozone production in regions with high biogenic VOC emissions where $RONO_2$ chemistry is the dominant NO_x sink. I combine extensive chemical measurements from SOAS with a more limited 15-year measurement record at the same location to examine how changes in temperature affect ozone production at this location, and show that changes in soil microbial emissions of NO_x with temperature explain 40% of the increase of O_3 production with temperature. This finding suggests that even if anthropogenic emissions of NO_x continue to decline over the continental United States, hotter temperatures will

continue to be associated with worse air pollution.

In Chapter 5, I combine a broad suite of air- and ground-based observations to discuss the factors that control NO_x loss on a continental scale. I show that over the past decades, the portion of NO_x loss occurring through $RONO_2$ chemistry has significantly increased in many areas of the country. I show that this transition, combined with changes in the spatial pattern of NO_x emissions, has led to a more even distribution of NO_x across the continental United States.

In Chapter 6, I conclude with a discussion of the implications of the results presented in this dissertation and suggest possible ideas for future research.

Chapter 2

NO_x loss in the southeast United States

Adapted from P. S. Romer et al., The lifetime of nitrogen oxides in an isoprene-dominated forest, *Atmos. Chem. Phys.*, 16(12), 7623–7637, doi:10.5194/acp-16-7623-2016, 2016.

2.1 Introduction

The concentration and chemistry of nitrogen oxides ($NO_x \equiv NO + NO_2$) in Earth's troposphere has a significant and non-linear effect on the oxidative capacity of the atmosphere. This in turn affects the production, composition, and aging of aerosols and the lifetime of greenhouse gases such as methane. Concentrations of NO_x control the production of ozone, a respiratory health hazard, important oxidant, and greenhouse gas. In addition, the deposition of reactive nitrogen is an important source of nutrients in some ecosystems (e.g., Fowler et al., 2013).

NO_x is emitted by both anthropogenic and biogenic sources, including motor vehicles, power plants, forest fires, and soil bacteria (e.g., Dallmann and Harley, 2010; Mebust and Cohen, 2014; Hudman et al., 2012), and is temporarily or permanently removed from the atmosphere by chemical conversion to higher oxides of nitrogen. Across much of the globe, the balance of these sources and sinks is in a period of dramatic change, with large reductions of NO_x emissions occurring in North America and Europe and significant increases occurring in Asia (e.g., Russell et al., 2012; Curier et al., 2014; Reuter et al., 2014). Understanding the effects of changes in NO_x emissions on the concentration and spatial distribution of NO_x requires detailed knowledge of the chemistry and transport of NO_x and NO_x reservoirs. These reservoirs are poorly understood and represent a significant uncertainty in analyses of NO_x emissions and ozone production (e.g., Ito et al., 2007; Browne and Cohen, 2012; Mao et al., 2013).

The net chemical loss of NO_x is difficult to directly observe. Observational methods for determining the lifetime of NO_x are easiest to apply in the outflow of isolated emissions,

where the declining concentration of NO_x or the changing ratio of NO_x to total reactive nitrogen (NO_y) provide clear evidence for NO_x loss (e.g., Ryerson et al., 1998; Dillon et al., 2003; Alvarado et al., 2010; Valin et al., 2013). In rural and remote regions, emissions and concentrations of NO_x and NO_y are typically slowly varying over large distances (e.g., Browne et al., 2013), preventing the loss of NO_x from being directly observable. Nor can the lifetimes found in plume studies be easily translated into an appropriate lifetime in the regional background. Short-lived NO_x reservoirs such as peroxy acyl nitrate (PAN) can efficiently remove NO_x in a plume, but act as a source of NO_x in rural and remote regions (Finlayson-Pitts and Pitts, 1999). In addition, the non-linear interactions between NO_x and OH make the lifetime of NO_x in a fresh plume very different from its lifetime several hours downwind (e.g., Martinez et al., 2003; Valin et al., 2013).

To constrain the lifetime of NO_x in rural and remote regions, observations of reactive nitrogen species must be combined with an understanding of the chemical transformations between NO_x and its higher oxides. If the production, loss, and fate of these higher oxides are accurately understood, then the lifetime of NO_x can be calculated by tracing the flow of reactive nitrogen through the system. Here, we evaluate the daytime lifetime of NO_x in the rural southeast United States, using measurements taken from 1 June – 15 July 2013 as part of the Southern Oxidant and Aerosol Study (SOAS). In situ measurements of volatile organic compounds (VOCs), atmospheric oxidants, and a wide range of reactive nitrogen compounds are used to determine the production and loss rates for nitric acid, alkyl and multifunctional nitrates, and peroxy nitrates. These rates are used to assess the lifetime of NO_x in this region.

2.2 The NO_y family and the lifetime of NO_x

During the day, NO_x is lost by associating with other radicals to produce higher oxides of nitrogen, primarily nitric acid, alkyl and multifunctional nitrates ($\Sigma ANs = \Sigma RONO_2$), and peroxy nitrates ($\Sigma PANs = \Sigma R(O)OONO_2$) (e.g., Day et al., 2003; Perring et al., 2010). The sum of these and other higher oxides such as N_2O_5 and HONO are collectively known as NO_z ($NO_z \equiv NO_y - NO_x$).

NO_x is oxidized to produce the major daytime classes of NO_z through reactions (R2.1), (R2.2b), and (R2.3).

$$NO_2 + OH + M \rightarrow HNO_3 + M \tag{R2.1}$$

$$NO + RO_2 + M \rightarrow RONO_2 + M \tag{R2.2b}$$

$$NO_2 + R(O)O_2 + M \rightleftharpoons R(O)OONO_2 + M \tag{R2.3}$$

NO_x can also be converted to NO_z through reactions of the NO_3 radical. Although these reactions are most important at night, previous studies have shown that NO_3 chemistry can

produce NO_z during the day if concentrations of alkenes are high (e.g., Fuentes et al., 2007; Mogensen et al., 2015; Ayres et al., 2015).

The production and fate of different NO_z species determine the lifetime of NO_x. Some of these species are short-lived and re-release NO_x back to the atmosphere within hours of being formed. If the lifetime for the conversion of an NO_z species back to NO_x is shorter than typical NO_x lifetimes in the atmosphere, then NO_x and these NO_z species interact, and their concentrations will approach a steady-state ratio. As NO_x is removed from the system, some of the short-lived NO_z species dissociate, buffering the concentration of NO_x. In this way, the presence of NO_x reservoirs directly extends the lifetime of NO_x.

One method to take this buffering into account when calculating the lifetime of NO_x is to consider the sum of NO_x and all NO_z species with lifetimes to re-release of NO_x shorter than the atmospheric lifetime of NO_x. We define this sum as short-lived reactive nitrogen, or NO_{SL}. The remaining forms of reactive nitrogen are defined as long-lived reactive nitrogen (NO_{LL}). The division between NO_{SL} and NO_{LL} depends on the lifetime of NO_x. For the initial discussion in this chapter, we use a provisional lifetime of 7 hours to divide NO_z species between NO_{SL} and NO_{LL}. This cutoff is in the middle of the range of NO_x lifetimes found in plume studies (e.g., Ryerson et al., 1998; Dillon et al., 2003; Alvarado et al., 2010; Valin et al., 2013). The provisional cutoff chosen as a starting point does not affect the final results.

In areas well removed from large NO_x sources, NO_x and its short-lived reservoirs interconvert significantly faster than the rate of change of NO_x. Under these conditions, the lifetime of NO_x(τ_{NO_x}) is equal to the lifetime of NO_{SL}. If the conversion of NO_{LL} to NO_{SL} is negligible, then the lifetime of NO_x can be calculated by Eq. (2.1).

$$\tau_{NO_x} = \tau_{NO_{SL}} = \frac{[NO_{SL}]}{\mathcal{L}(NO_{SL})} \tag{2.1}$$

Throughout this chapter, we use $\mathcal{L}$(X) to indicate the gross loss rate of the compound or class of compounds X.

The relationship and interactions between NO_{SL} and NO_{LL}, and their typical compositions in the planetary boundary layer, are shown in Fig. 2.1. In the summertime at mid-latitudes, peroxy nitrates typically release NO_x within hours of being formed (LaFranchi et al., 2009), making them a component of NO_{SL}. Under these same conditions, nitric acid typically converts back to NO_x on timescales of 100 hours or greater (Finlayson-Pitts and Pitts, 1999) and is a component of NO_{LL}. The fate and lifetime of $\Sigma RONO_2$, the third major component of NO_z, remain poorly understood, making it uncertain whether $\Sigma RONO_2$ act as a component of NO_{SL} or NO_{LL} (Perring et al., 2013, and references therein). This is especially true for the multifunctional, biogenically-derived nitrates that are the predominant component of $\Sigma RONO_2$ in forested areas (e.g., Beaver et al., 2012).

Recent studies of multifunctional nitrates suggest that the main daytime loss pathways of these species are deposition, reaction with OH, photolysis, and heterogeneous hydrolysis to produce nitric acid (e.g., Darer et al., 2011; Browne et al., 2013; Lee et al., 2014a; Müller

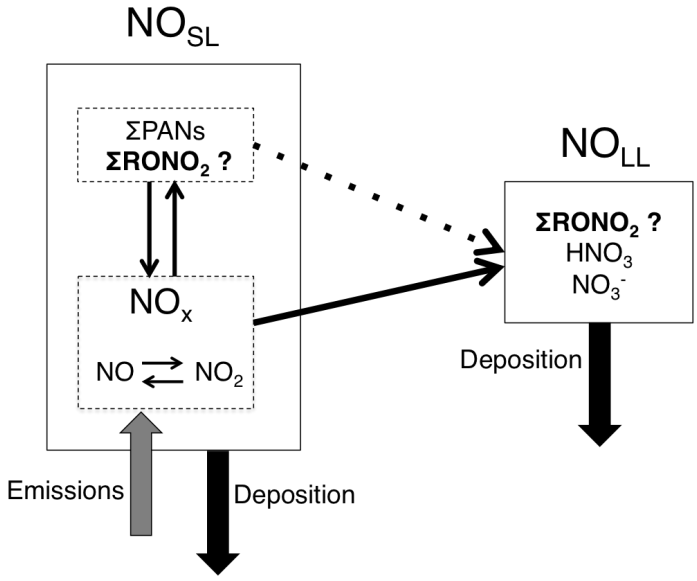

Figure 2.1: A schematic representation of the chemistry of NO_{SL} and NO_{LL}, showing the typical components of both classes.

et al., 2014; Nguyen et al., 2015; Lee et al., 2016). These recent studies, combined with the extensive measurements made during SOAS, allow us to provide new constraints on the lifetime and fate of $\Sigma RONO_2$ and therefore to more accurately determine the lifetime of NO_x.

2.3 Instrumentation and measurements

The primary ground site for SOAS was located in Bibb County, Alabama (32.90289° N, 87.24968° W) at the Centreville (CTR) long-term monitoring site in the SouthEastern Aerosol Research and CHaracterization (SEARCH) Network (Hansen et al., 2003). This location is 40 km southeast of Tuscaloosa (population 95,000), and 90 km southwest of Birmingham (population 210,000). Comparison with long-term measurements indicate that the summer of 2013 was cooler and cloudier than typical for previous summers (Hidy et al., 2014). Gas-phase measurements used in this study were located on a 20 m walk-up tower at the edge of the forest. Nitrate ion and meteorological parameters were measured in a clearing approximately 50 m away from the tower.

A nearly complete suite of reactive nitrogen species, including NO, NO_2, $\Sigma PANs$, $\Sigma RONO_2$, HNO_3, and NO_3^-, was measured during SOAS. NO was measured using the chemiluminescence instrument described in Min et al. (2014). The reaction of ambient NO with added excess O_3 formed excited NO_2^* molecules. A fraction of these fluoresce, and the emitted photons were collected on a red-sensitive photomultiplier tube (Hamamatsu H7421-50). Cal-

ibrations were performed every 2 hours by diluting NO standard gas (5.08 ppm ± 5% NO in N_2, Praxair) to 3–20 ppb in zero air and adding it to the instrument inlet. The mixing ratio was corrected for enhanced quenching by water vapor (Thornton et al., 2000) using co-located measurements of relative humidity and temperature.

NO_2, ΣPANs, and Σ$RONO_2$ were measured via thermal dissociation laser-induced fluorescence (TD-LIF), as described by Day et al. (2002). Ambient air was drawn into a multipass White cell, where a 532 nm Nd-YAG laser excited the NO_2 molecules, and their fluorescence signal was collected on a photomultiplier tube (Hamamatsu H7421-50). The same instrument was used to measure the sum of peroxy nitrates and the sum of alkyl and multifunctional nitrates by first passing the air through a heated oven, where the organic nitrates dissociated to form NO_2. Organic nitrates present in the particle phase undergo evaporation and thermal dissociation in the heated ovens to form NO_2. The TD-LIF measurement of Σ$RONO_2$ therefore includes alkyl and multifunctional nitrates in both the gas and particle phases, but does not include HNO_3 or particle-phase inorganic nitrate (Day et al., 2002; Rollins et al., 2010). All of the channels were calibrated by injecting NO_2 standard gas (5.03 ppm ±5% NO_2 in N_2, Praxair) and corrected for enhanced quenching by water vapor.

Nitric acid was measured in the gas phase by chemical ionization mass spectrometry (CIMS), using CF_3O^- as the reagent ion (Crounse et al., 2006). The ions were quantified using a compact time-of-flight mass spectrometer, and the instrument was calibrated in the field using isotopically labeled nitric acid. Particle-phase inorganic nitrate (NO_3^-) was measured using a monitor for aerosols and gases (MARGA) (Allen et al., 2015). Ambient air was drawn through a rotating wet-walled denuder which collected water-soluble gas-phase compounds. Particle-phase compounds were captured by a steam-jet aerosol collector downstream of the denuder. Water soluble ions from both phases were then quantified via ion chromatography. This measurement of NO_3^- is designed to be specific to inorganic nitrate, and is not affected by $RONO_2$ in the particle phase (Allen et al., 2015).

Measurements of reactive nitrogen species are summarized in Fig. 2.2. Concentrations of NO_{SL} compounds (NO, NO_2, and ΣPANs) are shown in Fig. 2.2A. Afternoon concentrations of NO_2 and NO were typically around 220 ppt and 50 ppt respectively. After sunset, NO dropped to near zero, and NO_2 began to increase. At sunrise, NO concentrations rapidly rose to over 200 ppt between 6 am and 8 am Central Standard Time (CST) while NO_2 decreased sharply. By 11 am, when the daytime boundary layer was well developed, the concentrations of NO and NO_2 returned to their typical afternoon values. Concentrations of ΣPANs were 160 ppt at sunrise, increased to a maximum concentration of 300 ppt at 9 am and declined slowly throughout the rest of the day.

Concentrations of HNO_3 and inorganic NO_3^-, components of NO_{LL}, are shown in Fig. 2.2B. Both species increased slowly after sunrise and reached a maximum combined concentration of 300 ppt at 1 pm, before declining to a combined concentration of 175 ppt at night. The total concentration of Σ$RONO_2$ in both the gas and particle phase, whose partitioning into NO_{SL} and NO_{LL} is not known, is shown in Fig. 2.2C. Σ$RONO_2$ concentrations averaged 150 ppt during the night and increased sharply after sunrise. After reaching a maximum

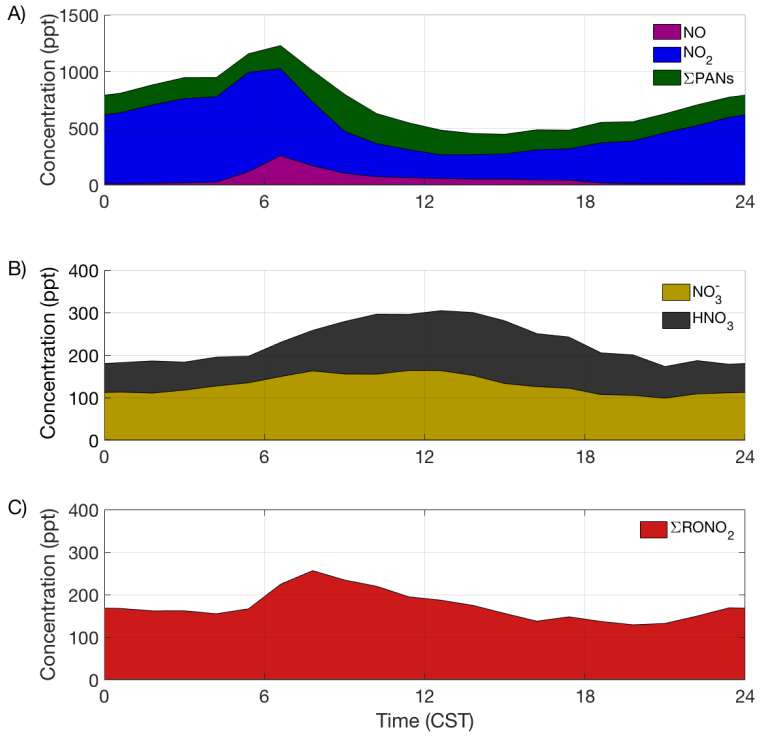

Figure 2.2: Diurnal cycle of measured reactive nitrogen species during SOAS. Reactive nitrogen species are classified as likely components of NO_{SL} (Fig. 2.2A), likely components of NO_{LL} (Fig. 2.2B) or unknown (Fig. 2.2C). The classification into NO_{SL} and NO_{LL} is based on typical summertime afternoon lifetimes. The measurement of HNO_3 represent nitric acid in the gas phase, while the measurement of NO_3^- represents inorganic nitrate in the particle phase. The measurement of $\Sigma RONO_2$ includes alkyl and multifunctional nitrates in both the gas and particle phase.

of 250 ppt at 8 am, $\Sigma RONO_2$ concentrations declined slowly to a minimum of 125 ppt at sunset.

OH, HO_2, and OH reactivity (OHR) were measured via fluorescence assay by gas expansion (FAGE) of OH. A 308 nm dye laser excited the OH radicals and their fluorescence was detected by an electronically gated microchannel plate detector (Faloona et al., 2004). Calibration of the system was performed by in situ generation of OH radicals via photolysis of water vapor. Chemical zeroing was performed by periodically adding C_3F_6 to the sampling inlet in order to quantify the interference from internally generated OH observed in previous field campaigns (Mao et al., 2012). HO_2 was measured in a second channel by adding NO to chemically convert HO_2 to OH. The amount of added NO was regulated such that HO_2 but not RO_2 was converted to OH (Fuchs et al., 2011). OHR was measured by drawing ambient air through a flow tube and mixing it with a fixed concentration of OH. At the end of the flow tube, the concentration of OH was measured. The OH Reactivity is determined by the

slope of the OH signal versus reaction time (Mao et al., 2009).

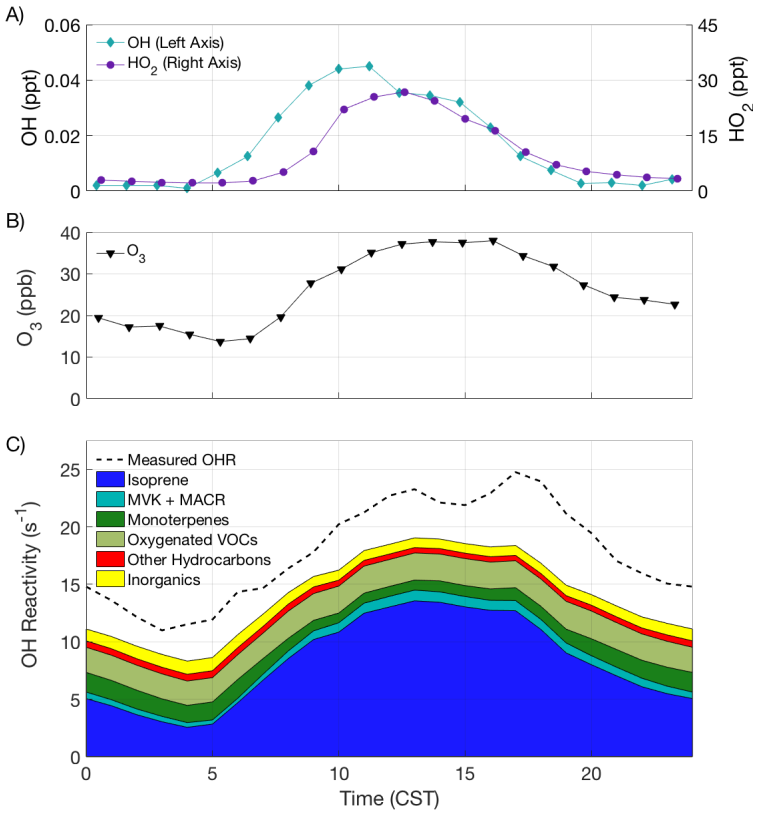

Figure 2.3: Diurnal cycle of OH, HO_2, O_3 and VOCs during SOAS. The top plot shows the concentration of OH and HO_2; the middle plot shows the concentration of O_3; the bottom plot shows the VOC Reactivity.

Measured concentrations of OH peaked at 0.045 ppt and concentrations of HO_2 at 30 ppt during SOAS (Fig. 2.3A). Both OH and HO_2 increased slowly throughout the morning and reached their maximum in the early afternoon. Concentrations then fell as the sun set, with OH usually dropping below 0.01 ppt by 7 pm. The measured OH Reactivity was high, reaching an afternoon peak of close to 25 s^{-1} (Fig. 2.3C). OHR decreased throughout the night, reaching a minimum of 10 s^{-1} just before sunrise.

Measurements of ozone were made using a Cavity Ring Down Spectrometer (Washenfelder et al., 2011). O_3 is chemically converted to NO_2 by reaction with excess NO, and the resulting NO_2 is measured by cavity ring-down spectroscopy at 404 nm. The concentration of ozone increased from a minimum of 15 ppb at sunrise to a maximum of 38 ppb in the late afternoon (Fig. 2.3B).

Volatile organic compounds were measured primarily by gas chromatography-mass spectrometry (GC-MS). Samples were collected in a liquid-nitrogen cooled trap for five minutes, and then transferred by heating onto an analytical column, and detected using an

electron-impact quadrupole mass-spectrometer (Goldan et al., 2004; Gilman et al., 2010). This system was able to quantify a wide range of compounds including alkanes, alkenes, aromatics, isoprene, and multiple monoterpenes. The sum of methyl vinyl ketone (MVK) and methacrolein (MACR) was measured using a proton transfer reaction time of flight mass spectrometer (PTR-TOF-MS) (Kaser et al., 2013). The interference in this measurement from the decomposition of isoprene hydroperoxides on instrument inlets (Rivera-Rios et al., 2014) is not corrected for, and increases the uncertainty in this measurement by approximately 20%.

VOC measurements at the site show that the OHR was dominated by reaction with biogenic compounds. Figure 2.3C shows the OH Reactivity of individually measured compounds as a stacked area plot. In the daytime, isoprene accounted for nearly half of the total reactivity, while VOCs typically attributed to anthropogenic activities, including alkanes, aromatics, and simple alkenes, were responsible for less than 10% of the measured OHR. Not included in Fig. 2.3C is the reactivity of VOCs whose reaction with OH does not lead to net loss of OH, and therefore does not contribute to the measured OHR. These compounds, primarily isoprene hydroperoxides (ISOPOOH) and C5-hydroxyaldehydes (HPALD), have an average daytime reactivity of 2 s^{-1}. The sum of individual reactivities shows a similar diurnal pattern to the measured OHR, and accounts for 70–85% of the total. Unknown biogenic emissions, small aldehydes and alcohols, and other 2nd and 3rd generation VOC oxidation products are all possible contributors to the missing reactivity (e.g., Di Carlo et al., 2004; Goldstein and Galbally, 2007; Pusede et al., 2014; Kaiser et al., 2016). Meteorological parameters including temperature and solar radiation were measured by Atmospheric Research and Analysis as part of SEARCH.

2.4 The production and loss of individual NO_x reservoirs

Nitric acid

In the boundary layer, the production of nitric acid is typically followed by deposition and thus leads to the permanent removal of reactive nitrogen from the atmosphere. Nitric acid can undergo photolysis or reaction with OH to produce NO_x, but these processes are slow (Burkholder et al., 1993; Atkinson et al., 2006), with an average calculated rate during SOAS of less than 0.2 ppt h^{-1}. Gas-phase nitric acid can also partition into aerosols. Nitric acid is long lived in the particle phase and is typically lost by re-evaporation into the gas phase (e.g., Hennigan et al., 2008). The loss of nitric acid through deposition of aerosols is typically negligible compared to its gas-phase deposition (e.g., Zalakeviciute et al., 2012). Because nitric acid releases NO_x so slowly, it is a component of NO_{LL}.

The deposition velocity (v_{dep}) of HNO_3 in the gas phase was measured during SOAS by Nguyen et al. (2015). Around midday, when the boundary layer is well developed, the deposition velocity can be combined with the boundary layer height (BLH) to calculate a

loss rate of HNO_3 (2.2).

$$\mathcal{L}(HNO_3) = \frac{v_{dep}}{BLH} \cdot [HNO_3] \tag{2.2}$$

Using this method, we find the lifetime of nitric acid in the gas and particle phase to be 6 hours at noon. In the late afternoon, changing boundary layer dynamics make this calculation of the loss rate inaccurate (e.g., Papale et al., 2006; Millet et al., 2015). The loss of nitric acid in the late afternoon was therefore calculated by fitting periods of consistent decay between 3 pm and 7 pm with an exponential curve. By fitting only the periods of consistent decay, we aim to select for periods where the production of nitric acid is at a minimum and the observed net decay of nitric acid is similar to its gross loss rate. Because nitric acid reversibly partitions between the gas and particle phases, the lifetime was calculated based on the concentration of nitric acid in both phases. The lifetime calculated using this method is 5^{+3}_{-2} hours, similar to the lifetime of nitric acid calculated using Eq. (2.2) at noon.

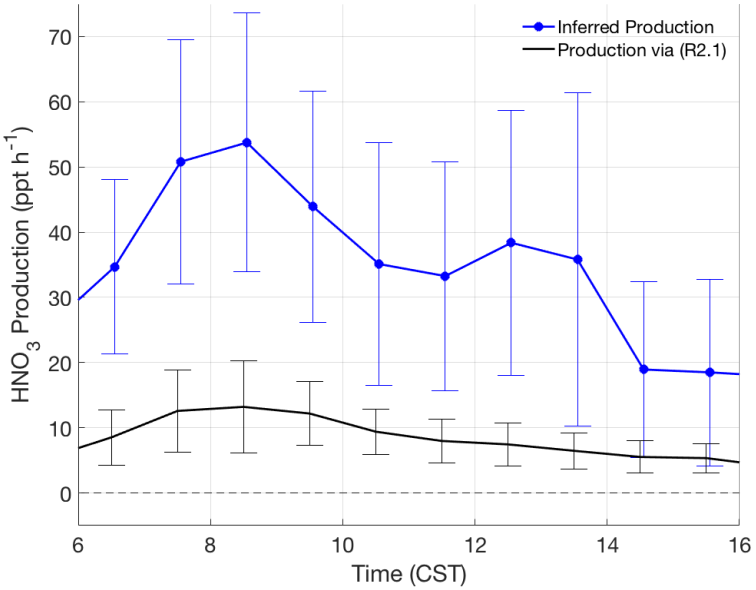

Figure 2.4: Production rates of nitric acid during SOAS calculated from the reaction of OH + NO_2 (black) and inferred from the concentration and deposition rate of nitric acid (blue). The vertical bars show the systematic and random uncertainty in the calculated rates, as described in the text.

By combining the loss rate of nitric acid with the rate of change of its concentration, we can calculate an inferred production rate of nitric acid (Fig. 2.4). This inferred production rate for each hour is defined as the difference between the rate of change in the concentration of nitric acid and the loss rate. The rate of change was determined as the slope of a best-fit line of the concentration of nitric acid versus time for each hour.

Since the calculation of the inferred production rate considers only the hour-to-hour change in nitric acid and not its gross concentration, the inferred production rate is not

affected by distant nitric acid sources. We find small (less than 15%) variation in the concentration of NO_x with wind direction and no correlation of the inferred production rate around noon with sulfate (a power plant tracer) or benzene (an urban tracer). As the transport time from these sources to the CTR site is significantly greater than 1 hour, this result is not surprising. The changing boundary layer height could significantly impact the inferred production rate of nitric acid during the early morning, but it is likely unimportant at midday.

Also shown in Fig. 2.4 is the rate of nitric acid production from the reaction of $OH + NO_2$ (R2.1), using the rate constant measured by Mollner et al. (2010). The vertical bars for the inferred rate represent the combined effects of the uncertainty in both the fit of concentration v. time and in the calculated nitric acid lifetime, as well as the day-to-day variations in the observations. The vertical bars shown for the production of nitric acid from the $OH + NO_2$ reaction include both the systematic and random errors in the measurements of OH and NO_2 and in the rate coefficient, $k_{OH + NO_2}$, combined in quadrature.

Between 10 am and 2 pm, when photochemistry is most active, the inferred production rate is 3–4 times larger than the rate of reaction (R2.1), a difference of approximately 30 ppt h^{-1}. The most likely explanation for the missing nitric acid production during this time is the heterogeneous hydrolysis of $RONO_2$. This has been proposed as an important source of nitric acid over the Canadian boreal forest (Browne et al., 2013), and the hydrolysis of tertiary alkyl nitrates on atmospherically relevant timescales has been observed in several laboratory experiments (e.g., Darer et al., 2011; Liu et al., 2012; Rindelaub et al., 2015). If $RONO_2$ are being converted to nitric acid, this process should appear as a sink in the budget of $\Sigma RONO_2$. If other processes are responsible for the missing nitric acid source, these would not affect the budget of $\Sigma RONO_2$. Only the conversion of $\Sigma RONO_2$ to nitric acid will lead to a missing source of nitric acid and a missing sink of $\Sigma RONO_2$.

Alkyl and multifunctional nitrates

Previous observational studies have found that the production of $\Sigma RONO_2$ is rapid in forested regions (e.g., Day et al., 2009; Beaver et al., 2012; Fry et al., 2013; Browne et al., 2013), but the subsequent fates of these biogenic nitrates are not well constrained. During the day, $RONO_2$ compounds are produced primarily from the reaction of organic peroxy radicals (RO_2) with NO. Most of the time, this leads to the formation of RO and NO_2 (R2.2a), but a fraction of the time produces an organic nitrate (R2.2b). The branching ratio $k_{R2.2b}/(k_{R2.2b} + k_{R2.2a})$ is designated α and varies with the structure of the R group, as well as the temperature and pressure.

$$NO + RO_2 \rightarrow RO + NO_2 \tag{R2.2a}$$

$$NO + RO_2 + M \rightarrow RONO_2 + M \tag{R2.2b}$$

Organic peroxy radicals are produced in the daytime troposphere predominantly by the reaction of OH with VOCs and are lost through reaction with NO, HO_2, and RO_2, or through unimolecular isomerization. These radicals reach steady state within seconds, allowing the production of $\Sigma RONO_2$ via reaction (R2.2b) to be calculated via Eq. (2.3).

$$P(\Sigma \mathrm{RONO_2}) = \sum_{R_i} \alpha_i \cdot f_{\mathrm{NO}_i} \cdot k_{\mathrm{OH+R_i}} \cdot [\mathrm{R_i}] \cdot [\mathrm{OH}] \tag{2.3}$$

The value f_{NO} represents the fraction of RO_2 radicals that are lost by reaction with NO. This value was calculated separately for each measured VOC and is equal to the rate of reactions R2.2b and R2.2a, divided by the sum of all RO_2 loss rates. Rate constants for the reaction of RO_2 radicals with NO, HO_2, and other RO_2 radicals are taken from the Master Chemical Mechanism v3.2 (Saunders et al., 2003) for all species other than isoprene and methacrolein. The reactions of isoprene-derived RO_2 radicals are based on the LIM-1 scheme described by Peeters et al. (2014), with the rate of unimolecular isomerization scaled to match the rate of HPALD formation observed in chamber experiments by Crounse et al. (2011). For methacrolein, we include the isomerization rate described by Crounse et al. (2012). Unimolecular isomerization is not included for any other RO_2 species. Concentrations of RO_2 radicals are calculated iteratively at each point until they converge.

Values of $k_{\mathrm{OH+R_i}}$ and α_i are taken from Atkinson and Arey (2003) and Perring et al. (2013) respectively, with the following exceptions. An α of 0.26 is used for α-pinene, following Rindelaub et al. (2015). An α of 0.12 is used for isoprene. This is in the middle of the range of branching ratios for isoprene (0.09–0.15) found in recent experiments (e.g., Paulot et al., 2009; Teng et al., 2015; Xiong et al., 2015).

The missing OH Reactivity (Fig. 2.3C) is included in this calculation as a generic VOC that forms RO_2 radicals that react with the same kinetics as $CH_3CH_2O_2$. This is appropriate if the missing reactivity is composed of small or highly oxygenated compounds (Perring et al., 2013). If the missing VOC Reactivity has a significant contribution from large hydrocarbons, then α for this reactivity should be higher.

The daytime production of $\Sigma RONO_2$ also includes a minor contribution from the reaction of NO_3 with alkenes, via reactions (R2.4) and (R2.5).

$$\mathrm{NO_2 + O_3 \rightarrow NO_3 + O_2} \tag{R2.4}$$

$$\mathrm{NO_3 + R \rightarrow RONO_2} \tag{R2.5}$$

Concentrations of isoprene and monoterpenes were sufficiently elevated during SOAS that reaction with these compounds is a significant fraction of the total daytime loss of NO_3. Calculations following Ayres et al. (2015) indicate that this pathway produces $RONO_2$ at an average rate of 10 ppt h^{-1}.

The calculated total rate of $\Sigma RONO_2$ production via (R2.2b) and (R2.5) is rapid, averaging approximately 90 ppt h^{-1} between 8 am and 4 pm (Fig. 2.5). The oxidation of

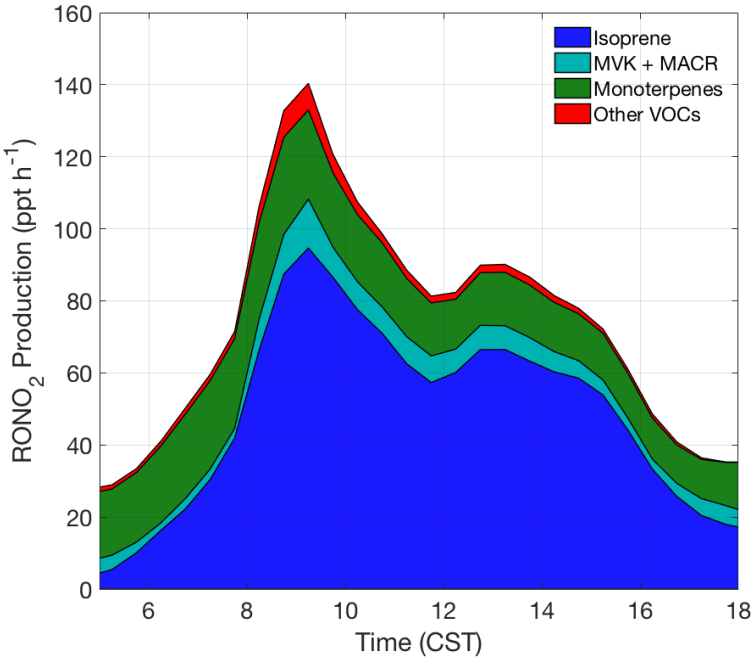

Figure 2.5: Average daytime production of $\Sigma RONO_2$, categorized based on VOC precursors.

isoprene accounts for over three-quarters of the production of $\Sigma RONO_2$, and monoterpenes account for an additional 15%. Based on the uncertainty in each term in Eq. (2.3), the total systematic uncertainty in the production rate of $\Sigma RONO_2$ is estimated to be $\pm 50\%$ (one sigma). The largest contribution to the total uncertainty comes from the calculation of f_{NO} for isoprene. Reported uncertainties for the rate constants and radical concentrations involved in RO_2 loss (Boyd et al., 2003; Ghosh et al., 2010; Crounse et al., 2011; Peeters et al., 2014) combine to give an overall uncertainty of $\pm 35\%$ in f_{NO} for isoprene. Uncertainty in the values of alpha and the nature of the missing VOCR are also significant contributions to the total uncertainty. The effects of boundary layer growth are not accounted for, but are unlikely to be important after 10 am (e.g., Xiong et al., 2015). The 55% uncertainty constrains the average $\Sigma RONO_2$ production rate to between 50 and 145 ppt h^{-1}.

Rapid production of $\Sigma RONO_2$ decreases the NO_x lifetime only if it leads to the long-term removal of NO_x from the atmosphere. This can occur either if the alkyl and multifunctional nitrates produced are themselves long lived, or if they have short lifetimes but are lost primarily to deposition or to conversion to a different NO_z species that is long-lived. Despite rapid production of $\Sigma RONO_2$ during the day, the diurnal cycle of $\Sigma RONO_2$ exhibits a decrease between 9 am and 7 pm (Fig. 2.2C), implying that the $\Sigma RONO_2$ loss rate must be rapid.

While $\Sigma RONO_2$ does not build up over the course of a day, their concentration is strongly correlated with their instantaneous production rate in the afternoon (Fig. 2.6). We inter-

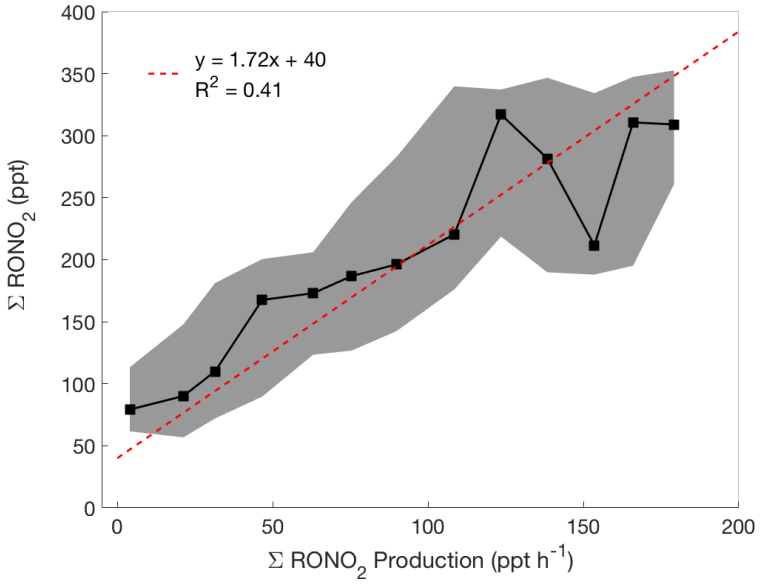

Figure 2.6: The concentration of $\Sigma RONO_2$ versus their production rate during the afternoon (12 pm – 4 pm). The black squares show the median in each bin, and the shaded grey area the interquartile range. A linear fit to all points gives a slope of 1.7 h.

pret these two results to indicate that $\Sigma RONO_2$ is short-lived and near steady-state in the afternoon. A least-squares fit between $\Sigma RONO_2$ production and concentration gives a slope of 1.7 hours and an intercept of 40 ppt. If $\Sigma RONO_2$ is near steady-state, then the slope of this correlation is equal to the $\Sigma RONO_2$ lifetime. The intercept of 40 ppt is interpreted as the large-scale background of long-lived $RONO_2$ during summertime at mid-latitudes. This background is likely composed of small monofunctional alkyl nitrates, since these compounds typically have lifetimes of days or weeks in the summertime troposphere (e.g., Clemitshaw et al., 1997). Ethyl and isopropyl nitrate were measured by GC-MS during SOAS, and show a consistent concentration of ∼20 ppt, explaining 50% of the intercept. Previous observations over North America suggest that the summed concentration of small monofunctional nitrates not measured during SOAS is likely also around 20 ppt in the southeast United States, accounting for the other 50% (e.g., Schneider et al., 1998; Blake et al., 2003b; Russo et al., 2010).

A lifetime of 1.7 hours for the reactive component of $\Sigma RONO_2$ is roughly consistent with previous estimates. Perring et al. (2009) found a lifetime of 1.5–2.5 h for $\Sigma RONO_2$ in the southeast United States, based on the correlation between $\Sigma RONO_2$ and formaldehyde. Multiple studies have also found evidence for rapid loss of $RONO_2$ through particle-phase processing in the southeast United States (e.g., Pye et al., 2015; Lee et al., 2016). This reactive component is likely composed of larger, multifunctional nitrates that can be lost rapidly by oxidation, deposition, or hydrolysis (Darer et al., 2011; Lee et al., 2014a; Nguyen et al., 2015).

Because most $RONO_2$ are short-lived, they do not serve as a permanent sink of NO_x directly. To establish whether $\Sigma RONO_2$ is a component of NO_{SL} or NO_{LL}, the fate of $\Sigma RONO_2$ must be understood. Conversion of an alkyl nitrate to another alkyl nitrate does not affect the measurement of $\Sigma RONO_2$ and therefore does not contribute to the calculated 1.7 hour lifetime. The only other NO_y compounds produced by alkyl nitrate oxidation that have been observed in laboratory experiments are NO_x and nitric acid (e.g., Darer et al., 2011; Lee et al., 2014a). These two products are thought to arise from completely different mechanisms in the oxidation of $\Sigma RONO_2$. NO_x is produced either during the gas-phase oxidation of nitrates (Lee et al., 2014a) or by the photolysis of carbonyl nitrates (Müller et al., 2014), while nitric acid is produced only by the heterogeneous hydrolysis of hydroxy-nitrates (Darer et al., 2011). The question of whether $RONO_2$ to nitric acid conversion is occurring is therefore equivalent to the question of whether deposition and the sum of all gas-phase loss processes are sufficient to explain the 1.7 h lifetime of $\Sigma RONO_2$. If these processes cannot explain the short lifetime of $\Sigma RONO_2$, then the unaccounted-for loss is likely due to heterogeneous formation of nitric acid.

An upper limit to the gas-phase oxidation rate of $\Sigma RONO_2$ can be calculated using measurements of $\Sigma RONO_2$ by assuming that all alkyl and multifunctional nitrates react with OH and O_3 at the same rate as isoprene hydroxy-nitrates and that these reactions all lead to loss of $\Sigma RONO_2$. Over three-quarters of the $\Sigma RONO_2$ produced during SOAS were isoprene hydroxy-nitrates (Fig. 2.5), making the average loss rate of $\Sigma RONO_2$ close to the rate for isoprene hydroxy-nitrates. In addition, under low-NO_x conditions, the most likely products of $RONO_2$ oxidation are either NO_x or carbonyl nitrates (Lee et al., 2014a). Studies by Müller et al. (2014) and Xiong et al. (2016) indicate that carbonyl nitrates are rapidly photolyzed to release NO_x. If the photolysis rate is fast enough, then it is a reasonable approximation to treat $RONO_2$ as releasing NO_x every time they are oxidized.

Only $RONO_2$ present in the gas phase are likely to undergo deposition or reaction with OH or O_3. Observations during SOAS indicate that 20% of $\Sigma RONO_2$ may be in the particle phase during the afternoon (Lee et al., 2016); however, even if we assume that all $\Sigma RONO_2$ are gas-phase, the rate of gas-phase oxidation plus the rate of deposition measured by Nguyen et al. (2015) during SOAS is insufficient to explain the loss of $\Sigma RONO_2$ in the afternoon (Fig. 2.7, filled areas). Since isoprene hydroxy-nitrates and most other first-generation nitrates must be further oxidized before undergoing photolysis, we do not include photolysis as a separate loss process in Fig. 2.7. Nitrates produced in the oxidation of compounds such as MVK and MACR can undergo photolysis without reacting with OH first, but these are a minor fraction of the total $\Sigma RONO_2$ production rate (Fig. 2.5).

If the gap between the individual loss processes and the overall loss rate of $\Sigma RONO_2$ is attributed entirely to $\Sigma RONO_2$ hydrolysis, then the rate of nitric acid production from $\Sigma RONO_2$ would be 65 ppt h^{-1}. This is two-thirds of the total $\Sigma RONO_2$ production rate, and roughly equal to the calculated production rate of tertiary nitrates (Peeters et al., 2014; Rindelaub et al., 2015). Laboratory experiments have shown that, in general, tertiary nitrates undergo hydrolysis far faster than primary or secondary nitrates (Darer et al., 2011; Hu et al., 2011), making it likely that the rate of $\Sigma RONO_2$ hydrolysis is similar to the rate

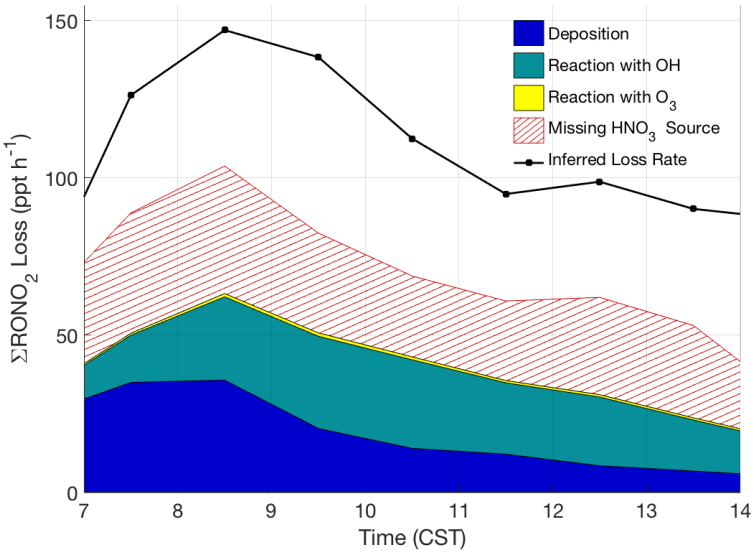

Figure 2.7: Loss rates and fates of $\Sigma RONO_2$ during SOAS. The black line shows the loss rate of $\Sigma RONO_2$ based on the difference between the calculated production rate and the observed change in concentration. The shaded areas show the rates of known $\Sigma RONO_2$ loss processes, and the hatched area shows the missing nitric acid source.

of tertiary $\Sigma RONO_2$ production.

While the simultaneous presence of a significant missing source of nitric acid and a missing sink of $\Sigma RONO_2$ supports the idea that $RONO_2$ to nitric acid conversion is occurring, the missing sink of $\Sigma RONO_2$ is approximately a factor of two larger than the missing source of nitric acid (Fig. 2.7, hatched area). The discrepancy between the two calculations of the $RONO_2$ hydrolysis rate could be accounted for by uncertainty in the measurements, in the calculated production rate of $\Sigma RONO_2$, or in the calculated lifetime of nitric acid. As the data from SOAS are insufficient to determine which of these interpretations is correct, we use the average of the missing nitric acid production rate and the missing $\Sigma RONO_2$ loss rate as our best estimate of the $\Sigma RONO_2$ hydrolysis rate.

Using this average, the rate of $RONO_2$ hydrolysis to produce nitric acid is 45 ppt h^{-1} between 10 am and 2 pm. When this is combined with the loss of $\Sigma RONO_2$ by deposition, 55% of the $\Sigma RONO_2$ produced lead to the permanent removal of NO_x from the atmosphere. Using the hydrolysis rate calculated from only the nitric acid budget or only the $\Sigma RONO_2$ budget changes this fraction to 35 or 75%. The remaining fraction of locally produced $\Sigma RONO_2$ is assumed to re-release NO_x back to the atmosphere through oxidation and photolysis.

Based on the lifetime and fate calculated here, locally-produced $\Sigma RONO_2$ has a lifetime to re-release of NO_x of just under 4 hours, making them part of NO_{SL}. At the same time, deposition and the rapid conversion of reactive multifunctional nitrates to nitric acid means that the formation of $\Sigma RONO_2$ leads to the significant removal of NO_{SL}, and therefore NO_x,

from the atmosphere.

Peroxy nitrates

Peroxy nitrates are produced through the association of a peroxy acyl radical with NO_2 (R2.3). While non-acyl peroxy radicals can also associate with NO_2, the product is extremely unstable and decomposes within seconds in the summertime boundary layer. Peroxy nitrates are primarily lost by thermal dissociation to form NO_2 and a peroxy acyl radical. This acyl radical can either react with NO_2 to reform a peroxy nitrate, or react with NO or HO_2 to form an acyloxy radical or a peracid. The lifetime of peroxy nitrates therefore depends on the temperature and the relative concentrations of NO_2, NO, and HO_2 (LaFranchi et al., 2009). Rate constants from Orlando and Tyndall (2012) and Atkinson et al. (2006) for the reactions of peroxy acyl nitrate and acyl peroxy radical were used to calculate the lifetime of peroxy nitrates during SOAS.

During the day, peroxy nitrates re-release NO_x on timescales of 1–2 hours and are a component of NO_{SL}. The production of peroxy nitrates therefore does not contribute to the net loss of NO_{SL}, but still affects the lifetime of NO_{SL} by adjusting the amount of NO_x available for reactions that produce $\Sigma RONO_2$ or nitric acid. At SOAS, the ratio of peroxy nitrates to NO_x is typically around 0.7 at midday.

There are other loss processes of peroxy nitrates. The reaction of OH with methacryloyl peroxy nitrate (MPAN) is rapid, but MPAN is typically a minor component of total peroxy nitrates (LaFranchi et al., 2009). The deposition rate of peroxy nitrates was not measured during SOAS, but previous measurements in a ponderosa pine forest estimate the deposition velocity to be between 0.5 and 1.3 cm s^{-1} (Wolfe et al., 2009; Min et al., 2012). Using this range of deposition velocities gives a total deposition loss rate of peroxy nitrates of 5 ± 3 ppt h^{-1} in the afternoon.

2.5 The photochemical lifetime of NO_x and NO_{SL}

The measured concentrations and calculated production and loss rates of each individual NO_z species can be combined to determine the lifetime of NO_{SL}. This lifetime depends on the distribution of NO_z between NO_{SL} and NO_{LL} and the chemical transformations between these two classes. If a 7 hour lifetime to re-release of NO_x is used as the provisional dividing line between NO_{SL} and NO_{LL}, then in the afternoon NO_{SL} was composed of NO_x, ΣPANs, and the reactive component of $\Sigma RONO_2$. As discussed earlier, both peroxy nitrates and $\Sigma RONO_2$ have lifetimes to re-release of NO_x of less than 4 hours. During the same time, NO_{LL} was composed of nitric acid and unreactive $RONO_2$. We interpret the y-intercept in the correlation between $\Sigma RONO_2$ production and concentration (Fig. 2.6) to represent a 40 ppt background of unreactive $RONO_2$, likely composed of small monofunctional nitrates. We treat all $\Sigma RONO_2$ greater than this constant background as short-lived.

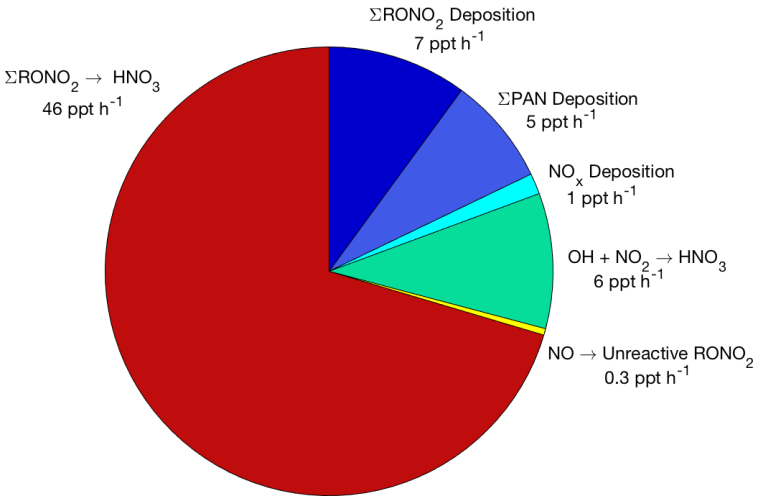

Figure 2.8: The average breakdown of NO_{SL} loss between 10 am and 2 pm during SOAS.

The lifetime of NO_{SL} can then be calculated as $\tau_{NO_{SL}} = [NO_{SL}]/\mathcal{L}(NO_{SL})$. The individual processes that lead to loss of NO_{SL} and their average value between 10 am and 2 pm during SOAS are shown in Fig. 2.8. The loss of short-lived reactive nitrogen is dominated by the hydrolysis of $\Sigma RONO_2$ to produce nitric acid. This single process accounts for 65% of the total NO_{SL} loss.

NO_{SL} is also converted to NO_{LL} during SOAS through the association of OH and NO_2 to produce nitric acid and the production of small, unreactive alkyl nitrates. The deposition of both peroxy nitrates and $\Sigma RONO_2$, as well as the uptake of NO_x by plants, also leads to the loss of NO_{SL}. Based on the deposition velocity of NO_x over vegetation measured by Breuninger et al. (2013), the rate of NO_x uptake was calculated to be approximately 1 ppt h^{-1}. A 50% uncertainty in the $\Sigma RONO_2$ hydrolysis rate, combined in quadrature with the uncertainties from the other NO_{SL} loss processes, gives the overall uncertainty in the NO_{SL} loss rate of $\pm$ 25 ppt h^{-1}.

When combined with the average concentration of NO_{SL} of 700 ppt during this same time period, the lifetime of NO_{SL}, and therefore the photochemical lifetime of NO_x, is calculated to be 11 ± 5 hours. This calculated lifetime of NO_{SL} is used as the cutoff between NO_{SL} and NO_{LL}. Changing the cutoff from our provisional value of 7 hours to 11 hours does not change the partitioning of NO_y between these two classes.

The long lifetime of NO_x calculated here is qualitatively consistent with the partitioning of NO_y during SOAS. The concentration of NO_{SL} is approximately twice as large as NO_{LL} during the afternoon (Fig. 2.2). In the absence of large fresh emissions of NO_x, this implies that the conversion of NO_{SL} to NO_{LL} must be slow, in agreement with our calculations. More quantitative calculations of the NO_x lifetime using the ratio of NO_{SL} to NO_{LL} or NO_x to NO_y have been developed for analyses of plumes (e.g., Kleinman et al., 2000; Ryerson et al., 2003) but are not adaptable to this data set.

This NO_x lifetime is longer than the lifetime of NO_x calculated in fresh plumes, where observational studies have found lifetimes of 5–8 hours (e.g., Ryerson et al., 1998; Alvarado et al., 2010; Valin et al., 2013). These studies focus solely on the chemistry of NO_x rather than NO_{SL} and recognition of the buffering effect of organic nitrates would extend the lifetimes found in these studies. In addition, the average noontime concentration of OH observed during SOAS was up to a factor of 5 lower than values typically observed in urban areas (e.g., Mao et al., 2010; Rohrer et al., 2014). Lower concentrations of OH slow the rate of atmospheric oxidation, leading to longer lifetimes of NO_x.

If lower OH and the production of NO_x from peroxy nitrates were the only differences between polluted areas and the regional background, then the lifetime of NO_x during SOAS would be significantly longer than 10 hours. However, the production of $\Sigma RONO_2$ is extremely rapid and the deposition and hydrolysis of these species accounts for the majority of the NO_x removal in this rural region. The VOC mixture present in the southeast United States leads to very high values of OH Reactivity and α, both of which enhance the production of $\Sigma RONO_2$. High concentrations of VOCs also lead to lower OH concentrations and slower production of nitric acid by reaction (R2.1). Moving from urban centers to rural or remote regions is therefore also a move from nitric acid- to $RONO_2$-dominated NO_x chemistry. Changes to our understanding of the production and fate of alkyl and multifunctional nitrates will therefore have a large impact on predictions of the lifetime of NO_x and NO_{SL}, with subsequent impacts on the concentration and distribution of NO_x across a region.

2.6 Conclusions

Measurements in a low-NO_x, high-VOC region provide new insights into the lifetime and chemistry of NO_x and NO_{SL} in rural areas. NO_{SL} is found to have an average lifetime of 11 ± 5 hours, longer than the lifetimes of NO_x observed in plume studies, which do not account for buffering by short-lived NO_z species. The long lifetime of NO_{SL} makes it relatively evenly distributed across the region and allows small inputs of NO_x to sustain the concentrations of NO_{SL} observed during SOAS.

The long daytime lifetime of NO_{SL} found here indicates that NO_x emitted on one day will persist into the night where NO_3 is often the most important oxidant (Brown and Stutz, 2012). Depending on the chemistry taking place, NO_{SL} could either be efficiently removed from the atmosphere at night, or remain in the atmosphere until the next day. To fully understand the transport and distribution of NO_x across a region the daytime chemistry of NO_x discussed here must be combined with additional analyses of the nighttime chemistry of NO_x and NO_y (e.g., Brown et al., 2009; Crowley et al., 2011; Ayres et al., 2015).

The production and loss of $\Sigma RONO_2$ are found to be the most important variables in controlling the lifetime of NO_{SL}. $\Sigma RONO_2$ was observed to have a lifetime of under 2 hours during the afternoon. This estimate is in line with many previous estimates of $\Sigma RONO_2$ lifetimes, and indicates that $\Sigma RONO_2$ is an important short-lived NO_x reservoir. Observations of both nitric acid and $\Sigma RONO_2$ during SOAS provide strong evidence that

both gas-phase oxidation to produce NO_x and particle-phase hydrolysis to produce nitric acid are important chemical loss processes for $\Sigma RONO_2$. Comparison of the nitric acid and $\Sigma RONO_2$ budgets indicate that between 30 and 70% of the alkyl and multifunctional nitrates produced are converted to nitric acid. Further laboratory and field studies are necessary to better constrain this percentage and to understand the mechanisms that control it.

The vast majority of $\Sigma RONO_2$ is formed during the oxidation of biogenic hydrocarbons, while much of the NO_x is emitted by anthropogenic activities. In this way, the formation of $RONO_2$ represents an important anthropogenic-biogenic interaction, where the oxidation of biogenic VOCs serves to remove anthropogenic pollution from the atmosphere. In rural and remote regions, the interactions between NO_y, HO_x, and VOCs are complex and bi-directional. As NO_x emissions decrease, $\Sigma RONO_2$ will likely become an even more important part of the NO_y budget, making it increasingly important that their chemistry and loss be taken into consideration when calculating the lifetime and fate of NO_x.

Chapter 3

Constraints on aerosol nitrate photolysis as a potential source of HONO and NO_x

3.1 Introduction

Nitrogen oxides ($NO_x \equiv NO + NO_2$) are a central component of atmospheric chemistry, affecting air quality, climate, and ecosystem health. The concentration of NO_x regulates the concentration of major atmospheric oxidants and controls the pathways of atmospheric oxidation. Accurate knowledge of the chemical sources and sinks of NO_x is therefore vital to understanding atmospheric oxidation and predicting how air quality will respond to changes in anthropogenic emissions or to changes in the global climate system.

On a global scale, the largest sink of NO_x is oxidation of NO_2 by OH to form HNO_3 (Stavrakou et al., 2013). In the lower troposphere, gas-phase HNO_3 is removed by wet and dry deposition, with an overall lifetime of only a couple days. Chemical removal of HNO_3 is much slower, with a lifetime to photolysis or oxidation by OH of 15–30 days in the troposphere (Dulitz et al., 2018). In remote locations, even this slow rate can be relevant and act as an important source of NO_x.

HNO_3 can also partition into aerosols, forming inorganic particle-phase nitrate (NO_3^-). For fine particles, this typically occurs via thermodynamic partitioning of ammonium nitrate between the gas and particle phases, while for coarse-mode particles, nitrate production more commonly occurs via surface reaction of gas-phase HNO_3 with sea-salt or mineral dust particles (Stelson and Seinfeld, 1982; Dentener et al., 1996; McNaughton et al., 2009). Dry deposition is slow for most particles, but particle-phase nitrate can be lost by wet deposition, or it can be lost by re-partitioning between phases as gas-phase HNO_3 is lost by deposition (e.g., Pusede et al., 2016). Throughout this chapter, we use HNO_3 to refer to the sum of gas-phase nitric acid and inorganic particle-phase nitrate.

Previous studies examining the chemical evolution of NO_x and HNO_3 in the absence of

fresh emissions have found varying results. While Bertram et al. (2007) and Neuman et al. (2006) found good agreement between observations and models, several other studies (e.g., Hauglustaine et al., 1996; Gao et al., 1999; Perkins et al., 2001) reported observations that could not be explained with known chemistry. To reconcile models and observations, multiple pathways for the conversion of HNO_3 to NO_x or HONO have been proposed, a process termed re-noxification. Various re-noxification pathways have been proposed in areas ranging from the upper troposphere (e.g., Chatfield, 1994; Gao et al., 1999; Perkins et al., 2001), the marine boundary layer (e.g., Hauglustaine et al., 1996; Reed et al., 2017; Ye et al., 2017a; Kasibhatla et al., 2018), rural forests (e.g., Zhou et al., 2003, 2011), and areas of continental outflow (e.g., Ye et al., 2016). Recently, several of these studies have suggested that HNO_3 is rapidly photolyzed in aerosols to form NO_2 or HONO, at a rate between 10 and 300 times faster than the rate of gas-phase HNO_3 photolysis (Ye et al., 2016, 2017a,b; Reed et al., 2017; Kasibhatla et al., 2018), and it is this process that we investigate here.

Most of the previous studies of this process were primarily focused on the potential for particle-phase nitrate photolysis to explain observations of HONO. To complement the approach of previous studies, we examine the consequences of rapid nitrate photolysis on concentrations of NO_x and HNO_3. Because HONO is itself rapidly lost by photolysis to produce NO, the effect of nitrate photolysis on NO_x chemistry does not depend on whether HONO or NO_x is the direct product. Past studies investigating aerosol nitrate photolysis have reported their results as an enhancement factor (EF), relating the rate of nitric acid photolysis in the particle phase to that in the gas-phase (3.1), and we follow that convention here.

$$j_{p\mathrm{HNO_3}} = EF \cdot j_{g\mathrm{HNO_3}} \tag{3.1}$$

While mechanistic studies of aerosol nitrate photolysis are limited, investigations of photolysis in solution or on surfaces help explain how large enhancements of aerosol-phase nitrate photolysis could occur. In solution, the cross section of NO_3^- is enhanced by a factor of 25 at 310 nm over that of gas-phase HNO_3, likely due to symmetry-breaking of the NO_3^- ion caused by hydration (Svoboda et al., 2013). At the same time, the quantum yield of NO_3^- is reduced from near unity in the gas-phase to 0.01 in bulk solution, likely due to recombination of the photolysis products in the solvent cage (Warneck and Wurzinger, 1988; Nissenson et al., 2010).

In contrast, nitric acid or nitrate adsorbed on surfaces is not fully enclosed in a solvent cage and is therefore expected to have an enhanced cross section without a significant decrease in the quantum yield. Experimental results have confirmed that the cross section of HNO_3 can be enhanced by up to a factor of 1000 at 308–310 nm when adsorbed onto the surface of aluminum or ice, while the quantum yield of surface-adsorbed HNO_3 on the same surfaces was 0.60 or greater (Zhu et al., 2008, 2010). Thus, if a significant portion of aerosol nitrate is located on or near the aerosol surface, where its quantum yield remains high, then it is plausible that its photolysis could be enhanced multiple orders of magnitude over that of gas-phase nitric acid. The likely role of surface chemistry further suggests that physical properties of the aerosols, including size distribution and viscosity, could have a significant

impact on the effective nitrate photolysis rate.

With a sufficiently fast rate, nitrate photolysis could have major impacts on our understanding of tropospheric NO_x chemistry. At the upper end of the proposed photolysis rates, loss of HNO_3 via particle-phase photolysis would be significantly faster than dry deposition, greatly extending the lifetimes of both NO_x and total reactive nitrogen (NO_y). If the lifetime of NO_x is significantly longer than currently thought, it would suggest major gaps in our understanding of NO_x emissions or NO_x chemistry, and could in turn change our understanding of O_3 production and the most effective ways to reduce air pollution.

The ratio of NO_x to HNO_3, which we refer to as R_{obs}, provides crucial information about the chemistry of HNO_3. R_{obs} has been used in past studies to investigate both the production and loss of HNO_3 (e.g., Chatfield, 1994; Hauglustaine et al., 1996; Gao et al., 1999; Perkins et al., 2001; Neuman et al., 2006). As a ratio of two concentrations, R_{obs} is relatively unaffected by the concentration of NO_y or the total volume of emissions encountered. By eliminating the effects of emissions and dilution, analysis of R_{obs}, rather than absolute HNO_3 concentration, helps isolate the effects of HNO_3 production and loss.

In this chapter, we present new constraints on the rate of particulate nitrate photolysis, based on observations of NO_x and HNO_3 collected onboard the NASA DC-8 aircraft during the KORUS-AQ field campaign. Using R_{obs} to evaluate HNO_3 production and loss, we demonstrate that the fastest proposed nitrate photolysis rates ($EF \geq 50$) are inconsistent with our current understanding of nitric acid production. Small to moderate enhancement of particulate nitrate photolysis ($1 \leq EF \leq 30$) is found to be most consistent with the observations. Comparisons of the data from KORUS-AQ with several other airborne observations show that the results from KORUS-AQ are not anomalous, and confirm that particle-phase nitrate photolysis is at most a minor HNO_3 loss pathway on a global scale. However, we cannot eliminate the possibility that there are periods or environments where particulate nitrate photolysis is extremely rapid.

3.2 Materials and methods

Observations

Primary observations were taken onboard the NASA DC-8 aircraft as part of the Korea-United States Air Quality Study (KORUS-AQ) during May and June 2016. The DC-8 component of KORUS-AQ consisted of 20 science flights based out of Osan Air Force Base, located approximately 50 km south of Seoul. Crucial observations used in this analysis include NO_x, gas-phase HNO_3, particle-phase nitrate, hydroxyl radical (OH), a wide range of volatile organic compounds (VOCs), and the spectrally-resolved actinic flux (used to calculate the gas-phase HNO_3 photolysis rate). Throughout the analysis, we use measurements of particle-phase nitrate from bulk aerosols collected onto filters and analyzed by ion chromatography. A full list of species used in this analysis and the techniques used to measure them are listed in Table 3.1.

Table 3.1: Measurements from KORUS-AQ used in this analysis.

Species	Technique	Principal Investigator	Reference
NO_2, $\Sigma RONO_2$, $\Sigma PANs$	TD-LIF[a]	R. Cohen	Day et al. (2002)
NO, NO_y, O_3	CL[b]	A. Weinheimer	Walega et al. (1991)
HNO_3, gas-phase	CIMS[c]	P. Wennberg	Crounse et al. (2006)
HNO_3, particle-phase	Filter-IC[d]	J. Dibb	Dibb et al. (1999)
OH, HO_2	FAGE[e]	W. Brune	Faloona et al. (2004)
VOCs	WAS-GC[f]	D. Blake	Blake et al. (2003a)
Oxygenated VOCs	PTR-MS[g]	A. Wisthaler	Wisthaler et al. (2002)
HCHO	DFGAS [h]	A. Fried	Richter et al. (2015)
CO, CH_4	TDLAS[i]	G. Diskin	Sachse et al. (1987)
$j_{g\mathrm{HNO_3}}$	CAFS[j]	S. Hall	Shetter and Müller (1999)

[a]Thermal Dissociation Laser-Induced Fluorescence; [b]Chemiluminescence; [c]Chemical-Ionization Mass Spectrometry; [d]Ion Chromatography; [e]Fluorescence Assay by Gas Expansion; [f]Whole Air Samples, followed by Gas Chromatography; [g]Proton Transfer Reaction Mass Spectrometry; [h]Difference Frequency Generation Absorption Spectroscopy; [i]Tunable Diode Laser Absorption Spectroscopy; [j]CCD Actinic Flux Spectroradiometry.

Additional data were obtained from the NASA LaRC Airborne Science Data for Atmospheric Composition website, from a set of six field deployments on the DC-8: INTEX-NA, MILAGRO, INTEX-B, ARCTAS-B, DC3, and SEAC4RS. A map of all seven deployments is shown in Fig. 3.1. Restricting our analysis to a single platform allows us to use many of the same instruments across all seven campaigns. All of the campaigns include measurements of NO_x, HNO_3 in the gas and particle phase, $\Sigma RONO_2$, peroxy acyl nitrates, and VOCs; all but one (SEAC4RS) include measurements of OH, although measurements of OH from INTEX-NA, MILAGRO, and INTEX-B include an interference from internally generated OH that can be important in some low-altitude environments (Mao et al., 2012). NO on previous campaigns was always measured by chemiluminescence, but the instrument and group responsible was not consistent. On INTEX-NA, NO was measured by the Brune group from Penn State, on INTEX-B by the Huey group from Georgia Tech, and on DC3 and SEAC4RS by the Ryerson group from NOAA ESRL.

Airmass age and plume evolution

To distinguish between airmasses with fresh emissions and those that are highly aged, we use the ratio of 2-butyl nitrate to *n*-butane (2BN/nB) as a chemical clock (Bertman et al., 1995; Perring et al., 2010). 2-butyl nitrate has very few direct emissions, rather it is produced almost exclusively by the OH oxidation of *n*-butane and is lost by photolysis and oxidation.

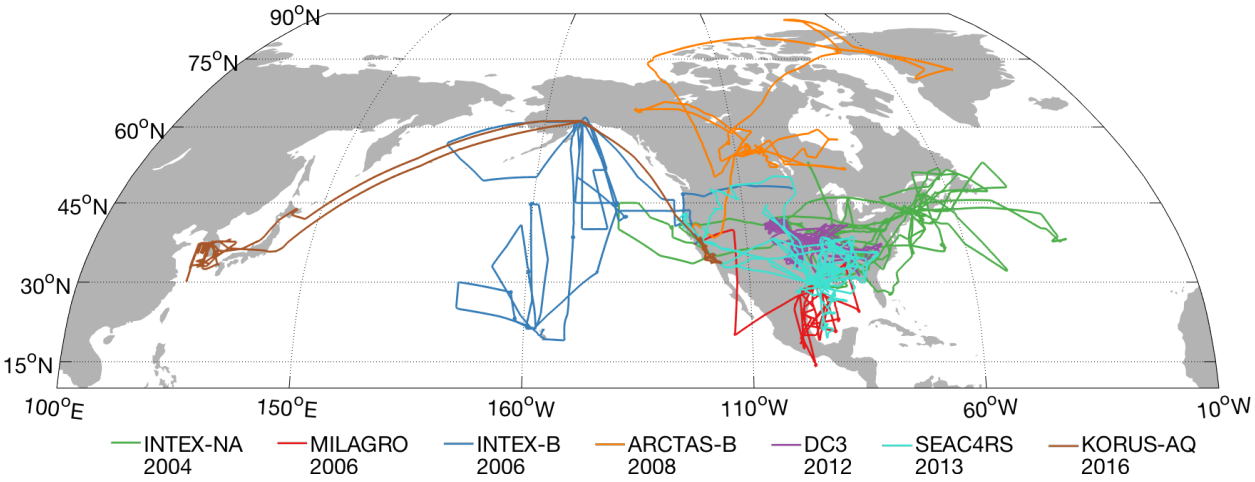

Figure 3.1: Map of measurements taken on all seven campaigns used in the extended analysis. The first phase of ARCTAS deployment (ARCTAS-A) was not included because conditions in the springtime Arctic (low light, high halogens) make it difficult to compare against other spring/summertime measurements.

2-butyl nitrate has a lifetime of weeks in the troposphere, compared to a lifetime of 1–2 days for *n*-butane (Clemitshaw et al., 1997). The 2BN/nB ratio is therefore expected to increase monotonically with airmass age, and can be used to sort airmasses from the freshest emissions to the most highly aged.

Box modeling

Box modeling was used in two ways to compare observations against predictions with different EF's. First, box modeling was used in a limited way to estimate instantaneous production and loss of NO_x and HNO_3 via routes that are not fully constrained from measurements. Secondly, a more comprehensive box model was used to study the evolution of advected plumes over the Yellow Sea. The framework and kinetics used for both applications are described here, while details specific to each application are described in their respective sections.

Simulations were run using the Framework for 0-Dimensional Atmospheric Modeling (F0AM), with chemical kinetics from the Master Chemical Mechanism v3.3.1 (MCM) (Wolfe et al., 2016; Jenkin et al., 2015). Accurate modeling of R_{obs} requires inclusion of all the HNO_3 sources present in the atmosphere, including several multiphase mechanisms not included in the MCM. The hydrolysis of alkyl and multifunctional nitrates ($\Sigma RONO_2$) on aerosols produces HNO_3 and in some forested areas has been found to be the largest source of HNO_3 (Browne et al., 2013; Romer et al., 2016). In the remote marine boundary layer, hydrolysis of halogen nitrates ($XONO_2$ = $BrONO_2$, $ClONO_2$, or $IONO_2$) on aerosols can be major HNO_3 sources (Sherwen et al., 2016). Finally, formation and hydrolysis of N_2O_5 can produce HNO_3,

often the largest HNO_3 source at night (Brown and Stutz, 2012). Modifications to the MCM to include these mechanisms are described below. To include the uncertainty in many of the parameters, multiple simulations were run testing a range of values for each parameter. The values listed below are the median or best-guess estimates for these parameters. A full list of parameters specified or added to F0AM and their uncertainty ranges is included in Tables 3A.1–3A.4 of the appendix to this chapter.

Inorganic halogen chemistry was added to the model following the scheme described in Sherwen et al. (2016). Total amounts of reactive chlorine, bromine, and iodine (Cl_y, Br_y, and I_y) were specified and allowed to partition freely between different halogen species. Average total concentrations of Cl_y, Br_y, and I_y were set at 7 ppt, 2.5 ppt, and 2.5 ppt respectively, based on averages from the modeling studies of Schmidt et al. (2016), Sherwen et al. (2016), and Hossaini et al. (2016).

Multiphase chemistry was added to the model through reactive uptake reactions onto a fixed aerosol surface area concentration. A reactive uptake parameter (γ) of 0.005 was applied to all $RONO_2$ with a tertiary nitrate group, equal to that assumed by Fisher et al. (2016) for isoprene hydroxy nitrates. When using observed $\Sigma RONO_2$ concentrations, which are not isomer specific, a γ of 0.002 was applied to all nitrates. A γ of 0.10 was used for all three $XONO_2$ species, in between the laboratory values for uptake onto aqueous solution (0.03, Deiber et al., 2004) and uptake onto sulfate aerosol (0.80, Hanson et al., 1996). A constant γ value of 0.014 was included for N_2O_5 chemistry, in the middle of the range found by McDuffie et al. (2018).

All the modeling studies were focused on plumes advected over the ocean, and therefore no emissions were included in the model. Dilution was included as a first-order decay of model concentrations towards a prescribed background concentration. The average dilution rate was set to 1.7×10^{-5} s^{-1}, based on the rate of decrease of CO with increasing 2BN/nB ratio observed during KORUS-AQ, following the methods of Perring et al. (2010) and Ebben et al. (2017). The average daytime boundary-layer deposition velocity for gas-phase HNO_3 used in the model is 2 cm s^{-1} (Ganzeveld and Lelieveld, 1995; Nguyen et al., 2015). The effective boundary layer height was set to 1300 m, based on observed temperature profiles over the Yellow Sea.

3.3 NO_x and HNO_3 chemistry during KORUS-AQ

Boundary layer measurements during KORUS-AQ typically found high concentrations of HNO_3 and NO_x, although there was significant variation in the concentration of both species (Fig. 3.2). To gain greater sensitivity to the chemical loss processes of HNO_3, we restrict our analysis to observations in the boundary layer over the Yellow Sea. The air over the Yellow Sea was highly aged and contained high concentrations of NO_y, averaging 6 ± 2 ppb. Together, these properties limit the chemical production of HNO_3 and emphasize the loss processes of HNO_3.

Boundary layer observations over the Yellow Sea are shown as the blue bars in Fig. 3.2. R_{obs} was typically extremely low, and was significantly lower than the ratios observed in the free troposphere (red bars in Fig. 3.2), indicating that boundary-layer chemistry, and not dilution, is controlling the ratio.

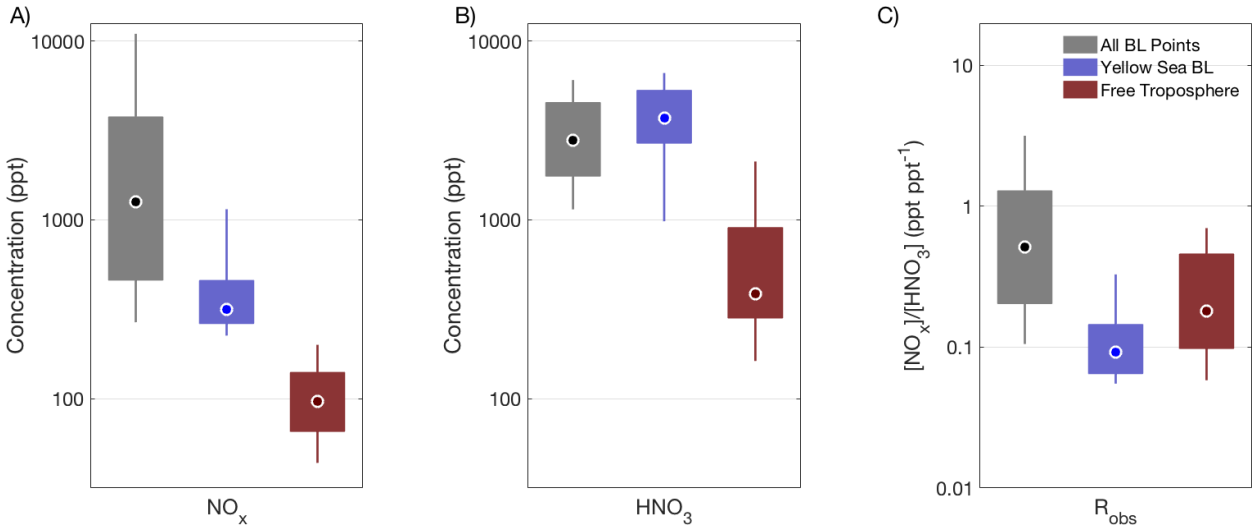

Figure 3.2: Distribution of NO_x, HNO_3 (gas + particle), and R_{obs} in three different regions during KORUS-AQ: all points in the boundary layer (gray bars), points in the boundary layer over the Yellow Sea (blue bars) and all points in the lower free troposphere (between 2 and 4 km, red bars). In each bar, the black dot shows the median value, the thick bar the inter-quartile range, and the thin line the 10^{th}-90^{th} percentiles.

To examine the compatibility of the observations with different proposed EF's, we compare R_{obs} with the calculated far-field ratios (R_{FF}), the predicted ratio of NO_x to HNO_3 in highly aged air. Because HNO_3 is not directly emitted to the atmosphere but is a product of NO_x oxidation, in an isolated plume R_{obs} starts at a maximum value and decreases to approach a far-field ratio set by the relative forward and backward conversion rates between NO_x and HNO_3. This behavior has been seen in past studies of NO_x chemistry in the outflow of plumes, which have found that R_{obs} decreases consistently as plumes evolves (e.g., Hauglustaine et al., 1996; Bertram et al., 2007; Pérez et al., 2009; Perring et al., 2010; Nault et al., 2016; Ebben et al., 2017). None of these studies observed an increase in R_{obs} with airmass age. Therefore, R_{obs} is expected to always be greater than or equal to R_{FF}.

R_{FF} can be calculated algebraically from the effective first-order chemistry of NO_x and HNO_3, described by the system of differential equations (3.2)–(3.3). The eigenvector of the system with the largest associated eigenvalue gives the predicted ratio of NO_x to HNO_3 in

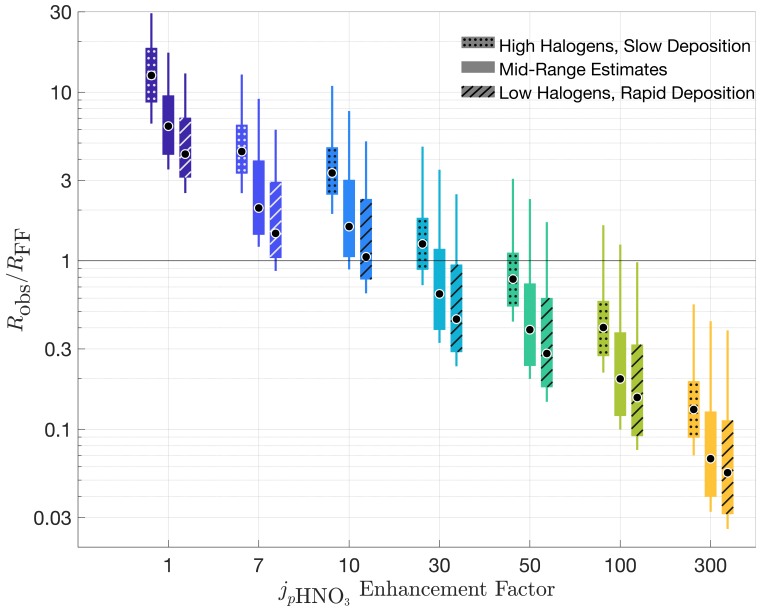

Figure 3.3: Comparison of R_{obs} to R_{FF} in the boundary layer over the Yellow Sea. Each individual bar shows a boxplot of the ratio of ratios, calculated using in situ data for every observation over the Yellow Sea. For every value of EF tested, R_{FF} was calculated 3 different ways, using different assumptions for the production of nitric acid via halogen chemistry and the deposition velocity of nitric acid, corresponding to the range of values in Table 3A.1. In each bar, the black dot shows the median value, the thick bar the inter-quartile range, and the thin line the 10^{th}–90^{th} percentiles. The boxplots are spaced equally and position along the x-axis does not correspond to EF on either a linear or a log scale.

infinitely aged air.

$$\frac{d[NO_x]}{dt} = -k_{forward}[NO_x] + k_{backward}[HNO_3] - k_{removal}[NO_x] \quad (3.2)$$

$$\frac{d[HNO_3]}{dt} = k_{forward}[NO_x] - k_{backward}[HNO_3] - k_{dep}[HNO_3] \quad (3.3)$$

The effective rate constants in these equations were calculated using observations from the DC-8, supplemented by box modeling of unmeasured species, using the parameters specified in Table 3A.1. For each observation over the Yellow Sea, an independent box model simulation was run to calculate the steady-state concentration of RO_2 radicals and of halogen nitrates.

$k_{forward}$, the effective rate constant for conversion of NO_x into HNO_3, includes the oxidation of NO_2 by OH and the production of HNO_3 by $RONO_2$, $XONO_2$, and N_2O_5 hydrolysis. $k_{forward}$ was calculated using in situ observations of OH, NO_2, $\Sigma RONO_2$, and aerosol surface area, and modeled concentrations of $XONO_2$ and N_2O_5 The backwards conversion rate,

k_{backward}, includes contributions from gas-phase HNO_3 photolysis and oxidation and particle-phase photolysis. k_{backward} uses measured values of HNO_3, OH, and $j_{g\text{HNO}_3}$, and different assumed EF values. The loss of HNO_3 by deposition, k_{dep} was calculated using a deposition rate of 2 cm s^{-1} for gas-phase nitric acid and a rate of 0.2 cm s^{-1} for particle-phase nitrate, weighted by the fraction of HNO_3 in each phase. k_{removal} represents the combined effects of other routes for NO_x removal, including oxidation to PAN and $RONO_2$, and was calculated based on the modeled RO_2 radical distribution.

Figure 3.3 shows the ratio of ratios $R_{\text{obs}}/R_{\text{FF}}$ for several different values of the assumed EF. In addition to our best-guess estimates, Fig. 3.3 also shows sensitivity tests using high- and low-end estimates of halogen concentrations and HNO_3 deposition velocity, listed in Table 3A.1. Because observed air masses may not yet have reached far-field conditions, $R_{\text{obs}}/R_{\text{FF}}$ is expected to always be greater than or equal to 1, setting an upper limit on the maximum EF compatible with the observations. Using our best-guess estimates for the unknown parameters, an EF of up to 10 is consistent with the observations. With more generous assumptions, an EF of up to 30 is plausible. However, when an EF of 50 or greater is used, over 75% of the R_{FF}'s are greater than the observed ratios and are therefore incompatible with the observations.

3.4 Lagrangian modeling of KORUS-AQ observations

To complement the analysis shown in Fig. 3.3, and to confirm that $R_{\text{obs}}/R_{\text{FF}} < 1$ could not be produced by changing chemistry in an evolving plume, we also ran a series of Lagrangian simulations examining the evolution of NO_y over the Yellow Sea. The effect of enhanced particle-phase HNO_3 photolysis was tested by comparing the results from simulation runs with 7 different EF's: 1, 7, 10, 30, 50, 100, and 300.

Due to significant uncertainties in many of the input parameters, random sampling was used to test the effects of different chemical parameters (Table 3A.2), initial conditions (Table 3A.3), and background concentrations (Table 3A.4). Lacking detailed atmospheric measurements over China, we use as initial conditions the 5% of points observed during KORUS-AQ with the lowest 2BN/nB ratios. A random point from these observations was selected independently for each simulation, and the measured concentrations at that point were used as initial conditions for that run. Similarly, background concentrations were taken as a random sample from observations in the lower free troposphere (2–4 km) over the Yellow Sea. Gas-particle partitioning of HNO_3 was included as a fixed parameter that we varied based on the observations. During KORUS-AQ, the gas-phase fraction of HNO_3 ($f_g = \frac{g\text{HNO}_3}{g\text{HNO}_3 + p\text{HNO}_3}$) in the boundary layer ranged from 0.3 to 0.7 (interquartile range), with a median of 0.51. For parameters that were not measured (e.g., $[Br_y]$), a plausible range of values was constructed with the same best-guess estimate as used in the calculation of R_{FF}, and a random value from within that distribution was chosen independently for each simulation run.

100 different simulations were run for each EF, and each simulation was run for 10 days. To ensure that the comparison of model results to observations is not biased by different airmass ages, only a portion of each model simulation was included. To match the distribution of modeled and observed airmass ages, a random sample of 100 2BN/nB ratios was generated that matched the observed distribution of 2BN/nB over the Yellow Sea; then, for each of the model runs, only the timesteps with the modeled 2BN/nB ratios that most closely matched the random sample were selected. This gives a sub-sample of each model run with nearly the same distribution of airmass ages as those observed over the Yellow Sea. The sub-sample of each model run was further limited to daylight hours (solar zenith angle $\leq 45°$), to match the conditions when the DC-8 sampled air over the Yellow Sea.

The selected model points from each of the 100 different simulations for each EF were aggregated, and then compared primarily with R_{obs} (Fig. 3.4A), as well as with concentrations of NO_x, HNO_3, ΣPANs, and OH (Fig. 3.4B–E). Model results and observations are presented as probability distributions, with the median highlighted as a circle (modeled) or a diamond (observed). The modeled distribution reflects both variation in the initial and background concentrations used, as well as uncertainty in the unmeasured model parameters.

The model runs with the lowest EF's (1–10) are found to most closely reproduce R_{obs}. The overall spread in modeled R is greater than that observed over the Yellow Sea, suggesting that the range of model parameters used is broader than that encountered in reality. The model runs with higher EF's (50–300) cannot reproduce values of R_{obs} of 0.06 or less, and at the highest EF values, many of the model runs predict R values of 0.3–1, values almost never observed over the Yellow Sea during KORUS-AQ. For a given EF, the spread in modeled NO_x to HNO_3 ratios was mostly explained by variation in parameters that controlled either the physical loss of HNO_3 or the gross production rate of HO_x radicals. This includes the background concentration and deposition velocity of HNO_3, relative humidity, temperature, and background O_3 concentration.

Perhaps surprisingly, the increase in modeled R with increasing EF is not due to changes in the concentration of HNO_3 but instead is due to changes in NO_x (Fig. 3.4B–C). The median concentration of HNO_3 shows almost no change with increasing EF, indicating that the concentration of HNO_3 is controlled in large part by dilution and deposition rather than chemistry.

The concentration of NO_x is much more sensitive to EF, likely reflecting the dominance of chemical processes to the NO_x budget. The model most closely reproduces the observed NO_x distribution at low EF's, but generally underestimates NO_x and overestimates PAN, indicating difficulties in the representation of PAN chemistry (Fig. 3.4B,D). Higher EF's are also associated with greater concentrations of OH, due to increased HO_x cycling by NO (Fig. 3.4E).

Based on the results of Fig. 3.4, the observations over the Yellow Sea can be most accurately reproduced with low EF's, of 1–30. As the model does not take into account wet deposition or the effects of enhanced aerosol nitrate photolysis on background HNO_3 concentrations, an EF of 30 represents a likely upper limit to the true enhancement factor.

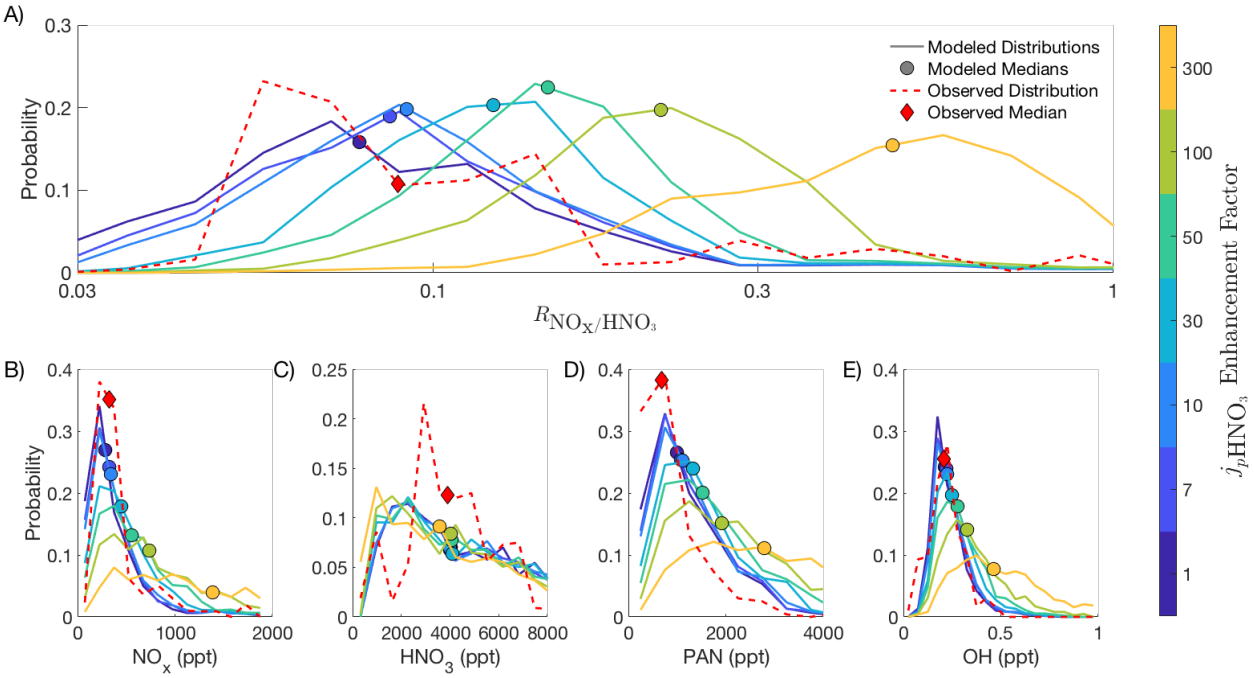

Figure 3.4: Probability distribution functions of R_{obs}, NO_x, HNO_3, ΣPANs, and OH from observations over the Yellow Sea and comparison with Lagrangian plume models using different assumed EF's.

3.5 Comparison of KORUS-AQ to other measurements

To examine whether the results from KORUS-AQ are representative, we extend the analysis of R_{obs}/R_{FF} to six additional airborne campaigns conducted over the past 15 years on the NASA DC-8. In order to focus the analysis on airmasses where HNO_3 loss is most important, we only include observations of highly aged air, which we define as points with 2BN/nB greater than 0.06. The observations were further limited to the lowest 1.3 km above ground level.

Combined results from all seven campaigns are shown in Fig. 3.5. The top panel shows the distribution of R_{obs} found in highly aged air. The bottom panel extends the analysis of Fig. 3.3 and presents the results for the case where $EF = 10$ and using our best-guess assumptions about deposition and heterogeneous chemistry (Table 3A.1). R_{FF} for SEAC4RS was calculated using a constant OH concentration of 0.18 ppt. The results from KORUS-AQ are generally in line with those from other campaigns, although there is significant variation. At $EF = 10$, INTEX-NA, MILAGRO, INTEX-B, and KORUS-AQ, all have a 25th percentile of R_{obs}/R_{FF} close to 1, while ARCTAS, DC3, and SEAC4RS have a 25th percentile R_{obs}/R_{FF} of 2–4.

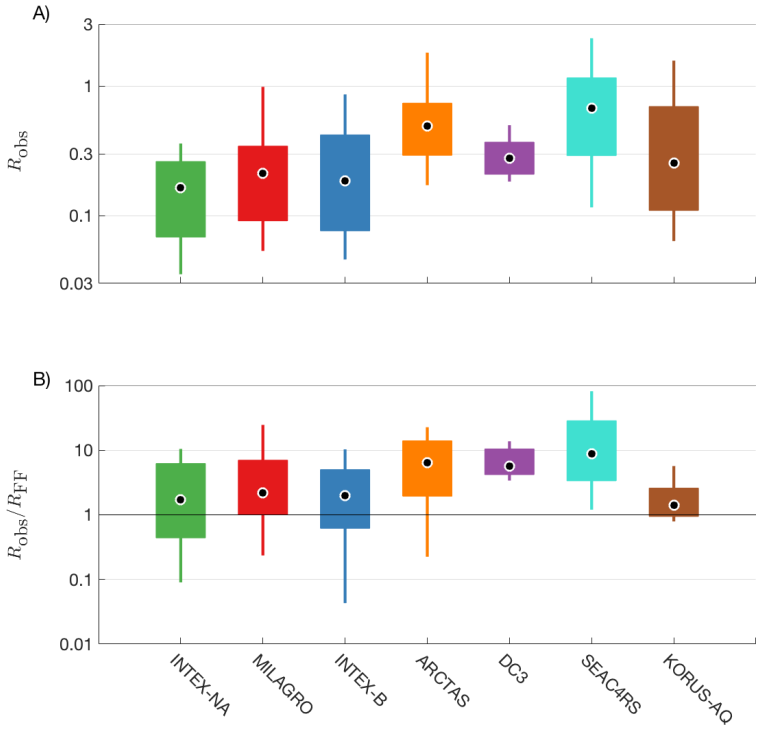

Figure 3.5: Analysis from KORUS-AQ extended to six additional campaign deployments. Panel A shows the observed far-field ratios of NO_x/HNO_3; Panel B shows the the ratio of ratios R_{obs}/R_{FF}, calculated assuming $EF = 10$ and $v_{dep,\ HNO_3} = 2$ cm s^{-1}.

One possible explanation for the variety in R_{obs}/R_{FF} is that there is significant variation in the rate of particulate nitrate photolysis between different environments. Previous studies of HNO_3 photolysis on surfaces and in particles collected on filters have also found significant variability in the reported photolysis rates (Ndour et al., 2009; Baergen and Donaldson, 2013; Ye et al., 2017b). These studies found, among other factors, that the rate of nitrate photolysis depends significantly on the total concentration of particulate nitrate (Ye et al., 2017b), the presence of mineral dust aerosols (Ndour et al., 2009), and relative humidity (Ndour et al., 2009).

The wide range of environments sampled over seven field deployments provide an opportunity to search for these expected behaviors in ambient data. Figure 3.6 plots R_{obs} in highly aged airmasses for all deployments as a function of NO_y, Ca^{2+}, and relative humidity (RH). NO_y is used as a proxy for nitrate loading that is not directly used in the calculation of R_{obs}. Particle-phase Ca^{2+}, measured by the same filter technique as aerosol nitrate, is used as a proxy for the presence of mineral dust. All other factors being equal, an increase in nitrate photolysis will cause increased HNO_3 to NO_x conversion, leading to higher values of R_{obs}. As shown in Fig. 3.6, this is not observed for any of the three parameters. Decreasing NO_y and increasing RH are associated with a slight decrease in R_{obs}, reverse of what is

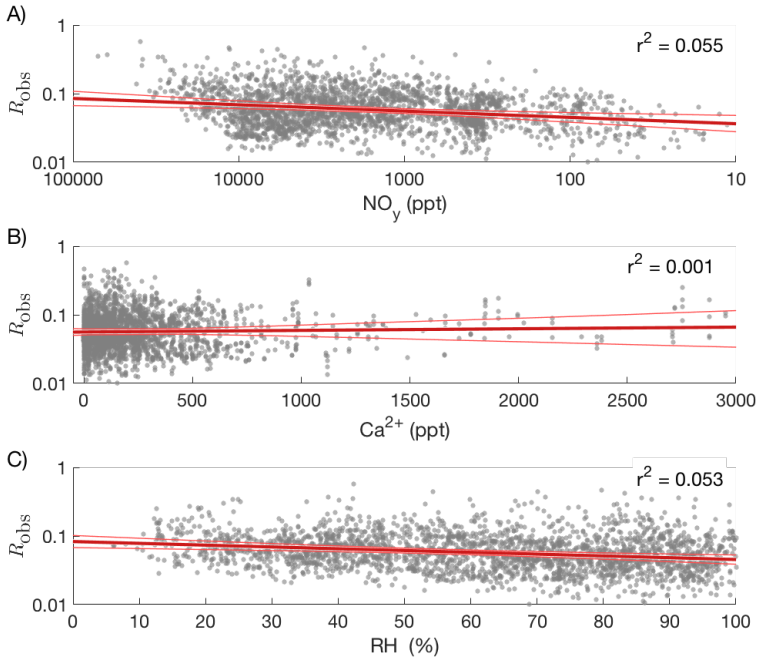

Figure 3.6: R_{obs} in highly-aged airmasses as a function of total NO_y (Panel A), Ca^{2+} (Panel B), and relative humidity (Panel C). Note the reversed x-axis in Panel A, so that moving to the right on all panels is expected to correspond to an increase in nitrate photolysis rate and therefore an increase in R_{obs}. The thick red line represents a linear fit to all data points; the thin red lines show the error in the fit calculated by bootstrap sampling.

expected based on Ye et al. (2017b) and Ndour et al. (2009), and Ca^{2+} shows no relation to R_{obs}. Changing whether these variables were treated on a linear or log scale, or including the effects of airmass age, did not greatly affect the trend of any of these variables with R_{obs}. However, without direct measurements of either the nitrate photolysis rate or HONO concentration, our power to find short periods of rapid HNO_3 photolysis is limited.

3.6 Discussion and conclusions

The observed NO_x/HNO_3 ratios are inconsistent with the hypothesis that HNO_3 undergoes photolysis 50–300 times faster in the particle phase than in the gas-phase, unless there is a major source of HNO_3 not represented in our calculations. This result is consistent across seven different sampling campaigns. Using our best guess about the deposition velocity of HNO_3 and the contribution of unmeasured halogens to HNO_3 production, an enhancement factor of up to 10 is consistent with R_{obs} measured over the Yellow Sea. Using more generous assumptions for these parameters, an enhancement factor of up to 30 is consistent. Because these calculations compare observed NO_x to HNO_3 ratios with those predicted in infinitely

aged air and do not take into account wet deposition, these EF's are an upper limit to the true average photolysis rate. While particle-phase nitrate photolysis was the primary focus of this analysis, these results are likely generalizable, and suggest an upper limit to the average daytime first-order re-noxification rate of inorganic aerosol nitrate of 1.4×10^{-6} s^{-1} – 4.1×10^{-6} s^{-1}.

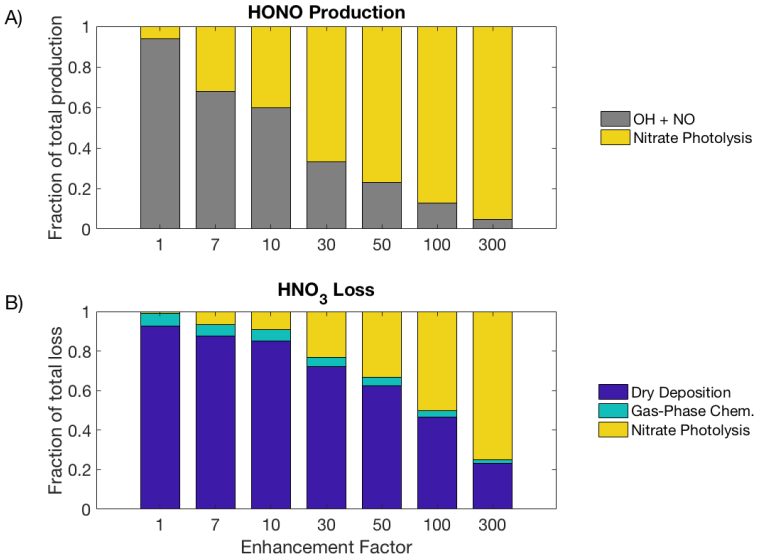

Figure 3.7: Effect of different particulate nitrate photolysis rates on the production of HONO (Panel A) and the loss of HNO_3 (Panel B), shown as a stacked bar graph. Each segment corresponds to the average fraction of total production or loss caused by a single pathway. Chemical rates were calculated using the average of all observations from all seven campaigns in the boundary layer in highly aged air, using the best-guess parameters in Table 3A.1.

Even moderately rapid nitrate photolysis could explain a significant fraction of the unexplained NO_x and HONO source in some remote regions. Figure 3.7 shows the effect of different assumed EF's on the HONO and HNO_3 budgets. At $EF = 10$, nitrate photolysis would account for an average of 40% of total HONO production, but only 10% of HNO_3 loss, indicating that moderate rates of nitrate photolysis would have a much larger effect on the predicted HONO concentrations than the predicted HNO_3 concentrations. Under these conditions, the lifetime of HNO_3 to chemical removal would decrease from 460 h without aerosol nitrate photolysis to 106 h when $EF = 10$. While this is a significantly shorter lifetime to chemical removal of HNO_3 than previously thought, it is still much longer than the lifetime of HNO_3 to removal by deposition. By turning aerosol nitrate into a source of NO_x, moderate EF's could also help resolve discrepancies between modeled and observed ratios of NO_x to HNO_3 in the remote atmosphere.

The wide range of measured and inferred rates of nitrate photolysis and the disagreement

between studies considering the budget of HONO and studies considering the budget of HNO_3 highlight the continued uncertainty in the chemistry of HONO and HNO_3. At the moment, we do not find evidence that particle-phase HNO_3 photolysis is extremely rapid, suggesting that if regional or global modeling studies include this pathway in their mechanisms, they should use an enhancement factor of 30 or less. On a global scale, nitrate photolysis is significantly slower than wet and dry deposition, making re-noxification pathways at most a minor HNO_3 loss process. While even moderate enhancements of particle nitrate photolysis could help explain observations of HONO in the remote troposphere, the effects of nitrate photolysis on ozone and NO_x are likely to be smaller than recently proposed.

Appendix 3A Parameters used in box model calculations

Table 3A.1: Parameters used in the calculation of R_{FF}.

Parameter	Low-End	Best-Guess	High-End
Cl_y (ppt)	4.0	7.0	10.0
Br_y (ppt)	1.2	2.5	4.5
I_y (ppt)	2.0	2.5	4.4
γ_{ClONO_2}	0.01	0.10	0.30
γ_{BrONO_2}	0.02	0.10	0.80
γ_{IONO_2}	0.02	0.10	0.80
γ_{RONO_2}	0.001	0.002	0.010
MW_{RONO_2} (kg)	0.120	0.120	0.120
$v_{dep,\,HNO_3}$ (cm s^{-1})[a]	1	2	4

[a] Gas-phase only, daytime average.

Table 3A.2: Parameters used for Lagrangian plume modeling. Median values chosen to match best-guess estimates in the calculation of R_{FF}. The 5^{th} and 95^{th} percentiles were set to best match the low-end and high-end estimates using either a normal or a log-normal distribution.

Parameter	Median Value	5^{th}–95^{th} percentiles
Pressure (mbar)	960	880–990
Temperature (K)	291	287–296
Relative humidity (%)	47	21–80
Altitude (km)	0.46	0.16–1.2
Latitude (°N)	20	10–30
HNO_3 gas-phase fraction	0.51	0.12–0.88
Aerosol surface area (μm^2 cm^{-3})	38	10–134
k_{dil} (s^{-1})	1.7e-05	1.1e-05–2.3e-05
$v_{\mathrm{dep,\,HNO_3}}$ (cm s^{-1})[a]	2.0	1.1–4.0
$\gamma_{\mathrm{ClONO_2}}$	0.10	0.017–0.60
$\gamma_{\mathrm{BrONO_2}}$	0.10	0.015–0.68
$\gamma_{\mathrm{IONO_2}}$	0.10	0.015–0.68
$\gamma_{\mathrm{RONO_2}}$	0.005	0.003–0.009
$\gamma_{\mathrm{N_2O_5}}$	0.014	0.007–0.039
Br_y (ppt)	2.5	1.3–5.0
Cl_y (ppt)	7.0	4.3–11.3
I_y (ppt)	2.5	1.7–3.8

[a] Gas-phase only, daytime average.

Table 3A.3: Initial concentrations used for Lagrangian plume modeling.

Species	Median Concentration	5^{th}–95^{th} percentiles
O_3 (ppb)	33	6–77
NO (ppb)	18	4–56
NO_2 (ppb)	15	3–42
HNO_3 (ppb)	4.6	1.1–13
PAN (ppb)	2.1	0.7–5.1
Methane (ppb)	2050	1920–2240
CO (ppb)	320	180–540
Ethane (ppb)	3.5	2.0–7.2
Ethene (ppb)	1.1	0.34–19
Propane (ppb)	2.9	1.1–15
Propene (ppb)	0.21	0.05–5.5
n-Butane (ppb)	1.5	0.5–5.6
2-Butyl nitrate (ppb)	0.026	0.011–0.072
n-Pentane (ppb)	0.69	0.18–2.7
n-Hexane (ppb)	0.37	0.07–5.7
Toluene (ppb)	1.8	0.32–6.3
m-Xylene (ppb)	0.55	0.14–2.4
Isoprene (ppb)	0.3	0.04–0.6
α-Pinene (ppb)	0.016	0.004–0.054
Methanol (ppb)	19	8–42
Acetaldehyde (ppb)	2.5	0.7–7.1
Formaldehyde (ppb)	4.6	1.8–14
Additional VOCR (s^{-1})	1.4	1.4–1.4

Table 3A.4: Background concentrations used for Lagrangian plume modeling.

Species	Median Concentration	5^{th}–95^{th} percentiles
O_3 (ppb)	99	79–120
NO_x (ppb)[a]	0.14	0.07–0.20
HNO_3 (ppb)	2.6	1.3–3.4
PAN (ppb)	0.6	0.3–1.4
Methane (ppb)	1960	1930–2020
CO (ppb)	194	147–309
Ethane (ppb)	2.78	2.12–3.18
Ethene (ppb)	0.013	0.006–0.019
Propane (ppb)	0.80	0.44–1.0
Propene (ppb)	0.017	0.015–0.019
n-Butane (ppb)	0.096	0.07–0.265
2-Butyl nitrate (ppb)	0.025	0.016–0.029
n-Pentane (ppb)	0.02	0.008–0.07
n-Hexane (ppb)	0.01	0.004–0.05
Toluene (ppb)	0.005	0.002–0.17
m-Xylene (ppb)	0.012	0.006–0.015
Isoprene (ppb)	0.01	0.002–0.04
α-Pinene (ppb)	0	0–0
Methanol (ppb)	6.7	5.0–11.2
Acetaldehyde (ppb)	0.33	0.25–1.2
Formaldehyde (ppb)	0.506	0.35–3.1

[a] The partitioning of background NO_x between NO and NO_2 was assumed to match the instantaneous partitioning in the model.

Chapter 4

Effects of temperature-dependent NO_x emissions on continental ozone production

Adapted from P. S. Romer et al., Effects of temperature-dependent NO_x emissions on continental ozone production, *Atmos. Chem. Phys.*, 18(4), 2601–2614, doi:10.5194/acp-18-2601-2018, 2018.

4.1 Introduction

Elevated concentrations of tropospheric ozone are an important contributor to anthropogenic radiative forcing and are associated with increased human mortality and decreased crop yields (Myhre et al., 2013; World Health Organization, 2005; Booker et al., 2009). Observations of increased surface ozone concentrations on hotter days are widely reported, but the mechanisms driving this relationship are poorly understood in regions and climates with low concentrations of nitrogen oxides ($NO_x \equiv NO + NO_2$). Understanding the mechanisms driving these increases is critical to effectively regulating ozone pollution and predicting the effects of global warming on air quality.

Several previous studies (e.g., Sillman and Samson, 1995; Weaver et al., 2009; Pusede et al., 2014) have used in situ observations and chemical transport models to examine the relationships between ozone and temperature. Typically observed slopes range from 1–6 ppb $^{\circ}C^{-1}$, with greater values occurring in more polluted environments (Pusede et al., 2015). A few studies have also reported that this effect is nonlinear and can become significantly less strong at the highest temperatures (Steiner et al., 2010; Shen et al., 2016).

Increased ozone concentrations with temperature in urban areas can be well explained by increased ozone production caused by greater emissions of volatile organic compounds (VOCs) and decreased sequestration of NO_x in short-term reservoirs (Jacob and Winner, 2009). In contrast, there is little consensus about the mechanisms responsible for temperature-

dependent changes in ozone concentrations in rural and remote environments. Arguments in favor of large-scale changes in atmospheric circulation and in favor of local changes in the chemical production and loss of ozone have both been presented (Steiner et al., 2006; Barnes and Fiore, 2013). Regional stagnation episodes, often associated with elevated temperatures, allow ozone to accumulate over several days and are known to contribute significantly to the ozone-temperature relationship (Jacob et al., 1993). How various temperature-dependent chemical effects interact and their relative contributions to ozone production are not well understood outside of polluted environments.

Summer daytime ozone concentrations at rural sites in the United States typically range from 35–55 ppb (Cooper et al., 2012), sufficient to cause harm to humans, crops, and the climate. Epidemiological studies and meta-analyses investigating the relationship between ozone and daily mortality have found significant effects in small cities and rural locations, with some studies suggesting that increases in ozone may have a greater effect on daily mortality under less polluted conditions (Vedal et al., 2002; Ito et al., 2005; Atkinson et al., 2012). Studies of crop yield and plant health have traditionally used a threshold of 40 ppb when investigating the effects of ozone exposure, but many crops have been shown to experience reduced yields when exposed to ozone concentrations as low as 20 ppb (Pleijel et al., 2004; Booker et al., 2009). From a regulatory perspective, elevated regional background ozone can strongly exacerbate ozone pollution and the probability of regulatory exceedances in urban areas such as Houston, TX (Berlin et al., 2013). Understanding the behavior of O_3 in the rural and remote areas that cover the majority of the land area of the Earth is therefore crucial for effectively predicting and controlling air quality now and in the future.

In this chapter we use observations from Centreville, Alabama (CTR), a rural site in the southeastern United States, to investigate how temperature affects ozone production. Long-term monitoring from the SouthEastern Aerosol Research and CHaracterization (SEARCH) network shows that ozone increases significantly with temperature at this site (Fig. 4.1), despite being in a low-NO_x environment where the predicted response of the instantaneous ozone production rate to temperature is small (Pusede et al., 2015). We combine this record with extensive measurements from the Southern Oxidant and Aerosol Study (SOAS) in summer 2013 to explicitly calculate daily integrated ozone production and NO_x loss as a function of daily average temperature. We find that changes in local chemistry are important drivers of the increase in ozone concentrations observed at this site, and that increased NO_x emissions are responsible for 40% of the temperature-dependent increase in daily integrated ozone production. We expect similar effects to be present in other low-NO_x areas with high concentrations of VOCs, where the chemistry of alkyl and multifunctional nitrates is the majority pathway for permanent NO_x loss.

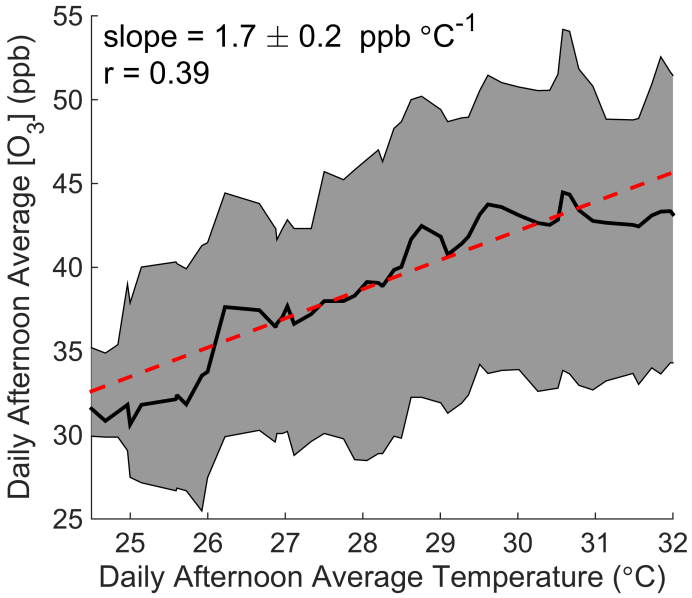

Figure 4.1: The O_3-temperature relationship in Centreville, Alabama. Daily afternoon (12 pm–4 pm) average ozone concentration is shown as a function of temperature from June–August 2010–2014 at the SEARCH CTR site. The black line and shaded gray region show the running median and interquartile range of ozone with temperature. The red line represents a fit to all daily data points.

4.2 Chemistry of ozone production and predicted response to temperature

Observed O_3-temperature relationships are caused by a combination of chemical changes to the production and loss of O_3 and changes to atmospheric circulation that determine advection and mixing. To begin separating these effects, we consider the chemical production of ozone (PO_3) and how it changes with temperature. Temperature-dependent changes in ozone production may be driven directly by temperature, or by another meteorological parameter that co-varies with temperature, such as solar radiation.

Ozone is produced in the troposphere when NO is converted to NO_2 by reaction with HO_2 or RO_2 in the linked HO_x and NO_x cycles (Fig. 4.2A). HO_2 and RO_2 radicals are generated in the HO_x cycle when a VOC reacts with OH in the presence of NO_x. In one turn of the cycle, the VOC is oxidized, OH is regenerated, and two molecules of O_3 are formed. The reactions that drive these catalytic cycles forward are in constant competition with reactions that remove radicals from the atmosphere, terminating the cycles. Termination can occur either through the association of two HO_x radicals to form inorganic or organic peroxides, or through the association of HO_x and NO_x radicals to form nitric acid or an organic nitrate.

The balance between propagating and terminating reactions causes PO_3 to be a non-

linear function of NO_x and the VOC reactivity (VOCR), as well as the production rate of HO_x radicals (PHO_x). The largest source of HO_x radicals in the summertime is the photolysis of O_3 followed by reaction with water vapor to produce OH; additional sources include the photolysis of formaldehyde and peroxides, ozonolysis of alkenes, and isomerization pathways in the oxidation of isoprene and other VOCs. To understand the response of ozone production to changes in chemistry, we use a simplified framework based on the balance of HO_x radical production and loss (Farmer et al., 2011).

Under high or moderate NO_x conditions, the primary loss process of HO_2 and RO_2 radicals is reaction with NO and the concentration of OH radicals can be expressed as a quadratic equation. To modify this approach to work under low-NO_x conditions, reactions between HO_x radicals must also be included, leading to a set of 4 algebraic equations that can be solved numerically (details given in Appendix 4A). Figure 4.2B shows the calculated rate of ozone production as a function of NO_x at two different VOC reactivities. Depending on atmospheric conditions, the ozone production rate can either be NO_x-limited, where additional NO_x causes PO_3 to increase, or NO_x-saturated, where additional NO_x suppresses ozone formation.

When considering day-to-day variations, the total amount of ozone produced over the course of a day ($\int PO_3$) is a more representative metric than the instantaneous ozone production rate. Total daily ozone production depends on all of the factors that affect PO_3 as well as their diurnal evolution. In places where ozone production is NO_x-limited, changes to chemistry with temperature that affect the NO_x loss rate ($\mathcal{L}NO_x$) can affect $\int PO_3$ by changing the amount of NO_x available for photochemistry later in the day (Hirsch et al., 1996).

Permanent NO_x loss occurs through two primary pathways in the troposphere: the association of OH and NO_2 to form HNO_3, and through the chemistry of alkyl and multifunctional nitrates ($RONO_2$). These organic nitrates are formed as a minor channel of the RO_2 + NO reaction, with the alkyl nitrate branching ratio α_i ranging from near zero for small hydrocarbons to over 0.20 for monoterpenes and long-chain alkanes (Perring et al., 2013). The overall alkyl nitrate branching ratio α_{eff} represents the reactivity-weighted average of α_i for all VOCs. While some fraction of $RONO_2$ quickly recycles NO_x to the atmosphere, a significant fraction η permanently removes NO_x through deposition and hydrolysis (e.g., Browne et al., 2013). Romer et al. (2016) determined that $\eta = 0.55$ during SOAS and was controlled primarily by the hydrolysis of isoprene hydroxy-nitrates. Because the hydrolysis rate is set primarily by the distribution of nitrate isomers, which does not change appreciably with temperature, we assume that η is constant with temperature in this study (Hu et al., 2011; Peeters et al., 2014). Deposition is only a minor loss process for $RONO_2$, therefore any changes in the deposition rate with temperature will have at most a minor effect on η.

NO_x also has several temporary sinks that can sequester NO_x, most importantly peroxy acyl nitrate (PAN). In the summertime southeastern United States, the lifetime of PAN is typically 1–2 hours, too short to act as a permanent sink of NO_x. Past studies in forested regions have found remarkably little variation in PAN with temperature, due to compensating changes in both its production and loss (e.g., LaFranchi et al., 2009). As a result, the

formation or destruction of PAN does not contribute significantly to net ozone production or NO_x loss and we do not include it in these calculations.

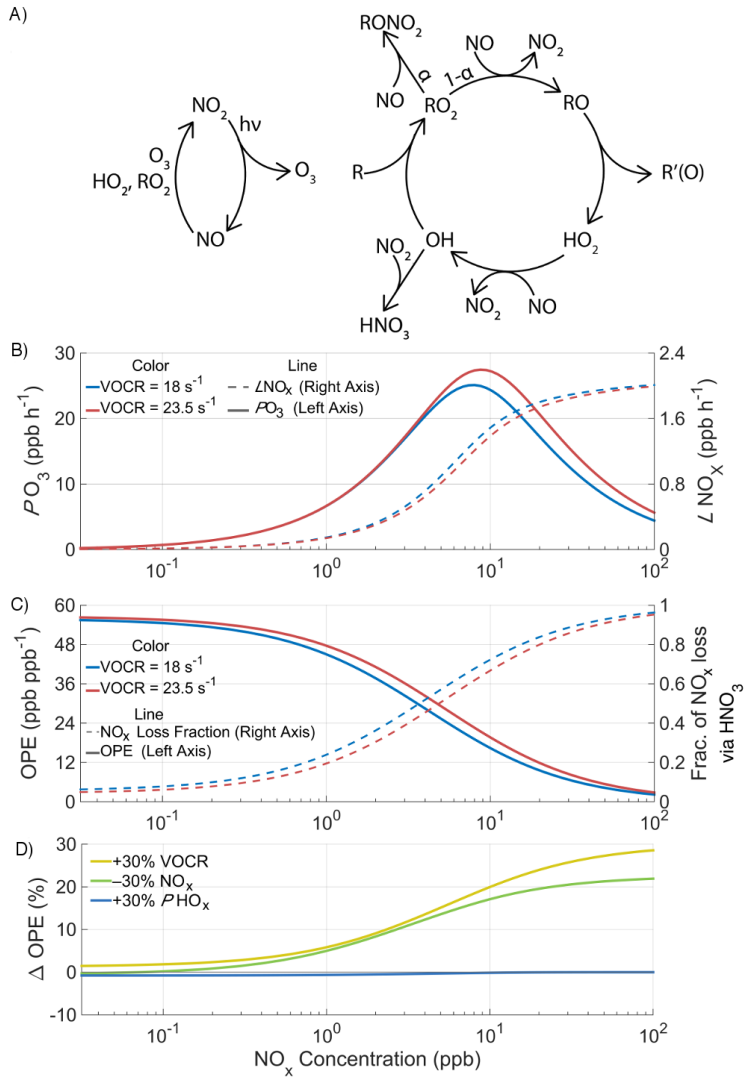

Figure 4.2: The chemistry of ozone production and NO_x loss in the troposphere. Panel A: Schematic of the linked NO_x and HO_x cycles that lead to net ozone production. Panel B: The calculated instantaneous O_3 production rate and NO_x loss rate as a function of NO_x and VOCR, with fixed PHO_x, η, and α_{eff}. Panel C: OPE and the fraction of NO_x loss that takes place via HNO_3 chemistry under the same conditions as above. Panel D: The percent change in ozone production efficiency caused by chemical changes as a function of NO_x.

The ozone production efficiency (OPE $\equiv P\text{O}_3/\mathcal{L}\text{NO}_x$) represents the number of ozone molecules formed per molecule of NO_x consumed and directly links the ozone and NO_x budgets. Because OPE accounts for changes in both $P\text{O}_3$ and $\mathcal{L}\text{NO}_x$, the temperature

response of OPE captures feedbacks in ozone production chemistry that $P\mathrm{O}_3$ alone does not.

As the concentration of $\mathrm{NO_x}$ decreases and VOCR increases, the fraction of $\mathrm{NO_x}$ loss that takes place via $\mathrm{HNO_3}$ chemistry decreases and the OPE increases (Fig. 4.2C). The relative importance of $\mathrm{HNO_3}$ and $\mathrm{RONO_2}$ chemistry determines the relationship between $P\mathrm{O}_3$ and $\mathcal{L}\mathrm{NO_x}$. When $\mathrm{HNO_3}$ is the most important $\mathrm{NO_x}$ loss pathway, $\mathrm{O_3}$ production and $\mathrm{NO_x}$ loss occur through separate channels. $\mathrm{O_3}$ production occurs when OH reacts with a VOC, generating $\mathrm{RO_2}$ and $\mathrm{HO_2}$ radicals; $\mathrm{NO_x}$ loss primarily occurs when OH reacts with $\mathrm{NO_2}$. Although these channels are linked by a shared dependence on OH, the relative importance of these pathways can vary. For example, under these conditions an increase in VOCR will cause $\mathrm{NO_x}$ loss to decrease, ozone production to increase, and OPE to increase (Fig. 4.2B–C).

In contrast, when $\mathrm{RONO_2}$ chemistry dominates $\mathrm{NO_x}$ loss, ozone production and $\mathrm{NO_x}$ loss are intrinsically linked by their shared dependence on the $\mathrm{RO_2} + \mathrm{NO}$ reaction. This reaction produces $\mathrm{O_3}$ in its main channel and consumes $\mathrm{NO_x}$ in the minor channel that forms organic nitrates, with the ratio between these two channels set by α_{eff}. Under these conditions, changes to the chemistry that do not affect α_{eff} have a minimal effect on OPE (Fig. 4.2D) and the OPE can be considered to be unvarying with temperature. An increase in VOCR or a decrease in $\mathrm{NO_x}$ will affect both $\mathrm{NO_x}$ loss and ozone production equally, because both processes are dependent on the same set of reactions. Because of this change in behavior, from variable OPE to fixed OPE, the drivers of the $\mathrm{O_3}$-T relationship are expected to be categorically different in areas where $\mathrm{RONO_2}$ chemistry dominates $\mathrm{NO_x}$ loss. As a result, the effects that cause $\mathrm{O_3}$ to increase with temperature in urban and other polluted regions, where $\mathrm{HNO_3}$ chemistry dominates $\mathrm{NO_x}$ loss, are unlikely to apply in areas with low concentrations of $\mathrm{NO_x}$ and high concentrations of reactive VOCs, where $\mathrm{RONO_2}$ chemistry is most important. In these areas, more $\mathrm{NO_x}$ must be oxidized in order to produce more $\mathrm{O_3}$.

4.3 Observed response of ozone production to temperature

Measurements during SOAS

The theoretical results presented in Fig. 4.2 can be compared to the observed behavior during SOAS. Measurements during SOAS have been described in detail elsewhere (e.g., Hidy et al., 2014; Romer et al., 2016; Feiner et al., 2016) and are summarized below. The primary ground site for SOAS was co-located with the CTR site of the SEARCH network (32.90289° N, 87.24968° W), in a clearing surrounded by a dense mixed forest (Hansen et al., 2003). Direct anthropogenic emissions of $\mathrm{NO_x}$ near this site are estimated to be low and predominantly from mobile sources (Hidy et al., 2014). Measurements taken as part of the SEARCH network were located on a 10 m tower approximately 100 m away from the forest edge, while the other measurements from the SOAS campaign used in this analysis

were located on a 20 m walk-up tower at the edge of the forest. Species measured on both the SOAS walk-up tower and the SEARCH platform were well correlated with each other, indicating that similar airmasses were sampled at both locations.

Several chemical and meteorological measurements used in this analysis, including NO_x, O_3, total reactive nitrogen (NO_y), and temperature, were collected by Atmospheric Research and Analysis (ARA) as part of SEARCH (Hidy et al., 2014). NO was measured using the chemiluminescent reaction of NO with excess ozone. NO_2 was measured based on the same principle, using blue LED photolysis to convert NO_2 to NO. The photolytic conversion of NO_2 to NO is nearly 100% efficient and does not affect higher oxides of nitrogen (Ryerson et al., 2000). Ozone was measured using a commercially available ozone analyzer (Thermo-Scientific 49i).

During the SOAS campaign, NO_2, total peroxy nitrates (ΣPANs), and total alkyl and multifunctional nitrates ($\Sigma RONO_2$) were measured via thermal dissociation laser-induced fluorescence, as described by Day et al. (2002). An NO chemiluminescence instrument located on the walk-up tower provided additional measurements of NO co-located with the other SOAS measurements (Min et al., 2014).

HO_x radicals were measured with the Penn State Ground-based Tropospheric Hydrogen Oxides Sensor (GTHOS), which uses laser-induced fluorescence to measure OH (Faloona et al., 2004). HO_2 was also measured in this instrument by adding NO to convert HO_2 to OH. C_3F_6 was periodically added to the sampling inlet to quantify the interference from internally generated OH (Feiner et al., 2016). Measurements of total OH reactivity (OHR $\equiv$ inverse OH lifetime) were made by sampling ambient air, injecting OH, and letting the mixture react for a variable period of time. The slope of the OH signal versus reaction time provides a top-down measure of OHR (Mao et al., 2009).

A wide range of VOCs were measured during SOAS using gas chromatography-mass spectrometry (GC-MS). Samples were collected in a liquid-nitrogen cooled trap for five minutes, then transferred by heating onto an analytical column, and detected using an electron-impact quadrupole mass-spectrometer (Gilman et al., 2010). This system is able to quantify a wide range of compounds including alkanes, alkenes, aromatics, isoprene, and multiple monoterpenes at a time resolution of 30 minutes. Methyl vinyl ketone (MVK) and methacrolein (MACR) were measured individually by GC-MS and their sum was also measured using a proton transfer reaction mass spectrometer (PTR-MS) (Kaser et al., 2013). The calculated rates of ozone production and NO_x loss do not change significantly depending on which measurement is used.

Average diurnal cycles of the main measurements used in this study during the SOAS campaign are shown in Fig. 4.3. Afternoon concentrations of NO_x averaged 0.3 ppb and concentrations of isoprene 5.5 ppb. Due to these low-NO_x, high-VOC conditions, $RONO_2$ chemistry was responsible for over three-quarters of the permanent NO_x loss (Romer et al., 2016). Daily average afternoon (12 pm–4 pm) ozone concentrations increased with daily average afternoon temperature during SOAS (2.3 ± 1 ppb $^\circ C^{-1}$). This trend is greater than the long-term trend reported by the SEARCH network, but the difference is not statistically significant.

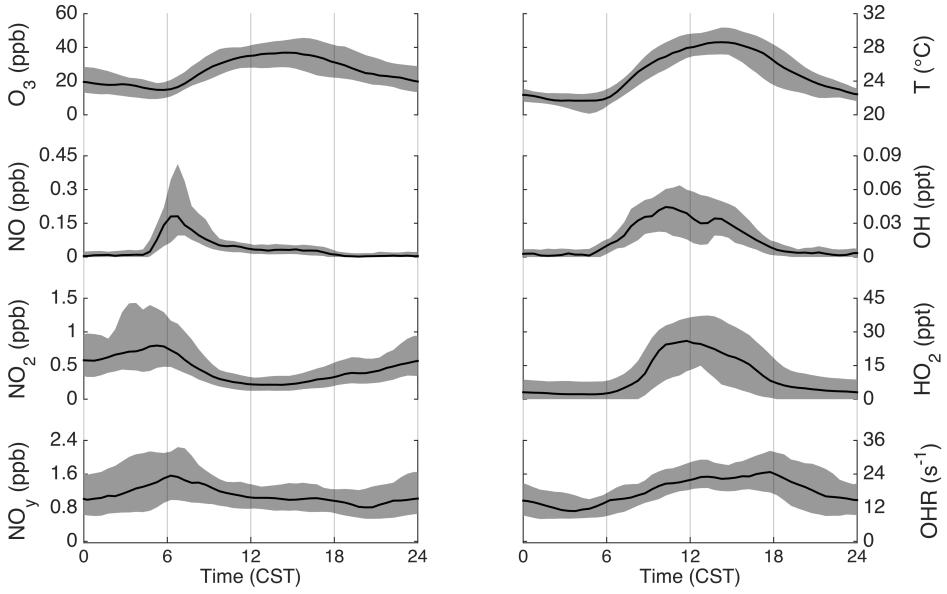

Figure 4.3: Diurnal cycle of the primary parameters used in this study as measured during SOAS. For each quantity the black line shows the hourly median and the shaded gray area shows the interquartile range.

Calculation of $\int PO_3$ and effects of temperature

Measurements of NO, NO_2, OH, HO_2, and a wide range of VOCs were used to calculate the steady-state concentrations of RO_2 radicals using the Master Chemical Mechanism v3.3.1, run in a MATLAB framework (Jenkin et al., 2015; Wolfe et al., 2016). Before 24 June, HO_2 measurements are not available and steady-state concentrations of both HO_2 and RO_2 were calculated. Input species were taken to 30 minute averages, and the model was run until radical concentrations reached steady state. Top-down measurements of OHR were used to include the contribution to ozone production from unmeasured VOCs.

To understand the day-to-day variation of ozone chemistry, the calculated ozone production rate was integrated from 6 am to 4 pm for each of the 24 days during the campaign period with greater than 75% data coverage of all input species. When plotted against daily average afternoon temperature, $\int PO_3$ is seen to increase strongly with temperature (2.3 ± 0.6 ppb $^{\circ}C^{-1}$, Fig. 4.4A). The change in $\int PO_3$ with temperature demonstrates that local chemistry is an important contributor to the observed O_3-T relationship; however, the observed O_3-T trend also includes the effects of chemical loss, advection, entrainment, and multi-day buildup on overall O_3 concentration (e.g., Baumann et al., 2000).

While elevated temperatures are associated with enhanced production of ozone, they are also associated with increased chemical loss. The chemical loss of ozone occurs through three

main pathways in this region: photolysis followed by reaction with H_2O, reaction with HO_2, and reaction with VOCs (Frost et al., 1998). The loss of O_3 was calculated for each of these pathways, and then integrated over the course of the day to determine total daily ozone loss ($\int \mathcal{L}O_3$). Chemical loss of ozone is found to increase with temperature (1.1 ± 0.3 ppb $^\circ C^{-1}$, Fig. 4.4B), but much less than the chemical production.

The difference between the trend in the net chemical production and loss of O_3 and the trend in ozone concentration gives a rough estimate of how non-chemical processes contribute to the ozone-temperature relationship. We calculate that non-chemical processes cause O_3 to increase by 1 ± 1.2 ppb $^\circ C^{-1}$. This approach does not take into account the interactions between chemical and non-chemical effects, such as how changes to advection and mixing may impact concentrations of VOCs, NO_x, and other reactants. Although the large uncertainty does not allow for quantitative analysis, qualitatively, chemical and non-chemical processes are both found to be important contributors to the ozone-temperature relationship. Other approaches, such as chemical transport models, that can more directly investigate and control specific physical processes are likely to be better suited to calculating the contribution of non-chemical processes to the ozone-temperature relationship (e.g., Fu et al., 2015).

Using the same calculated radical concentrations, the rate of NO_x loss was calculated as the rate of direct HNO_3 production plus the fraction η of alkyl nitrate production that leads to permanent NO_x loss. Figure 4.4C shows the increase in $\int \mathcal{L}NO_x$ with temperature for the SOAS campaign (0.05 ± 0.01 ppb $^\circ C^{-1}$). As expected from the importance of $RONO_2$ chemistry to NO_x loss, $\int \mathcal{L}NO_x$ and $\int PO_3$ are tightly correlated ($r^2 = 0.90$), and OPE is high (OPE average 45 ± 3 ppb ppb^{-1}) and is effectively constant with temperature (calculated trend 0.2 ± 0.6 $^\circ C^{-1}$). Therefore, the increase in $\int PO_3$ with temperature is not caused by more efficient production of ozone while the same amount of NO_x is consumed.

OPE can also be estimated from the ratio of odd oxygen ($O_x \equiv O_3 + NO_2$) to NO_x oxidation products ($NO_z \equiv NO_y - NO_x$) (Trainer et al., 1993). The afternoon ratio of O_x to NO_z during SOAS varied from 43–67 (interquartile range), slightly higher than the average ratio of $\int PO_3$ to $\int \mathcal{L}NO_x$. However, since the O_x to NO_z ratio includes the effects of chemical loss and transport, which the ratio of $\int PO_3$ to $\int \mathcal{L}NO_x$ does not, these two values are not expected to be equivalent, particularly in non-polluted areas.

The trend in $\int PO_3$ with temperature is robust and extends beyond the short temporal window of the SOAS campaign. Although long-term measurements of HO_x and VOCs are not available, the ozone production rate can be estimated from SEARCH measurements using the deviation of NO and NO_2 from photostationary state (Eq. 4.1) (Baumann et al., 2000; Pusede et al., 2015).

$$PO_3 = j_{NO_2}[NO_2] - k_{NO+O_3}[NO][O_3] \tag{4.1}$$

The NO_2 photolysis rate was parameterized as a quadratic function of total solar radiation (Trebs et al., 2009). Using this method and scaling the result to match the values calculated using steady-state RO_2 concentrations during SOAS, we find that $\int PO_3$ increased by 2.3 ± 0.8 ppb $^\circ C^{-1}$ during June–August 2010–2014 (Fig. 4.5). Without scaling, the long-term trend in

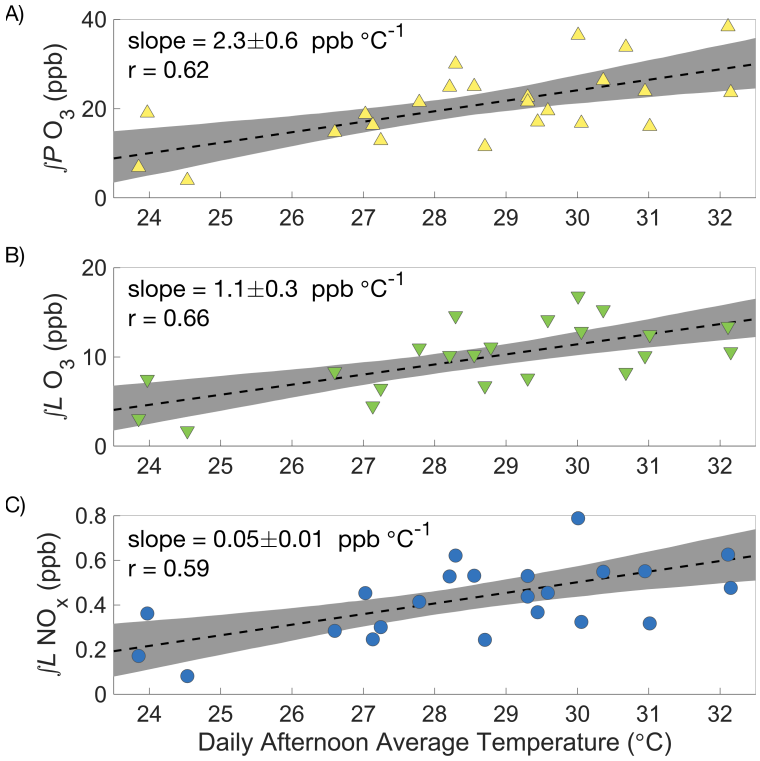

Figure 4.4: Observed dependence of daily $\int P\mathrm{O}_3$ (Panel A), $\int \mathcal{L}\mathrm{O}_3$ (Panel B), and $\int \mathcal{L}\mathrm{NO}_x$ (Panel C) on daily afternoon average temperature during SOAS. Each point shows the afternoon average temperature and integrated production or loss for a single day. Black lines show a least squares fit to all points; shaded areas show the 90% confidence limits of the fit calculated via bootstrap sampling.

$\int P\mathrm{O}_3$ with temperature is 4.0 ± 0.5 ppb $^\circ\mathrm{C}^{-1}$. Based on the long-term SEARCH record, we do not find evidence that the relationship between ozone concentration or ozone production changes significantly at the highest temperatures (the top 5% of observations). This agrees broadly with Shen et al. (2016), who found that ozone suppression at extreme temperatures to be uncommon in the southeastern United States.

4.4 Drivers of increased ozone production

While the increase in ozone production is accompanied by an observed increase in ozone concentration, the increase in NO_x loss is not accompanied by a significant decrease in NO_x concentration (-0.002 ± 0.01 ppb $^\circ\mathrm{C}^{-1}$, Fig. 4.6A). For this to occur, NO_x must have a source that increases with temperature to compensate for its increased loss. One possible explanation is that the increased thermal decomposition rate of peroxy nitrates (ΣPANs) causes less NO_x to be sequestered in these short-term reservoirs. This is not the case during

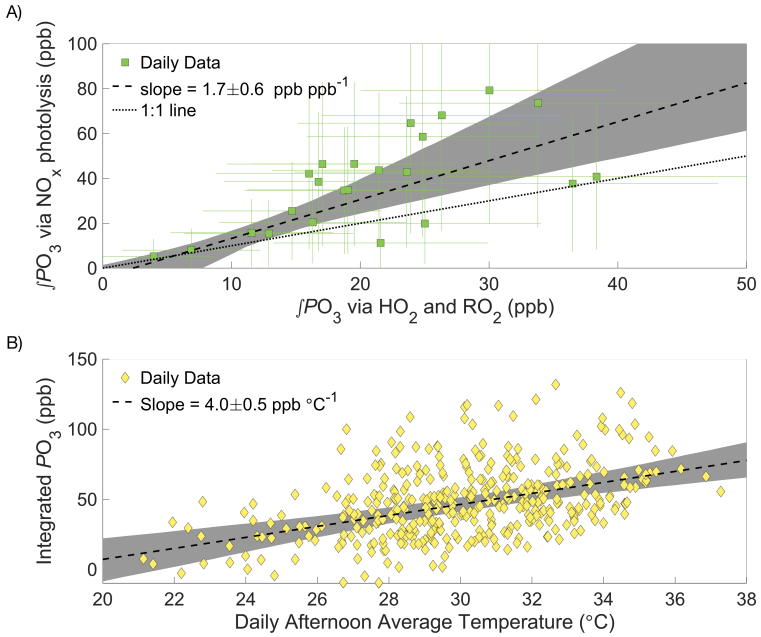

Figure 4.5: Comparison of daily integrated ozone production via two methods (Panel A) and long-term trend in $\int PO_3$ with temperature (Panel B). The reported slope in Panel A was calculated using a bivariate (York-type) fit accounting for the error in both x and y.

SOAS. The increased decomposition rate of peroxy nitrates is counteracted by an increase in their production rate, such that the average concentration of total peroxy nitrates shows no decrease with temperature (Fig. 4.6B).

More generally, increased transformations from NO_x oxidation products back into NO_x cannot explain the observations. The concentration of NO_y increases significantly with temperature (Fig. 4.6C). Because NO_y includes NO_x as well as all of its reservoirs and sinks, changes in the transformation rates between NO_x and its oxidation products cannot explain the increase of NO_y with temperature. There must be a source of NO_y, not just of NO_x, that increases with temperature.

Data from the SEARCH network indicate that the increase in NO_y with temperature observed during SOAS is primarily a local effect. Measurements from June–August 2010–2014 show a consistent increase of NO_y with temperature at the two rural monitoring sites in the network, but total NO_y decreases with temperature at the four urban and suburban sites (Table 4.1). The increase in NO_y with temperature therefore cannot be explained by regional meteorological effects, since those would lead to similar relationships between NO_y and temperature across the southeastern United States.

Measurements at night and in the early morning, before significant photochemistry has occurred, show a strong temperature-dependent increase of NO_x over the course of the night. Because surface wind speeds are low at night and the increase in NO_x at night is not accom-

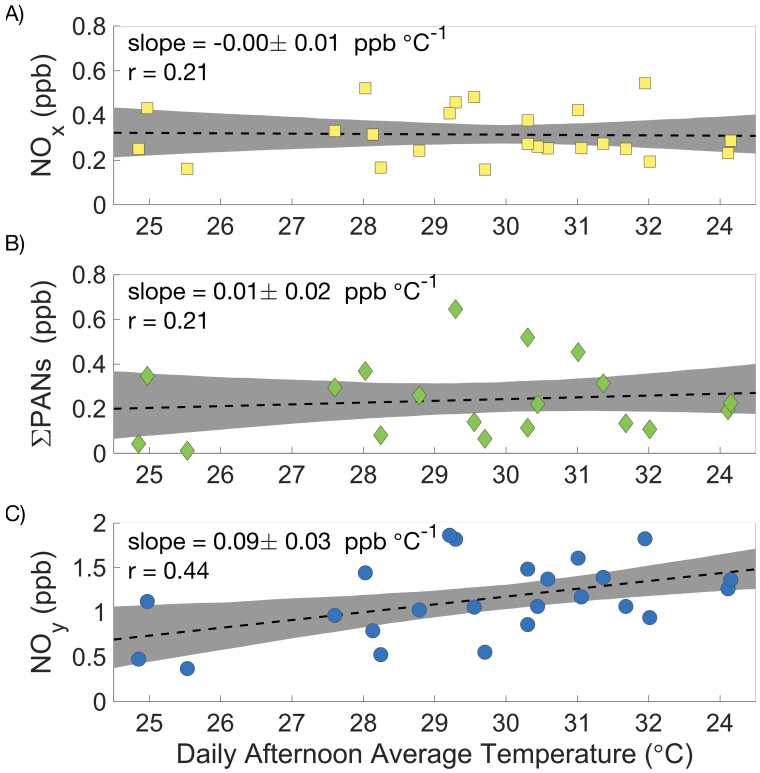

Figure 4.6: Afternoon average concentrations of NO_x (Panel A), ΣPANs (Panel B), and NO_y (Panel C) at the CTR site as a function of daily average afternoon temperature during SOAS.

panied by large increases in NO_x oxidation products, the increase in NO_x must be caused by emissions local to the CTR site.

The consistent increase of NO_x over the course of the night can be used to quantitatively measure the local NO_x emissions rate. Figure 4.7 shows the temperature-dependent increase of NO_x relative to the concentration of NO_x at 4 pm the day before, separating the effects of the previous day from the nighttime increase. Measurements from June–August 2010–2014 from the CTR SEARCH network site are used to obtain more representative statistics. The average rate of NO_x increase during the night is 0.095 ppb h^{-1}. To account for the chemical removal of NO_x, the cumulative loss of NO_x during the night was added to the observations. During SOAS, the nighttime loss of NO_x occurred almost exclusively through the reaction of NO_2 with O_3 to form NO_3, which then reacted with a VOC to form an organic nitrate (Ayres et al., 2015). N_2O_5 chemistry made a negligible contribution to total NO_x loss. The loss rate of NO_x during the night was therefore calculated as the rate of reaction of NO_2 with O_3. In this form, the rate of increase of the adjusted NO_x concentrations (NO_x*) is equal to the local NO_x emission rate. The emission rate of NO_x and its temperature dependence were calculated by a linear regression following the form of Eq. (4.2), where the adjusted

Table 4.1: Observed trend in NO_y with temperature at 6 SEARCH sites across all days June–August 2010–2014. GFP data only extends through 2012.

Site Name	Location	NO_y-T Slope (ppb $°C^{-1}$)
CTR	Rural	0.072 ± 0.009
YRK	Rural	0.043 ± 0.015
OAK	Suburban	-0.034 ± 0.016
JST	Urban	-0.037 ± 0.047
BHM	Urban	-0.312 ± 0.050
GFP	Urban	-0.050 ± 0.040

concentration of NO_x depends both on time (H = hours after 4 pm) and temperature (T).

$$NO_x^* = (\alpha T + \beta)H + b \tag{4.2}$$

In this regression, the fitted parameter α represents the increase of NO_x emissions with temperature and the average value of $\alpha T + \beta$ provides an estimated NO_x emission rate.

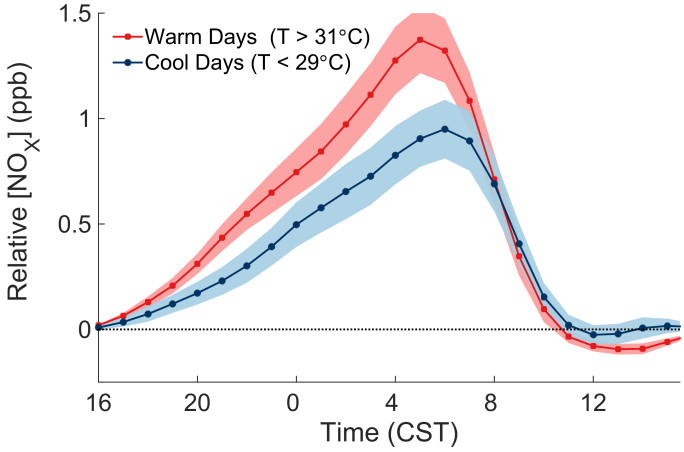

Figure 4.7: Concentrations of NO_x relative to their concentration at 4 pm the day before over June–August 2010–2014 at the CTR site. The thick lines and shaded areas show the hourly mean and 90% confidence interval of the mean for cooler and warmer days.

Because emissions are localized to the surface, the effective depth of the nighttime boundary layer must also be accounted for, which we estimate to be 150 m. This agrees well with the derived mixing heights from daily 5 am sonde launches at the Birmingham (BHM) airport (Durre and Yin, 2008) and past estimates of the nocturnal boundary layer height (e.g.,

Liu and Liang, 2010; VandenBoer et al., 2013), while it is significantly lower than the average ceilometer-reported 5 am boundary layer height of 400 m during SOAS.

After accounting for these factors, the NO_x emissions rate is calculated to be 7.4 ppt m s^{-1} or 4.2 ng N m^{-2} s^{-1}. Based on the change in slope with temperature, the emissions rate is estimated to increase by 0.4 ppt m s^{-1} $°C^{-1}$. The rise in NO_x emissions with temperature over 24 hours agrees to within the uncertainty with the increase of daily $\int \mathcal{L}NO_x$ with temperature, sufficient to explain why afternoon NO_x concentrations are not observed to decrease with temperature even as their loss rate increases.

The inferred local NO_x source bears all the hallmarks of soil microbial emissions (S_{NO_x}). Soil microbes emit NO_x as a byproduct of both nitrification and denitrification, and the rate of NO_x emissions correlates strongly with microbial activity in soil (Pilegaard, 2013). The inferred NO_x source is active during day and night, increases strongly with temperature, and is present in a rural area with low anthropogenic emissions. The only plausible source of NO_x that matches all of these constraints is soil microbial emissions near to the SOAS site. Soil NO_x emissions also depend on soil water content and nitrogen availability, neither of which is generally limiting in the southeastern United States (e.g., Hickman et al., 2010). The most likely anthropogenic sources of NO_x at this location are mobile sources, which are not thought to change significantly with temperature (Singh and Sloan, 2006) and therefore cannot explain the results of Fig. 4.7.

To calculate how the increase in NO_x emissions affects ozone production, we use the same chemical framework from Fig. 4.2. For each half-hour period the average value of the input parameters and their temperature dependence during the SOAS campaign were calculated (Fig. 4B.2). The diurnal cycle and trend with temperature of all model inputs were then used to calculate total daily ozone production as a function of temperature (Fig. 4B.1). By altering whether the temperature dependence for each parameter is included, the overall trend in $\int P O_3$ can be decomposed into individual components (Fig. 4.8). The effect of increased NO_x emissions was calculated by fixing the trend in NO_x with temperature to match the trend in $\int \mathcal{L}NO_x$. We find that the increase of NO_x emissions with temperature accounts for 40% of the increase in $\int P O_3$ with temperature, or approximately 0.9 ppb $°C^{-1}$. The other 60% is caused primarily by the increase of PHO_x with temperature. The increase in PHO_x with temperature is most likely caused by changes in solar radiation, which is well correlated with the total PHO_x rate and increases strongly with temperature. In contrast, water vapor is not correlated with total PHO_x. Although VOCR increases strongly with temperature, the $RONO_2$-dominated NO_x chemistry causes neither the ozone production rate nor the NO_x loss rate to be sensitive to this increase, leading to the minimal effect of VOCR on $\int P O_3$.

4.5 Conclusions

Changes in NO_x emissions with temperature have an outsized effect when considering the impacts of ozone on human health and climate. At the CTR site and other areas where OPE

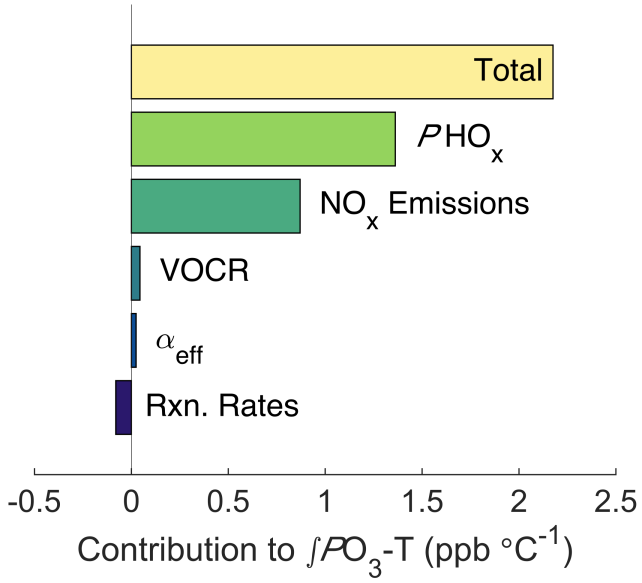

Figure 4.8: Decomposed effects of ozone and temperature. The top bar shows the model-calculated $\int PO_3$-T trend, all other bars show how the $\int PO_3$-T slope changes when the temperature dependence of each factor is removed.

does not vary with temperature, the total amount of ozone produced on weekly or monthly timescales is directly proportional to the amount of available NO_x. While faster oxidation on hotter days causes more ozone to be produced, without changes in NO_x emissions there would be an associated decrease in ozone production on subsequent days, because the NO_x necessary for ozone production would be depleted. In contrast, increased NO_x emissions can cause weekly or monthly average ozone concentrations to increase with temperature. Change in long-term average ozone concentrations is often more important to the ozone climate feedback and human health than day-to-day variation. The mechanisms described here are likely to be active in all areas with low concentrations of NO_x and high concentrations of reactive VOCs. Only regions where $RONO_2$ chemistry is the dominant pathway for NO_x loss have effectively constant OPE with temperature, but the effect of soil NO_x emissions on ozone production is widespread.

Past direct measurements of soil NO_x using soil chambers have found enormous variability, both between sites and within different plots in the same field. Pilegaard et al. (2006) found variability of a factor of over 100 between soil NO_x emissions in different European forests. Within the southeastern United States, direct measurements at forested sites have reported emissions rates ranging from 0.1–10 ng N m^{-2} s^{-1} (Williams and Fehsenfeld, 1991; Thornton et al., 1997; Hickman et al., 2010). Besides temperature, the most important variables affecting soil NO_x emissions are typically nitrogen availability and soil water content, as well as plant cover and soil pH (Pilegaard, 2013). In very wet environments, soil microbes

typically emit N_2O or N_2 instead of NO_x, and in arid environments soil emissions of HONO can be equal to or larger than soil NO_x emissions (Oswald et al., 2013). Although conditions at the CTR site are too wet and acidic for soil HONO emissions to be significant, in environments where soil HONO emissions are large, they would likely have an even greater effect on ozone production by acting as a source of both NO_x and HO_x radicals.

The variability between sites and the interaction between several biotic and abiotic factors make it difficult to apply regional or model estimates of soil NO_x emissions to a particular location. Our approach in this analysis, using observations of the nighttime atmosphere to determine the NO_x emissions rate, helps span the gap between soil chambers and the regional atmosphere. Although soil NO_x emissions depend on several environmental factors, process-driven models predict that the response of soil NO_x emissions to global warming will be driven primarily by the increase in temperature (Kesik et al., 2006).

While soil NO_x emissions have been known and studied for decades, the impacts of soil NO_x emissions on ozone from non-agricultural regions was often found to be insignificant compared to anthropogenic sources (e.g., Davidson et al., 1998). Years of declining anthropogenic NO_x emissions in the United States and recent higher estimates for forest soil NO_x emissions (e.g., Hickman et al., 2010) mean that this is no longer the case. Non-agricultural soil NO_x emissions may now account for nearly a third of total NO_x emissions in the summertime southeastern United States (Travis et al., 2016), and have significant effects on regional ozone production.

The rise in ozone production caused by increased NO_x emissions on hotter days established here suggests that the relationship between ozone and temperature will be positive under a wider range of conditions than previously thought. This includes 1. the pre-industrial atmosphere, 2. present day rural continental locations, and 3. future scenarios with dramatically reduced anthropogenic NO_x emissions.

1. In pre-industrial times, semi-quantitative measurements of ozone show significantly lower concentrations of ozone than currently observed in rural and remote regions or generally predicted by global models (Cooper et al., 2014). While $RONO_2$ chemistry establishes an upper limit to the ozone production efficiency under low-NO_x conditions, the significant contribution of S_{NO_x} to ozone production makes reconciling the semi-quantitative measurements with model predictions more difficult and suggests that natural emissions of NO_x in pre-industrial models may be over-estimated (Mickley et al., 2001).

2. In the present day, effective ozone regulation, especially on hot days, requires taking into account the effect of S_{NO_x}. Because these emissions are distributed over broad areas and are not directly anthropogenic, they present additional challenges to air quality management. Indirect approaches, such as changes to fertilizer application practices, have the potential to significantly reduce S_{NO_x} from agricultural regions (Oikawa et al., 2015). Decreases in direct anthropogenic NO_x emissions may also lead to a decrease in S_{NO_x} by decreasing the amount of nitrogen available to the ecosystem (Pilegaard, 2013).

3. In the future, because soil NO_x emissions lead to the formation of ozone, itself an important greenhouse gas, the increase of soil NO_x emissions with temperature represents a positive climate feedback and an additional link between changes to the nitrogen cycle and the environment. The effects of increased ozone pollution to plants, including reduced photosynthesis and slower growth, have the potential to alter the carbon cycle on a regional scale (Heagle, 1989; Booker et al., 2009). Soil NO_x emissions therefore represent an additional link between the nitrogen and carbon cycles that should be included when considering the consequences of a warming world.

Appendix 4A Analytic model of O_3 production

To conceptually understand O_3 production and NO_x loss, we use a simplified framework similar to that described by Farmer et al. (2011). This framework uses fixed values of total organic reactivity (VOCR), alkyl nitrate branching ratio α and loss efficiency η, NO_x, and HO_x radical production rate (PHO_x).

Since HO_x radicals are highly reactive, it is a valid assumption under nearly all NO_x concentrations that HO_x radicals are in steady-state and that PHO_x is equal to the gross HO_x loss rate (Eq. 4A.1).

$$\begin{aligned} PHO_x &= k_{OH+NO_2}[OH][NO_2] + \alpha \cdot k_{RO_2+NO}[RO_2][NO] + 2k_{HO_2+HO_2}[HO_2][HO_2] \\ &\quad + 2k_{RO_2+HO_2}[RO_2][HO_2] + 2k_{RO_2+RO_2}[RO_2][RO_2] \end{aligned} \tag{4A.1}$$

Individual HO_x radicals (OH, HO_2, and RO_2) can also be assumed to be in steady state, such that their production and loss are equal. Under low-NO_x conditions, the reactions that initiate and terminate the HO_x cycle must be included as well as the cycling rate. We further constrain the model by requiring that the concentration of HO_2 and RO_2 radicals be equal. This constraint is satisfied by introducing an additional parameter c which allows PHO_x to produce both HO_2 and OH radicals in a varying ratio. These constraints provide a system of 4 equations that can be solved numerically (Eq. 4A.2–4A.5).

$$[OH] = \frac{k_{HO_2+NO}[HO_2][NO] + c \cdot PHO_x}{VOCR + k_{OH+NO_2}[NO_2]} \tag{4A.2}$$

$$[RO_2] = \frac{[OH] \cdot VOCR}{k_{RO_2+NO}[NO] + k_{RO_2+HO_2}[HO_2] + 2k_{RO_2+RO_2}[RO_2]} \tag{4A.3}$$

$$[HO_2] = \frac{(1-\alpha)k_{RO_2+NO}[RO_2][NO] + (1-c)PHO_x}{k_{HO_2+NO}[NO] + 2k_{HO_2+HO_2}[HO_2] + k_{HO_2+RO_2}[RO_2]} \tag{4A.4}$$

$$[HO_2] = [RO_2] \tag{4A.5}$$

For the calculations in Fig. 4.2, the values of VOCR, α, and PHO_x were fixed at 18 s^{-1}, 0.06, and 1.15×10^7 molec. cm^{-3} s^{-1}. Rate constants are taken from the IUPAC chemical

kinetics database, assuming that all RO_2 radicals react with the kinetics of $CH_3CH_2O_2$ (Atkinson et al., 2006). The system of equations was solved numerically using the `vpasolve` function in MATLAB, subject to the constraints that [OH], [HO_2], and [RO_2] are positive and c is between 0 and 1.

The resulting concentrations of HO_x radicals can be used to calculate the rates of ozone production and NO_x loss using Eq. (4A.6)–(4A.9).

$$P\mathrm{O}_3 = (1-\alpha)k_{\mathrm{RO}_2+\mathrm{NO}}[\mathrm{RO}_2][\mathrm{NO}] + k_{\mathrm{HO}_2+\mathrm{NO}}[\mathrm{HO}_2][\mathrm{NO}] \quad (4\mathrm{A}.6)$$

$$P\mathrm{HNO}_3 = k_{\mathrm{OH}+\mathrm{NO}_2}[\mathrm{OH}][\mathrm{NO}_2] \quad (4\mathrm{A}.7)$$

$$P\Sigma\mathrm{RONO}_2 = \alpha \cdot k_{\mathrm{RO}_2+\mathrm{NO}}[\mathrm{RO}_2][\mathrm{NO}] \quad (4\mathrm{A}.8)$$

$$\mathcal{L}\mathrm{NO}_x = P\mathrm{HNO}_3 + \eta \cdot P\Sigma\mathrm{RONO}_2 \quad (4\mathrm{A}.9)$$

Appendix 4B Decomposition of the O_3-temperature relationship

The simplified HO_x model described above was used to decompose the contribution of different parameters to the increase of $\int P\mathrm{O}_3$ with temperature. Peroxy nitrates are not included in this model, but because there is no significant trend in ΣPANs with temperature their absence does not affect the results. To validate that this model gave accurate $\int P\mathrm{O}_3$ results, it was first run using inputs based on measured values for each half-hour period:

- Model inputs of NO_x were taken directly from measurements of NO and NO_2
- VOCR was calculated as the measured OHR minus the reactivity of species that do not form RO_2 radicals (e.g., CO, NO_2)
- $P\mathrm{HO}_x$ was calculated as equal to the measured rate of HO_x loss, using Eq. (4A.1) and measured HO_x radical concentrations
- α_{eff} was calculated as the reactivity-weighted average of α_i for all measured VOCs.

The comparison of $\int P\mathrm{O}_3$ calculated from the full data set and that from the steady-state HO_x model is shown in Fig. 4B.1A. The two calculations are well-correlated with a slope close to 1, showing that the steady-state HO_x model can accurately reproduce ozone production at this location.

To use this model to explore how ozone production changes with temperature, the diurnal cycle and trend in temperature of each of these inputs was calculated. Because the response to temperature is different at different times of day, the trend with temperature was calculated independently for each half-hour bin, and is shown in Fig. 4B.2. These trends were used to construct temperature-dependent diurnal cycles of each of the parameters, which were then used as inputs to the model at a range of daily average afternoon temperatures

from 24–32 °C. Figure 4B.1B shows that $\int PO_3$ calculated this way has a very similar trend with temperature as that using the full data set, although it cannot capture day-to-day variability not caused by temperature. The nonlinear shape of the trend with temperature is caused primarily by the imposed exponential increase of PHO_x with temperature. Using a linear or quadratic increase of PHO_x with temperature changes the shape of the increase but does not significantly affect the overall $\int PO_3$-T slope.

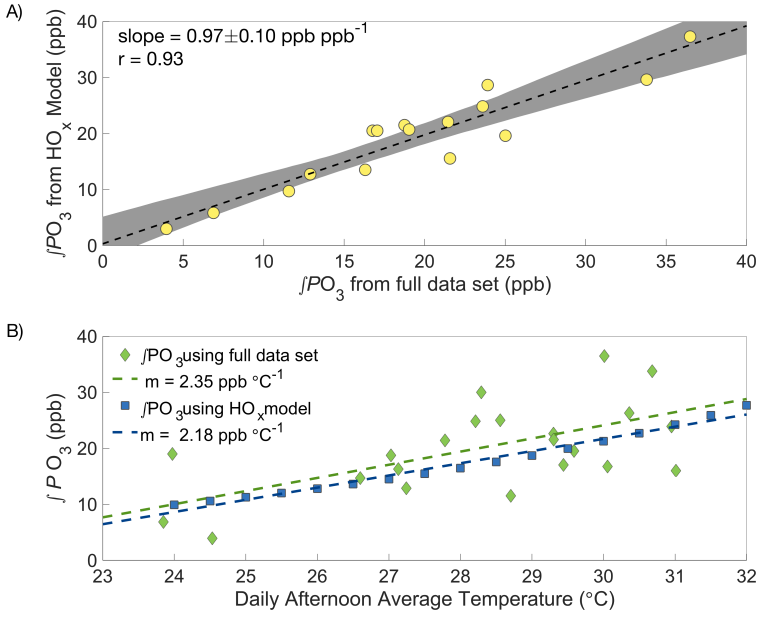

Figure 4B.1: Panel A: Comparison of $\int PO_3$ based on the full data set and simplified HO_x model; Panel B: comparison of the $\int PO_3$-T trend using all data (green diamonds) and HO_x model using only the diurnal cycle and trend with temperature of the inputs (blue squares).

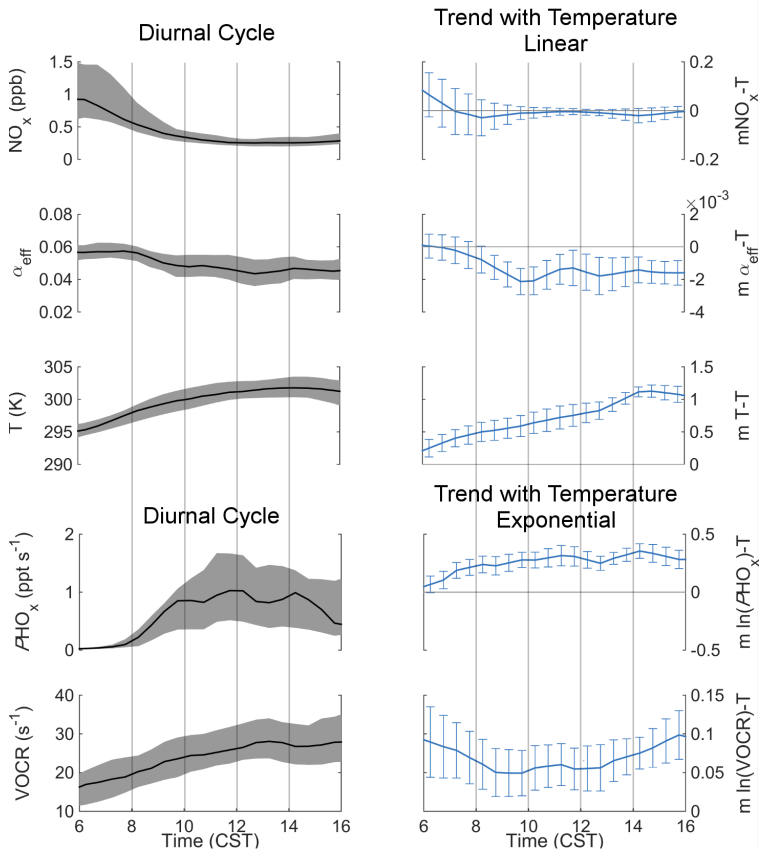

Figure 4B.2: Measurement inputs for the O_3-T decomposition, showing the observed diurnal cycle (left side) and trend with temperature (right side). The trends for VOCR and $P\mathrm{HO_x}$ are reported on a log-scale, representing an expected exponential increase with temperature. In the left column, the black lines and shaded gray areas show the median and interquartile range for each parameter; in the right column the line and error bars show the calculated trend and its associated uncertainty from a least-squares regression.

Chapter 5

The changing role of organic nitrates in the removal and transport of NO_x

5.1 Introduction

The chemistry of nitrogen oxides ($NO_x \equiv NO + NO_2$) controls the concentration of tropospheric oxidants, including OH, O_3, and NO_3. As a result, the concentration of NO_x plays a major role in the formation of toxic air pollutants including O_3 and aerosols and determining the lifetime of greenhouse gases such as methane. NO_x emissions also directly contribute to deposition of nitrogen to sensitive ecosystems (Fowler et al., 2013). Due to its harmful effects to the environment and human health, NO_x has been the target of emission control strategies since the 1970s, causing anthropogenic NO_x emissions to have decreased by a factor of 2 or more in the United States over the past 30 years (United States Environmental Protection Agency, 2018). Understanding the consequences of these past changes and predicting the results of future emissions reductions on the atmosphere requires a quantitative description of feedbacks between NO_x concentrations and NO_x chemistry.

After emission to the atmosphere, removal of NO_x occurs through two primary pathways: conversion to HNO_3 and conversion to alkyl and multifunctional nitrates ($RONO_2$). As described in Ch. 3, HNO_3 is nearly chemically inert in the troposphere, with a lifetime to reaction or photolysis of over 50 hours, and is removed almost entirely by wet and dry deposition. $RONO_2$ are a class of diverse molecules, with atmospheric lifetimes ranging from hours to days depending on the properties of the organic backbone (R-group). The loss of $RONO_2$ is divided among reactions that release NO_x from the R-group and recycle it back to the atmosphere, reactions that result in heterogeneous hydrolysis to form HNO_3, and direct deposition. The latter two pathways permanently remove NO_x from the atmosphere (Nguyen et al., 2015; Romer et al., 2016; Fisher et al., 2016). Other NO_x oxidation products, such as peroxy acetyl nitrate (PAN) or HONO can play an important role in the transport and redistribution of NO_x but do not lead to permanent NO_x removal.

Historically, direct HNO_3 production was thought to be the only important NO_x loss

pathway, with $RONO_2$ chemistry playing at most a minor role. However, several studies have shown that the rate of formation of $RONO_2$ in cities or forested regions can be competitive with or greater than the direct production rate of nitric acid (Rosen et al., 2004; Farmer et al., 2011; Browne et al., 2013; Romer et al., 2016; Sobanski et al., 2017).

The relative rate of HNO_3 and $RONO_2$ production is an important factor in setting the lifetime of NO_x (Romer et al., 2016) and affects the response of NO_x loss to temperature (Romer et al., 2018). Due to the different production pathways of HNO_3 and $RONO_2$, the relative production rate of HNO_3 and $RONO_2$ also controls how NO_x loss and ozone production are affected by changes to emissions of NO_x or VOCs. By terminating the radical chain reactions, the formation of $RONO_2$ serves to suppress ozone formation in polluted areas (Perring et al., 2010; Farmer et al., 2011; Edwards et al., 2013; Lee et al., 2014b). Several studies have also shown that $RONO_2$ can efficiently partition into aerosols, potentially explaining a large portion of secondary organic aerosol in a wide range of environments (Rollins et al., 2012; Pye et al., 2015; Xu et al., 2015b; Lee et al., 2016).

Here, we use in situ observations from a collection of 13 different field deployments to investigate how the relative production of $RONO_2$ and HNO_3 varies across the United States and how this fraction may change in the future. We show that the relative production of $RONO_2$ and HNO_3 in the daytime can be well described by the relative OH reactivity of NO_2 and the combined VOC mixture. As both anthropogenic NO_x and anthropogenic VOC emissions have decreased substantially over the past 20 years, the relative role of these two pathways has shifted as well. While the shift has generally been towards an increasing role for $RONO_2$ chemistry, the shift has been smallest in large cities and largest in the transitional regime around them. Combined with changing emissions patterns of NO_x, the shift in NO_x chemistry is leading to a flatter distribution of NO_x across the continental United States.

5.2 NO_x chemistry and production of $RONO_2$ and HNO_3

NO_x is emitted to the atmosphere as NO from a range of anthropogenic and biogenic sources, including motor vehicles, power plants, lightning, fires, and soil bacteria. Once in the atmosphere, NO interconverts with NO_2 on a timescale of minutes through reactions (R5.1)–(R5.2), forming the chemical family NO_x. When NO_x is combined with VOCs and hydrogen oxides (HO_x), a set of linked radical chain reactions is formed (R5.3–R5.6). As part of these reactions, two molecules of NO are oxidized to NO_2, leading to the net production of O_3 through reaction (R5.2).

$$NO + O_3 \longrightarrow NO_2 + O_2 \tag{R5.1}$$

$$NO_2 + h\nu + O_2 \longrightarrow O_3 + NO \tag{R5.2}$$

$$OH + R + O_2 \longrightarrow RO_2 + H_2O \tag{R5.3}$$

$$RO_2 + NO \longrightarrow RO + NO_2 \tag{R5.4a}$$

$$RO + O_2 \longrightarrow R'CHO + HO_2 \quad \text{(R5.5)}$$

$$HO_2 + NO \longrightarrow OH + NO_2 \quad \text{(R5.6)}$$

These reactions that propagate the catalytic cycle occur at the same time as reactions that remove NO_x from the atmosphere, terminating the cycle.

$$OH + NO_2 + M \longrightarrow HNO_3 + M \quad \text{(R5.7)}$$

$$RO_2 + NO + M \longrightarrow RONO_2 + M \quad \text{(R5.4b)}$$

Direct HNO_3 production occurs through the association of OH with NO_2 (R5.7). $RONO_2$ compounds are produced as a minor channel of the RO_2+NO reaction (R5.4b). Some fraction of the time α, these two radicals will associate to form an organic nitrate, with the balance producing O_3 via reaction (R5.4a). The branching ratio α is determined by the nature of the R-group as well as the temperature and pressure. Longer carbon backbones and lower temperatures increase α, while lower pressures and oxygenated functional groups decrease it (Wennberg et al., 2018). Typical values of α in the summertime continental boundary layer range from near 0 for small hydrocarbons and most oxygenated compounds to over 0.20 for large alkanes and alkenes (Perring et al., 2013).

The rate of total alkyl and multifunctional nitrate ($\Sigma RONO_2$) production can be calculated from the properties of individual VOCs measured in the atmosphere (5.1).

$$P(\Sigma RONO_2) = [OH] \sum_{R_i} [R_i] \cdot k_{OH+R_i} \cdot Y_{RO_{2i}} \cdot f_{NO_i} \cdot \alpha_i \quad (5.1)$$

In (5.1), $Y_{RO_{2i}}$ represents the yield of RO_2 radicals from VOC oxidation (typically 1) and f_{NO_i} represents the fraction of those RO_2 radicals that react with NO instead of reacting with HO_2 or undergoing unimolecular isomerization (e.g., Teng et al., 2017). f_{NO_i} is equal to 1 under polluted or moderately polluted conditions, but decreases in low-NO_x conditions.

If the contributions from individual VOCs are summed and averaged, the total production of $RONO_2$ can also be written in terms of the effective behavior of the VOC mixture (5.2), where VOCR is the sum of all measured VOC concentrations weighted by their reaction rate with OH.

$$P(\Sigma RONO_2) = [OH] \cdot VOCR \cdot Y_{RO_{2eff}} \cdot f_{NO_{eff}} \cdot \alpha_{eff} \quad (5.2)$$

In a similar fashion, the production of HNO_3 can be calculated via (5.3), where NO_2R is the NO_2 reactivity, or the concentration of NO_2 times k_{OH+NO_2}. At 298 K and 1 atm, 10 ppb of NO_2 is equivalent to an NO_2R of 2.3 s^{-1}.

$$P(HNO_3) = [OH] \cdot [NO_2] \cdot k_{OH+NO_2} = [OH] \cdot NO_2R \quad (5.3)$$

Total NO_x loss is the sum of the conversion to HNO_3 and conversion to $RONO_2$. The fraction of NO_x loss via $\Sigma RONO_2$ production can be expressed analytically as Eq. (5.4).

$$\frac{P(\Sigma\mathrm{RONO_2})}{P(\Sigma\mathrm{RONO_2}) + P(\mathrm{HNO_3})} = \left(1 + \frac{1}{\alpha_{\mathrm{eff}} \cdot f_{\mathrm{NO_{eff}}} \cdot Y_{\mathrm{RO_{2eff}}}} \times \frac{\mathrm{NO_2R}}{\mathrm{VOCR}}\right)^{-1} \tag{5.4}$$

The relative production of $\Sigma RONO_2$ and HNO_3 is seen to be controlled by two factors, the first describing the chemistry of RO_2 radicals (α_{eff}, $f_{\mathrm{NO_{eff}}}$, $Y_{\mathrm{RO_{2eff}}}$), and the second the ratio of NO_2R to VOCR, which describes whether OH is more likely to react with a VOC or with NO_2. Because Eq. (5.4) concerns fractional loss of NO_x, the concentration of OH, which affects $\Sigma RONO_2$ and HNO_3 production equally, does not appear in the result.

We show below that in the summertime continental boundary layer, the terms describing RO_2 radical chemistry vary significantly less than the NO_2R/VOCR ratio, allowing the relative importance of $RONO_2$ and HNO_3 chemistry to be roughly estimated from only a single variable.

5.3 Insights from 20 years of observations

Relative $RONO_2$ and HNO_3 production was calculated for 13 separate campaign deployments in the northern hemisphere over the past 20 years. Campaigns were selected that included measurements of $\Sigma RONO_2$, NO_x, HNO_3, O_3, HCHO, and a wide range of VOCs. Although they do not include measurements of $\Sigma RONO_2$, ITCT2k2 and CALNEX-P3 were also included to provide a pair of measurements of VOCs and NO_x in the same geographic location separated in time. A list of all campaigns used in this chapter is given in Table 5.1. Where available, measurements of OH and HO_2 were used to directly calculate RO_2 formation and loss; when these radicals were not available, OH, HO_2, and RO_2 radical concentrations were calculated iteratively based on the rate of HO_x radical production by O_3 and HCHO photolysis.

The fraction of total NO_x loss occurring via $RONO_2$ chemistry from all 13 of these campaigns is shown in Fig. 5.1A for points within the continental summertime boundary layer. Despite spanning a large range of environments, all 13 campaigns are well described by a single function of the form $(1 + b \cdot (^{\mathrm{NO_2R}}/_{\mathrm{VOCR}})^m)^{-1}$ (red line in Fig. 5.1). This roughly matches the expected form if the VOC mixture were constant between environments, and so all parameters other than the NO_2R/VOCR ratio remained constant (gray line in Fig. 5.1). However, the binned data exhibits a sharper transition from HNO_3-dominated to $RONO_2$-dominated NO_x loss, likely due to an increase in α_{eff} as NO_2R/VOCR decreases.

The calculated increase in fractional NO_x loss via $RONO_2$ chemistry as NO_2R/VOCR decreases is matched by an increase in the ratio of $\Sigma RONO_2$ to the sum of $\Sigma RONO_2$ and HNO_3 (Fig. 5.1B). However, the increase in fractional concentrations as NO_2R/VOCR decreases is much less than the increase in fractional production. At low NO_2R/VOCR ratios, the dominant $RONO_2$ species are typically short-lived and can undergo heterogeneous hydrolysis to produce HNO_3, as described in Ch. 2. This indirect source of HNO_3 can be the

Table 5.1: Field campaigns used in this chapter.

Campaign name	Format	Year	Base of Operations	Date
ITCT2k2	Airborne	2002	Monterey, CA	22 Apr – 19 May
INTEX-NA	Airborne	2004	Palmdale, CA	2 Jul
			Mascoutah, IL	7 Jul – 14 Jul
			Portsmouth, NH	16 Jul – 10 Aug
			Mascoutah, IL	12 Aug
INTEX-B	Airborne	2006	Houston, TX	4 Mar – 19 Mar
			Honolulu, HI	23 Apr – 28 Apr
			Anchorage, AK	1 May – 12 May
BEARPEX 2007	Ground	2007	Georgetown, CA	15 Aug –10 Oct
ARCTAS-B	Airborne	2008	Palmdale, CA	18 Jun – 24 Jun
			Cold Lake, Alberta, CAN	29 Jun – 8 Jul
			Thule, Greenland	8 Jul – 10 Jul
BEARPEX 2009	Ground	2009	Georgetown, CA	15 Jun – 31 Jul
CALNEX-P3	Airborne	2010	Ontario, CA	1 May – 22 Jun
CALNEX-SJV	Ground	2010	Bakersfield, CA	15 May – 30 Jun
DC3	Airborne	2012	Salina, KS	13 May – 30 Jun
SOAS	Ground	2013	Centreville, AL	1 Jun – 15 Jul
SEAC4RS	Airborne	2013	Houston, TX	8 Aug – 23 Sep
FRAPPÉ	Airborne	2014	Broomfield, CO	16 Jul –16 Aug
KORUS-AQ	Airborne	2016	Pyeongtaek, ROK	1 May – 14 Jun
			Palmdale, CA	17 Jun – 18 Jun

greatest source of HNO_3 in forested environments, and leads to the much weaker dependence of fractional concentration on NO_2R/VOCR than fractional NO_x loss.

The conclusion that variation in RO_2 parameters is small compared to the variation in the NO_2R/VOCR ratio does not hold outside of the summertime continental boundary layer. In the remote marine boundary layer or in the upper troposphere, α_{eff} is extremely low, as the dominant VOCs produce alkyl nitrates at yields of 0.01 or less (Mao et al., 2009; Perring et al., 2013). Under these conditions, HNO_3 production dominates NO_x loss even when NO_2R/VOCR is less than 0.03. Similarly, while $f_{\text{NO}_{\text{eff}}}$ can drop to near zero in remote marine environments, the combined observations over land show that background concentrations of NO_x are sufficient to keep $f_{\text{NO}_{\text{eff}}}$ above 0.20 over 95% of the time. By restricting our analysis to the summertime continental boundary layer, extremely low values of both α_{eff} and $f_{\text{NO}_{\text{eff}}}$ are avoided, and the relative production of $RONO_2$ and HNO_3 can be estimated from the NO_2R/VOCR ratio.

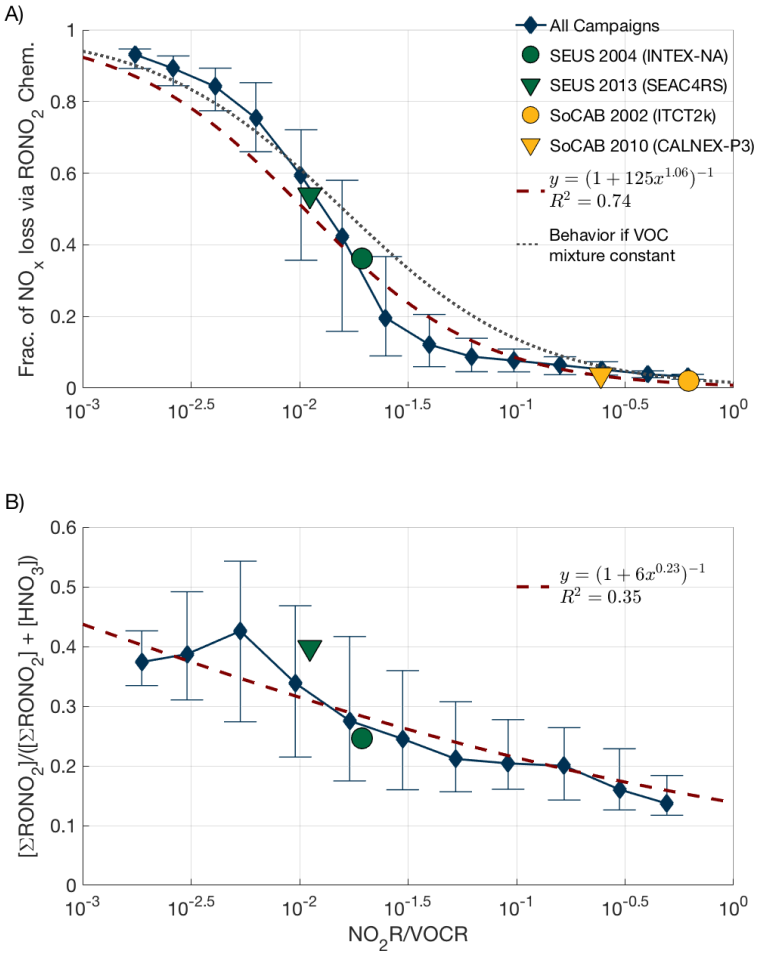

Figure 5.1: Comparison of the relative production rates of $\Sigma RONO_2$ and HNO_3 as a function of $NO_2R/VOCR$. Used data points are restricted to the continental summertime boundary layer (i.e., over land, less than 1.5 km above ground level, and average temperature > 10 °C). Panel A shows the fraction of NO_x loss attributable to $RONO_2$ chemistry, as well as a least-squares fit to the data and the expected behavior if α_{eff}, $f_{\text{NO}_{\text{eff}}}$, $Y_{\text{RO}_{2\text{eff}}}$ were constant. Panel B shows the ratio of $\Sigma RONO_2$ to the sum of HNO_3 and $\Sigma RONO_2$.

5.4 Trends over time

The simple dependence shown in Fig. 5.1A suggests that Eq. (5.4) could be used to understand trends in NO_x chemistry over time. Doing so requires replacing the observed variation across space for variation across time, which is not necessarily equivalent. However, two direct comparisons of fractional NO_x loss in the same environment but at different times are found to fall along the same curve as the variation between campaigns in different locations (Fig. 5.1). The first case, INTEX-NA and SEAC4RS, sampled the southeast United

States (SEUS) in 2004 and 2013; the second case, ITCT2k2 and CALNEX-P3, sampled the South Coast Air Basin (SoCAB) around Los Angeles, CA in 2002 and 2010. Averages from these pairs of campaigns are shown in Fig. 5.1A and all four points fall along the same overall curve. For INTEX-NA and SEAC4RS, the shift in chemistry towards the $RONO_2$-dominated regime is accompanied by a dramatic shift in the ratio of $\Sigma RONO_2$ and HNO_3 concentrations, where $\Sigma RONO_2$ concentrations were only 1/4 of HNO_3 in 2004 but were nearly equal in 2013. $\Sigma RONO_2$ measurements are not available for ITCT2k2 or CALNEX-P3, preventing a similar comparison from being made for those campaigns.

Together, these cases indicate that the trend from Fig. 5.1A can be used to predict changes in fractional loss if the trend in $NO_2R/VOCR$ is known. Over the past decade, satellite measurements of NO_2 show a significant decrease in national NO_2 concentrations, reporting an average decrease of 4.5–7 % per year between 2005 and 2011 (Russell et al., 2012). No comparable satellite observations of VOCs exist, but studies in multiple locations have reported a decrease in primary anthropogenic VOC concentrations of 5.5–7.5 % per year over 2000–2010 (Geddes et al., 2009; Warneke et al., 2012; Pollack et al., 2013; Pusede et al., 2014). In contrast, biogenic VOC concentrations have been either constant or increasing over that same time period (Geddes et al., 2009; Hidy et al., 2014). Oxygenated VOCs show no major trend with time, although there are few long-term measurements of these species (Geddes et al., 2009; Pusede et al., 2014).

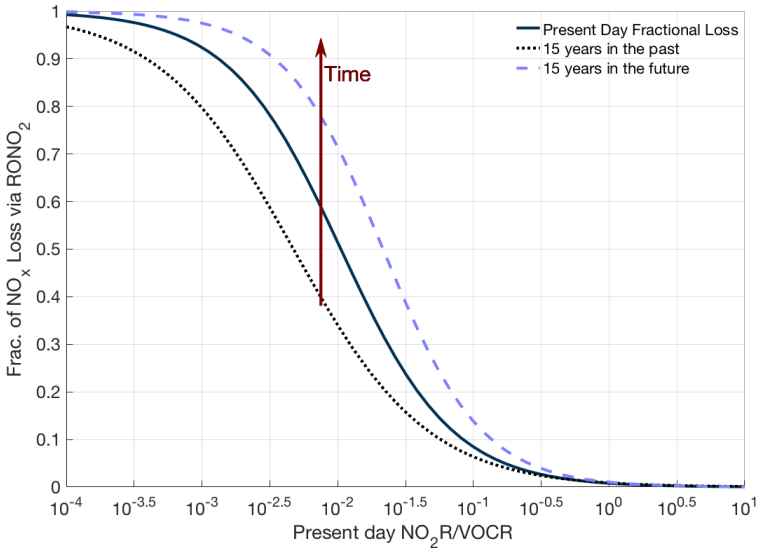

Figure 5.2: Predicted trends in fractional NO_x loss over time.

These varied trends in NO_x, anthropogenic VOCs, and biogenic VOCs indicate that $NO_2R/VOCR$ has not changed uniformly over the past decade. Past $NO_2R/VOCR$ ratios were calculated by assuming a 6.5 % yr^{-1} decrease in anthropogenic VOC concentrations, a 5.5 % yr^{-1} decrease in NO_x concentrations, and a 1.5 % yr^{-1} increase in biogenic VOC

concentrations over the past 15 years. We also extrapolate these same trends to estimate NO_2R/VOCR 15 years in the future. The calculated NO_2R/VOCR ratios are combined with the relationship from Fig. 5.1A to estimate fractional NO_x loss at different times (Fig. 5.2). While this chapter is focused on the variables that control NO_x oxidation, these changes in emissions will also have significant impacts on VOC oxidation and aerosol formation more broadly. For example, lower concentrations of NO_x will affect the yield of secondary organic aerosol (Xu et al., 2015a) and will increase the yield of peroxides and epoxides from isoprene oxidation (Teng et al., 2017).

Based on these trends, $RONO_2$ chemistry is seen to have become a larger portion of total NO_x loss over the past 15 years, although the change has not been evenly distributed. The similar trends in NO_x and anthropogenic VOCs cause there to have been little to no change in the regions with the highest NO_2R/VOCR ratios (typically large cities). The largest changes are projected to occur in regions with moderate NO_2R/VOCR ratios. In these regions, biogenic VOCs generally account for a greater fraction of the VOCR, leading to significant decreases in NO_2R/VOCR over the past 15 years. In addition, the response of fractional loss to changes in the NO_2R/VOCR ratio is magnified in areas where both $RONO_2$ and HNO_3 chemistry contribute to NO_x loss. In this transitional regime, if recent trends continue, the fraction of NO_x loss occurring via $RONO_2$ chemistry could double in the next 15 years. Many regions of the United States are therefore likely to transition from a regime where HNO_3 dominates NO_x loss to a mixed or $RONO_2$-dominated regime.

5.5 Impacts of the transition from the HNO_3 to the $RONO_2$ regime

The growing importance of $RONO_2$ chemistry to NO_x loss has several implications for air quality. Most directly, it means that understanding NO_x chemistry in all but the most polluted megacities requires including the effects of $RONO_2$ chemistry. More theoretically, the transition from HNO_3- to $RONO_2$-dominated NO_x loss affects how atmospheric chemistry will respond to changes in emissions of NO_x and VOCs. Because $RONO_2$ are produced in the same set of reactions that produce O_3, the fractional loss of NO_x via $\Sigma RONO_2$ chemistry is directly proportional to the ozone production efficiency (OPE), the ratio of ozone production to NO_x loss (5.5).

$$OPE = \frac{P\mathrm{O_3}}{\mathcal{L}\mathrm{NO_x}} = \frac{2 \cdot \mathrm{VOCR} \cdot Y_{\mathrm{RO_{2eff}}} \cdot f_{\mathrm{NO_{eff}}} \cdot (1 - \alpha_{\mathrm{eff}})}{\mathrm{NO_2R} + \mathrm{VOCR} \cdot Y_{\mathrm{RO_{2eff}}} \cdot f_{\mathrm{NO_{eff}}} \cdot \alpha_{\mathrm{eff}}} \propto \frac{P(\Sigma\mathrm{RONO_2})}{P(\Sigma\mathrm{RONO_2}) + P(\mathrm{HNO_3})} \quad (5.5)$$

Fundamentally, OPE represents the total amount of ozone produced for each molecule of NO_x emitted (Trainer et al., 1993; Kleinman et al., 1994). When considering ozone pollution on regional scales, OPE is a more comprehensive metric than $P\mathrm{O_3}$ because it accounts for ozone production both locally and further afield.

Figure 5.3 uses the analytical framework based on a simplified chemical mechanism from Ch. 4 to investigate how ozone and NO_x chemistry changes as a function of NO_2R/VOCR.

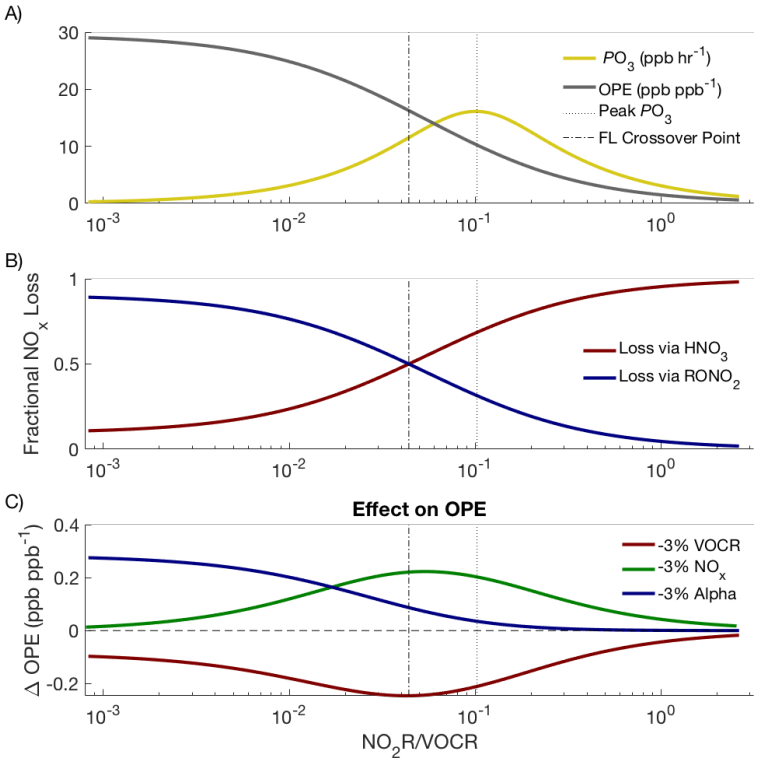

Figure 5.3: Theoretical picture of NO_x and O_3 chemistry, calculated using variable NO_x concentrations and fixed VOCR, PHO_x, and α_{eff}. Panel A shows how PO_3 and OPE change as NO_x changes; Panel B shows how the fractional NO_x loss changes as $NO_2R/VOCR$ decreases; Panel C shows that changes to NO_x and VOCR have their greatest effect on OPE not when PO_3 is at a maximum, but at the crossover point between the $RONO_2$-dominated and HNO_3-dominated regimes.

As the $NO_2R/VOCR$ ratio decreases, OPE increases, reaching an inflection point exactly at the crossover point between the HNO_3-dominated and $RONO_2$-dominated regimes (Fig 5.3A–B). For the polluted areas in the country, where HNO_3 is the dominant NO_x loss pathway, this means that, for example, interventions to improve air quality by reducing NO_x emissions will be fighting uphill, because every incremental decrease in NO_x emissions will be associated with a growing incremental increase in OPE (Fig. 5.3C).

As $RONO_2$ chemistry becomes a more important part of the NO_x budget, changes to α_{eff} have an increasing effect on OPE (Fig. 5.3C). Policy interventions that reduce VOCR but preferentially target high-α compounds (e.g., long-chain alkanes) could inadvertently increase ozone production or ozone production efficiency (Farmer et al., 2011; Perring et al., 2013).

In addition to the large effects on aerosol yield that changes to NO_x and VOC emissions have directly (e.g., Pusede et al., 2016; Zhang et al., 2018), changing emissions also affect

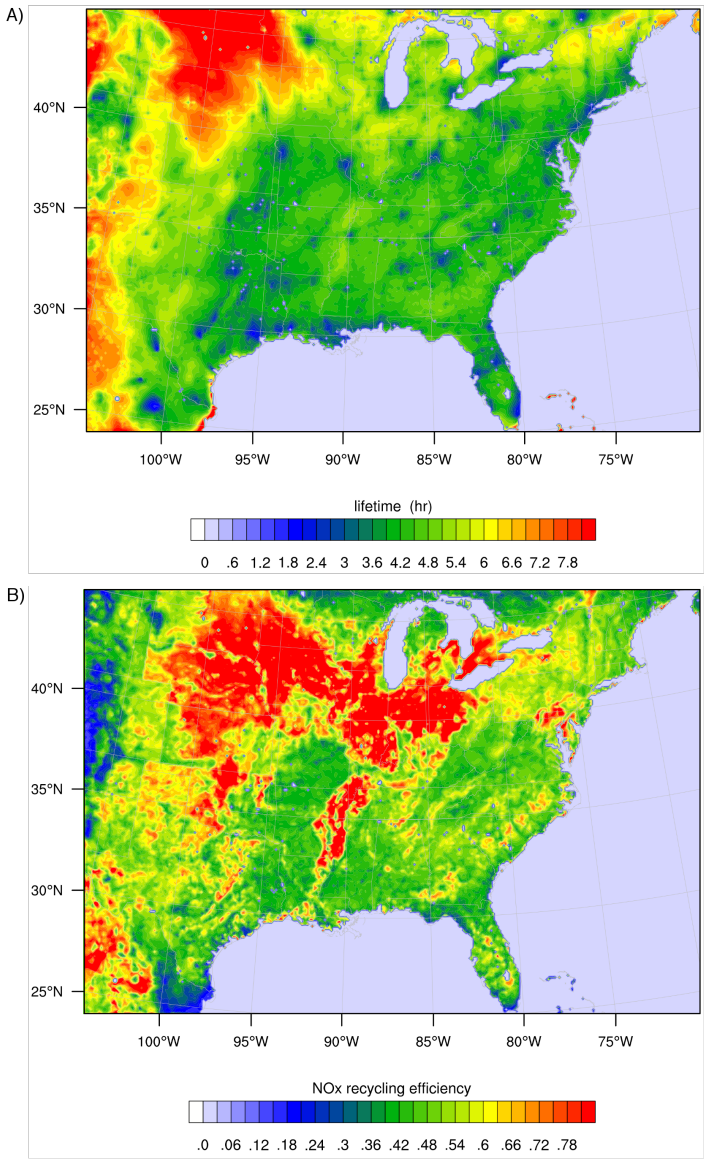

Figure 5.4: WRF-Chem simulation of $RONO_2$ chemistry over the southeast United States for summer 2013 as described in Zare et al. (2018). Panel A shows the overall lifetime of $\Sigma RONO_2$, defined as the concentration of $\Sigma RONO_2$ divided by the $\Sigma RONO_2$ loss rate. Panel B shows the average NO_x recycling efficiency, defined as the local rate of NO_x production from $\Sigma RONO_2$ oxidation divided by the rate of $\Sigma RONO_2$ production.

aerosols by changing the fate of NO_x. While both HNO_3 and $RONO_2$ can form aerosols (Stelson and Seinfeld, 1982; Pye et al., 2015), the properties of the resulting aerosols are likely to differ. Because HNO_3 is a strong acid, a shift towards $RONO_2$ chemistry is likely

to increase aerosol pH. In addition, an increase in the role of $RONO_2$ chemistry is likely to cause more of the nitrate aerosol to be organic rather than inorganic. This in turn has the potential to affect the viscosity and morphology of aerosols.

Further effects of changing NO_x chemistry arise from the distinct fates of $\Sigma RONO_2$ and HNO_3. Many $RONO_2$, especially those derived from isoprene, are remarkably reactive in the troposphere, with lifetimes of a few hours or less. A fraction of this $RONO_2$ loss returns NO_x to the atmosphere, allowing $RONO_2$ production to effectively transport NO_x downwind (Romer et al., 2016; Xiong et al., 2016). In contrast, HNO_3 is effectively chemically inert in the troposphere, with a chemical lifetime of 50 hours or more.

As a result of the differing chemical fates and lifetimes, transitioning from a HNO_3-dominated regime to a mixed or $RONO_2$-dominated regime has implications for the distribution of NO_x on regional to continental scales. If a greater fraction of NO_x in polluted or moderately polluted regions is converted into $RONO_2$ rather than HNO_3, then more of the NO_x may be re-released downwind, where it can participate in radical chemistry and ozone production. Simulations of $RONO_2$ chemistry using WRF-Chem and the RACM2_Berkeley2 mechanism (Zare et al., 2018) were used to investigate the $\Sigma RONO_2$ lifetime and NO_x recycling efficiency of $\Sigma RONO_2$ across the southeast United States in summer 2013 (Fig. 5.4). Across much of the region, $\Sigma RONO_2$ is calculated to have a lifetime of roughly 4 hours, and release of NO_x from $\Sigma RONO_2$ oxidation was between 40 and 75% of the instantaneous $\Sigma RONO_2$ production rate. Combined, these findings demonstrate a significant role for $RONO_2$ chemistry in the transport of NO_x between regions. The effects of organic nitrate chemistry on the distribution of NO_x is likely to vary greatly across the United States and should be studied in further detail.

Enhanced NO_x transport between source and receptor regions is one aspect of a combined trend that is transforming the spatial distribution of NO_x. Over the past decade, NO_x emissions reductions have been concentrated in the most polluted environments. In these areas, motor vehicles and power plants, the largest targets of emission control strategies, account for almost all of the NO_x emissions. In less polluted regions, less controllable sources of NO_x, including soil microbes (both in agricultural and non-agricultural regions), off-road vehicles, fires, and lightning, play a greater role in the NO_x budget, reducing the effectiveness of combustion-related NO_x emissions controls. In addition, hemispheric background concentrations of NO_x and O_3 have risen slightly over the past two decades (e.g., Cooper et al., 2012). The combination of all three of these trends suggests that the distribution of NO_x across the United States is getting flatter over time. This trend matches satellite observations of NO_2 over the continental United States. Fig. 5.5 shows the cumulative frequency distribution of summertime tropospheric NO_2 columns from 2005–2007 and 2015–2017 using the Berkeley High-Resolution (BEHR, Russell et al., 2011) v3.0A retrieval of data from the Ozone Monitoring Instrument (OMI), using simulated monthly a priori profiles. Over this time, the highest percentiles NO_2 concentrations have decreased and the lowest percentiles increased, leading to a significantly narrower distribution of NO_2 concentrations.

In summary, over the past 15 years, decreases in anthropogenic NO_x and VOC emissions have led to a significant shift in the mechanisms of NO_x loss. Many places where HNO_3

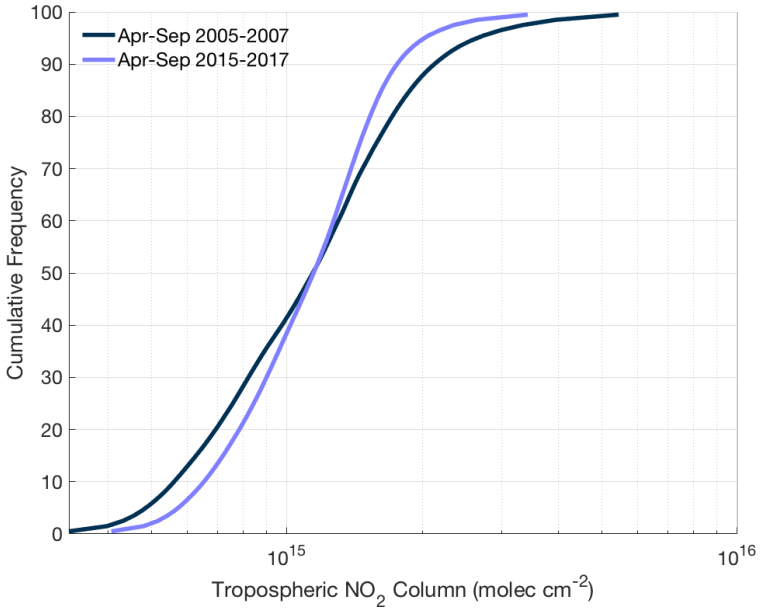

Figure 5.5: Cumulative frequency distribution of OMI tropospheric NO_2 columns over the continental United States using the BEHR retrieval for summer (Apr–Sep) in 2005–2007 and 2015–2017.

production dominated NO_x loss are now mixed or have switched to a situation where the majority of NO_x loss occurs through $RONO_2$ chemistry. If past trends continue, $RONO_2$ chemistry will grow to become an even more important fraction of NO_x chemistry in coming decades. As a result of this combination of changing NO_x chemistry, decreasing NO_x emissions, and increasing background concentrations, air pollution in the United States may transform from a highly local issue to a more extended regional one. Efforts to control air pollution focused only on local sources are less likely to be effective; future improvements in air quality and attaining the most recent National Ambient Air Quality Standards is likely to require coordinated efforts on regional scales to broadly reduce NO_x emissions.

Chapter 6

Conclusion

6.1 Summary

Over the past 30 years, the success of air quality regulations in the United States has led to dramatic increases in public health and significant changes in atmospheric chemistry. Continued improvements in air quality will require greater understanding of the chemical production and loss of NO_x and how they are affected by anthropogenic emissions and temperature. In this dissertation, I combined short-term field campaigns and long-term monitoring to describe new constraints on the fate of different NO_x oxidation products and analyze how the chemical removal of NO_x has changed over the past 15 years. I have described new frameworks for thinking about the lifetime of NO_x to aid in understanding the effects that changes in anthropogenic emissions and temperature have on the chemical removal of NO_x

The results in this dissertation add to the growing body of literature arguing that NO_x chemistry in rural and remote regions is significantly more active than often assumed. In the southeast United States, the rate of $\Sigma RONO_2$ formation peaks at over 100 ppt h^{-1}. To sustain the observed concentrations of NO_x and explain the nighttime buildup of NO_2, both significant local emission of NO_x and recycling of NO_x from $\Sigma RONO_2$ oxidation are necessary. Over the Yellow Sea, we find the possibility for moderate enhancements in aerosol nitrate photolysis over that of gas-phase HNO_3, suggesting cycling between NO_x and HNO_3 may be more rapid than currently represented in models, although less rapid than others have recently argued. The result is active, bi-directional cycling of NO_x, affecting the transport of NO_x and the response of O_3 production to temperature on regional scales.

One additional consequence of this rapid chemistry is that efforts to improve air quality in the United States should include efforts to reduce regional background NO_x and O_3 concentrations. Even in areas that are not in violation of the NAAQS, improvements in air quality are likely to lead to significant improvements in human and ecosystem health (Ito et al., 2005; Booker et al., 2009; Correia et al., 2013). From a regulatory standpoint, broad improvements in air quality would aid attainment in more polluted regions, as urban air

problems typically exist as a local enhancement on top of a regional background (e.g., Berlin et al., 2013).

Finally, the dramatic changes in atmospheric chemistry emphasize the need for high-quality measurements over long periods of time. At this point, there exists over 25 years of measurements from intensive field campaigns, although the data for some early campaigns are not easily available. Decisions for future campaign deployments must weigh the benefits of sampling a previously unexplored location or examining changes in a region over time. To complement the results from field campaigns, long-term monitoring measurements focused not only on regulatory compliance but on scientific inquiry can provide unique constraints on the changing chemistry over time. The SEARCH network, which operated for 25 years in the southeast United States (Hansen et al., 2003), was an excellent example of such a network, making it possible to examine the long-term trends in $P\mathrm{O}_3$ with temperature described in Ch. 4. The NCORE network, started in 2011, may one day provide a similar high-quality, long-term record (Scheffe et al., 2009).

6.2 Future work

The work presented in this dissertation is one part of ongoing research, aimed at broadly understanding $\mathrm{NO_x}$ chemistry in a wide range of environments, and raises several additional questions for future inquiry. I list some of these questions below:

1. How much of atmospheric $\mathrm{NO_x}$ is currently biogenic in origin? As direct anthropogenic $\mathrm{NO_x}$ emissions have declined, soil microbial emissions are becoming increasingly important to the $\mathrm{NO_x}$ budget. In Ch. 4, I showed signatures of significant biogenic $\mathrm{NO_x}$ sources at the SOAS site, suggesting that they could explain up to 50% of the total $\mathrm{NO_x}$ at this location. However, due to significant variability in measurements of soil $\mathrm{NO_x}$ emissions at different locations, this result cannot be extrapolated to the broader southeast United States. Trends in biogenic $\mathrm{NO_x}$ emissions over time also remain a significant unknown. Deposition of nitrogen to soils is thought to increase microbial $\mathrm{NO_x}$ emissions (Pilegaard et al., 2006), thus it is plausible that soil $\mathrm{NO_x}$ emissions have decreased over the past decades in conjunction with decreases in anthropogenic $\mathrm{NO_x}$ emissions. However, I know of no long-term measurements of soil $\mathrm{NO_x}$ fluxes in the United States available to test this hypothesis.

2. On what timescale does $\mathrm{NO_x}$ return to the atmosphere after deposition? I have assumed that deposition of any $\mathrm{NO_y}$ species could be treated as permanent removal of $\mathrm{NO_x}$ from the atmosphere, but some previous studies have raised the possibility for relatively rapid return of $\mathrm{NO_x}$ to the atmosphere after deposition. Zhou et al. (2011) suggested that $\mathrm{HNO_3}$ on surfaces could be rapidly photolyzed to produce HONO, and measurements in a ponderosa pine forest found surprisingly large upward fluxes of peroxy nitrates and $\mathrm{HNO_3}$, raising the possibility of rapid $\mathrm{NO_x}$ chemistry on or within tree leaves (Farmer and Cohen, 2008; Min et al., 2012).

3. What parameters control the rate of $RONO_2$ hydrolysis? While the results of Ch. 2, combined with recent laboratory studies, have convincingly shown that a large fraction of $\Sigma RONO_2$ is lost by hydrolysis, little is known about the precise mechanisms of this reaction. Recent modeling studies have either applied a fixed lifetime against hydrolysis or a reactive uptake parameter to irreversibly convert $RONO_2$ into aerosols (Fisher et al., 2016; Zare et al., 2018), neither of which reflects the likely complexity of the process. Studies of isoprene epoxydiols and N_2O_5 have all found steep dependencies of their hydrolysis rates on aerosol properties such as pH and water content (Gaston et al., 2014; McDuffie et al., 2018), suggesting that the rate of $RONO_2$ hydrolysis is likely to vary significantly between environments. Isomer-specific $RONO_2$ measurements could help untangle these dependencies and lead to better understanding of the fate and lifetime of $RONO_2$ in different environments.

Bibliography

Allen, H. M., Draper, D. C., Ayres, B. R., Ault, A., Bondy, A., Takahama, S., Modini, R. L., Baumann, K., Edgerton, E., Knote, C., Laskin, A., Wang, B., and Fry, J. L.: Influence of crustal dust and sea spray supermicron particle concentrations and acidity on inorganic NO_3^- aerosol during the 2013 Southern Oxidant and Aerosol Study, *Atmos. Chem. Phys.*, *15*(18), 10669–10685, doi: 10.5194/acp-15-10669-2015, **2015**.

Alvarado, M. J., Logan, J. A., Mao, J., Apel, E., Riemer, D., Blake, D., Cohen, R. C., Min, K.-E., Perring, A. E., Browne, E. C., Wooldridge, P. J., Diskin, G. S., Sachse, G. W., Fuelberg, H., Sessions, W. R., Harrigan, D. L., Huey, G., Liao, J., Case-Hanks, A., Jimenez, J. L., Cubison, M. J., Vay, S. A., Weinheimer, A. J., Knapp, D. J., Montzka, D. D., Flocke, F. M., Pollack, I. B., Wennberg, P. O., Kurten, A., Crounse, J., St. Clair, J. M., Wisthaler, A., Mikoviny, T., Yantosca, R. M., Carouge, C. C., and Le Sager, P.: Nitrogen oxides and PAN in plumes from boreal fires during ARCTAS-B and their impact on ozone: an integrated analysis of aircraft and satellite observations, *Atmos. Chem. Phys.*, *10*(20), 9739–9760, doi: 10.5194/acp-10-9739-2010, **2010**.

Andreae, M. O. and Merlet, P.: Emission of trace gases and aerosols from biomass burning, *Global Biogeochem. Cy.*, *15*(4), 955–966, doi: 10.1029/2000GB001382, **2001**.

Atkinson, R. and Arey, J.: Atmospheric Degradation of Volatile Organic Compounds, *Chem. Rev.*, *103*(12), 4605–4638, doi: 10.1021/cr0206420, **2003**.

Atkinson, R., Aschmann, S. M., Carter, W. P. L., Winer, A. M., and Pitts, J. N., Jr.: Alkyl Nitrate Formation from the NO_x–Air Photooxidations of C_2-C_8 *n*-alkanes, *J. Phys. Chem.*, *86*(23), 4563–4569, doi: 10.1021/j100220a022, **1982**.

Atkinson, R., Baulch, D. L., Cox, R. A., Crowley, J. N., Hampson, R. F., Hynes, R. G., Jenkin, M. E., Rossi, M. J., Troe, J., and IUPAC Subcommittee: Evaluated kinetic and photochemical data for atmospheric chemistry: Volume II – gas phase reactions of organic species, *Atmos. Chem. Phys.*, *6*(11), 3625–4055, doi: 10.5194/acp-6-3625-2006, **2006**.

Atkinson, R. W., Yu, D., Armstrong, B. G., Pattenden, S., Wilkinson, P., Doherty, R. M., Heal, M. R., and Anderson, H. R.: Concentration-Response Function for Ozone and Daily Mortality: Results from Five Urban and Five Rural U.K. Populations, *Environ. Health Persp.*, *120*(10), 1411–1417, doi: 10.1289/ehp.1104108, **2012**.

Ayres, B. R., Allen, H. M., Draper, D. C., Brown, S. S., Wild, R. J., Jimenez, J. L., Day, D. A., Campuzano-Jost, P., Hu, W., de Gouw, J., Koss, A., Cohen, R. C., Duffey, K. C., Romer, P., Baumann, K., Edgerton, E., Takahama, S., Thornton, J. A., Lee, B. H., Lopez-Hilfiker, F. D., Mohr, C., Wennberg, P. O., Nguyen, T. B., Teng, A., Goldstein, A. H., Olson, K., and Fry, J. L.: Organic nitrate aerosol formation via NO_3 + biogenic volatile organic compounds in the southeastern United States, *Atmos. Chem. Phys.*, *15*(23), 13377–13392, doi: 10.5194/acp-15-13377-2015, **2015**.

Baergen, A. M. and Donaldson, D. J.: Photochemical Renoxification of Nitric Acid on Real Urban Grime, *Environ. Sci. Technol.*, *47*(2), 815–820, doi: 10.1021/es3037862, **2013**.

Barnes, E. A. and Fiore, A. M.: Surface ozone variability and the jet position: Implications for projecting future air quality, *Geophys. Res. Lett.*, *40*(11), 2839–2844, doi: 10.1002/grl.50411, **2013**.

Baumann, K., Williams, E. J., Angevine, W. M., Roberts, J. M., Norton, R. B., Frost, G. J., Fehsenfeld, F. C., Springston, S. R., Bertman, S. B., and Hartsell, B.: Ozone production and transport near Nashville, Tennessee: Results from the 1994 study at New Hendersonville, *J. Geophys. Res.*, *105*(D7), 9137–9153, doi: 10.1029/1999JD901017, **2000**.

Beaver, M. R., St. Clair, J. M., Paulot, F., Spencer, K. M., Crounse, J. D., LaFranchi, B. W., Min, K. E., Pusede, S. E., Wooldridge, P. J., Schade, G. W., Park, C., Cohen, R. C., and Wennberg, P. O.: Importance of biogenic precursors to the budget of organic nitrates: observations of multifunctional organic nitrates by CIMS and TD-LIF during BEARPEX 2009, *Atmos. Chem. Phys.*, *12*(13), 5773–5785, doi: 10.5194/acp-12-5773-2012, **2012**.

Berlin, S. R., Langford, A. O., Estes, M., Dong, M., and Parrish, D. D.: Magnitude, Decadal Changes, and Impact of Regional Background Ozone Transported into the Greater Houston, Texas, Area, *Environ. Sci. Technol.*, *47*(24), 13985–13992, doi: 10.1021/es4037644, **2013**.

Bertman, S. B., Roberts, J. M., Parrish, D. D., Buhr, M. P., Goldan, P. D., Kuster, W. C., Fehsenfeld, F. C., Montzka, S. A., and Westberg, H.: Evolution of alkyl nitrates with air mass age, *J. Geophys. Res.*, *100*(D11), 22805–22813, doi: 10.1029/95JD02030, **1995**.

Bertram, T. H., Perring, A. E., Wooldridge, P. J., Crounse, J. D., Kwan, A. J., Wennberg, P. O., Scheuer, E., Dibb, J., Avery, M., Sachse, G., Vay, S. A., Crawford, J. H., McNaughton, C. S., Clarke, A., Pickering, K. E., Fuelberg, H., Huey, G., Blake, D. R., Singh, H. B., Hall, S. R., Shetter, R. E., Fried, A., Heikes, B. G., and Cohen, R. C.: Direct Measurements of the Convective Recycling of the Upper Troposphere, *Science*, *315*(5813), 816–820, doi: 10.1126/science.1134548, **2007**.

Bertram, T. H., Perring, A. E., Wooldridge, P. J., Dibb, J., Avery, M. A., and Cohen, R. C.: On the export of reactive nitrogen from Asia: NO_x partitioning and effects on ozone, *Atmos. Chem. Phys.*, *13*(9), 4617–4630, doi: 10.5194/acp-13-4617-2013, **2013**.

Blake, N. J., Blake, D. R., Simpson, I. J., Meinardi, S., Swanson, A. L., Lopez, J. P., Katzenstein, A. S., Barletta, B., Shirai, T., Atlas, E., Sachse, G., Avery, M., Vay, S., Fuelberg, H. E., Kiley, C. M., Kita, K., and Rowland, F. S.: NMHCs and halocarbons in Asian continental outflow during the Transport and Chemical Evolution over the Pacific (TRACE-P) Field Campaign: Comparison With PEM-West B, *J. Geophys. Res.*, *108*(D20), 8806, doi: 10.1029/2002JD003367, **2003**a.

Blake, N. J., Blake, D. R., Sive, B. C., Katzenstein, A. S., Meinardi, S., Wingenter, O. W., Atlas, E. L., Flocke, F., Ridley, B. A., and Rowland, F. S.: The seasonal evolution of NMHCs and light alkyl nitrates at middle to high northern latitudes during TOPSE, *J. Geophys. Res.*, *108*(D4), 8359, doi: 10.1029/2001JD001467, **2003**b.

Booker, F., Muntifering, R., McGrath, M., Burkey, K., Decoteau, D., Fiscus, E., Manning, W., Krupa, S., Chappelka, A., and Grantz, D.: The ozone component of global change: potential effects on agricultural and horticultural plant yield, product quality and interactions with invasive species, *J. Integr. Plant Biol.*, *51*(4), 337–351, doi: 10.1111/j.1744-7909.2008.00805.x, **2009**.

Boyd, A. A., Flaud, P.-M., Daugey, N., and Lesclaux, R.: Rate Constants for RO_2 + HO_2 Reactions Measured under a Large Excess of HO_2, *J. Phys. Chem. A*, *107*(6), 818–821, doi: 10.1021/jp026581r, **2003**.

Breuninger, C., Meixner, F. X., and Kesselmeier, J.: Field investigations of nitrogen dioxide (NO_2) exchange between plants and the atmosphere, *Atmos. Chem. Phys.*, *13*(2), 773–790, doi: 10.5194/acp-13-773-2013, **2013**.

Brown, S. S., Dubé, W. P., Fuchs, H., Ryerson, T. B., Wollny, A. G., Brock, C. A., Bahreini, R., Middlebrook, A. M., Neuman, J. A., Atlas, E., Roberts, J. M., Osthoff, H. D., Trainer, M., Fehsenfeld, F. C., and Ravishankara, A. R.: Reactive uptake coefficients for N_2O_5 determined from aircraft measurements during the Second Texas Air Quality Study: Comparison to current model parameterizations, *J. Geophys. Res.*, *114*(D7), D00F10, doi: 10.1029/2008JD011679, **2009**.

Brown, S. S. and Stutz, J.: Nighttime radical observations and chemistry, *Chem. Soc. Rev.*, *41*(19), 6405–6447, doi: 10.1039/C2CS35181A, **2012**.

Browne, E. C. and Cohen, R. C.: Effects of biogenic nitrate chemistry on the NO_x lifetime in remote continental regions, *Atmos. Chem. Phys.*, *12*(24), 11917–11932, doi: 10.5194/acp-12-11917-2012, **2012**.

Browne, E. C., Min, K.-E., Wooldridge, P. J., Apel, E., Blake, D. R., Brune, W. H., Cantrell, C. A., Cubison, M. J., Diskin, G. S., Jimenez, J. L., Weinheimer, A. J., Wennberg, P. O., Wisthaler, A., and Cohen, R. C.: Observations of total $RONO_2$ over the boreal forest: NO_x sinks and HNO_3 sources, *Atmos. Chem. Phys.*, *13*(9), 4543–4562, doi: 10.5194/acp-13-4543-2013, **2013**.

Burkholder, J. B., Talukdar, R. K., Ravishankara, A. R., and Solomon, S.: Temperature dependence of the HNO_3 UV absorption cross sections, *J. Geophys. Res.-Atmos.*, *98*(D12), 22937–22948, doi: 10.1029/93JD02178, **1993**.

Carter, W. P. and Atkinson, R.: Alkyl nitrate formation from the atmospheric photoxidation of alkanes; a revised estimation method, *J. Atmos. Chem.*, *8*(2), 165–173, doi: 10.1007/BF00053721, **1989**.

Chatfield, R. B.: Anomalous HNO_3/NO_x ratio of remote tropospheric air: Conversion of nitric acid to formic acid and NO_x?, *Geophys. Res. Lett.*, *21*(24), 2705–2708, doi: 10.1029/94GL02659, **1994**.

Chen, X., Hulbert, D., and Shepson, P. B.: Measurement of the organic nitrate yield from OH reaction with isoprene, *J. Geophys. Res.*, *103*(D19), 25563–25568, doi: 10.1029/98JD01483, **1998**.

Clemitshaw, K. C., Williams, J., Rattigan, O. V., Shallcross, D. E., Law, K. S., and Cox, R. A.: Gas-phase ultraviolet absorption cross-sections and atmospheric lifetimes of several C_2–C_5 alkyl nitrates, *J. Photochem. Photobio. A*, *102*(2), 117–126, doi: 10.1016/S1010-6030(96)04458-9, **1997**.

Cooper, O. R., Gao, R.-S., Tarasick, D., Leblanc, T., and Sweeney, C.: Long-term ozone trends at rural ozone monitoring sites across the United States, 1990–2010, *J. Geophys. Res. Atmos.*, *117*(D22), D22307, doi: 10.1029/2012JD018261, **2012**.

Cooper, O. R., Parrish, D. D., Ziemke, J., Balashov, N. V., Cupeiro, M., Galbally, I. E., Gilge, S., Horowitz, L., Jensen, N. R., Lamarque, J.-F., Naik, V., Oltmans, S. J., Schwab, J., Shindell, D. T., Thompson, A. M., Thouret, V., Wang, Y., and Zbinden, R. M.: Global distribution and trends of tropospheric ozone: An observation-based review, *Elem. Sci. Anth.*, *2*, 000029, doi: 10.12952/journal.elementa.000029, **2014**.

Correia, A. W., Pope, C. A., Dockery, D. W., Wang, Y., Ezzati, M., and Dominici, F.: Effect of Air Pollution Control on Life Expectancy in the United States: An Analysis of 545 U.S. Counties for the Period from 2000 to 2007, *Epidemiology*, *24*(1), 23–31, doi: 10.1097/EDE.0b013e3182770237, **2013**.

Crounse, J. D., Knap, H. C., Ørnsø, K. B., Jørgensen, S., Paulot, F., Kjaergaard, H. G., and Wennberg, P. O.: Atmospheric Fate of Methacrolein. 1. Peroxy Radical Isomerization Following Addition of OH and O_2, *J. Phys. Chem. A*, *116*(24), 5756–5762, doi: 10.1021/jp211560u, **2012**.

Crounse, J. D., McKinney, K. A., Kwan, A. J., and Wennberg, P. O.: Measurement of Gas-Phase Hydroperoxides by Chemical Ionization Mass Spectrometry, *Anal. Chem.*, *78*(19), 6726–6732, doi: 10.1021/ac0604235, **2006**.

Crounse, J. D., Paulot, F., Kjaergaard, H. G., and Wennberg, P. O.: Peroxy radical isomerization in the oxidation of isoprene, *Phys. Chem. Chem. Phys.*, *13*(30), 13607–13613, doi: 10.1039/C1CP21330J, **2011**.

Crowley, J. N., Thieser, J., Tang, M. J., Schuster, G., Bozem, H., Beygi, Z. H., Fischer, H., Diesch, J.-M., Drewnick, F., Borrmann, S., Song, W., Yassaa, N., Williams, J., Pöhler, D., Platt, U., and Lelieveld, J.: Variable lifetimes and loss mechanisms for NO_3 and N_2O_5 during the DOMINO campaign: contrasts between marine, urban and continental air, *Atmos. Chem. Phys.*, *11*(21), 10853–10870, doi: 10.5194/acp-11-10853-2011, **2011**.

Curier, R., Kranenburg, R., Segers, A., Timmermans, R., and Schaap, M.: Synergistic use of OMI NO_2 tropospheric columns and LOTOS–EUROS to evaluate the NO_x emission trends across Europe, *Remote Sens. Environ.*, *149*, 58–69, doi: 10.1016/j.rse.2014.03.032, **2014**.

Dallmann, T. R. and Harley, R. A.: Evaluation of mobile source emission trends in the United States, *J. Geophys. Res.*, *115*(D14), D14305, doi: 10.1029/2010JD013862, **2010**.

Darer, A. I., Cole-Filipiak, N. C., O'Connor, A. E., and Elrod, M. J.: Formation and Stability of Atmospherically Relevant Isoprene-Derived Organosulfates and Organonitrates, *Environ. Sci. Technol.*, *45*(5), 1895–1902, doi: 10.1021/es103797z, **2011**.

Davidson, E. A., Potter, C. S., Schlesinger, P., and Klooster, S. A.: Model Estimates of Regional Nitric Oxide Emissions from Soils of the Southeastern United States, *Ecol. Appl.*, *8*(3), 748–759, doi: 10.1890/1051-0761(1998)008[0748:MEORNO]2.0.CO;2, **1998**.

Day, D. A., Dillon, M. B., Wooldridge, P. J., Thornton, J. A., Rosen, R. S., Wood, E. C., and Cohen, R. C.: On alkyl nitrates, O_3, and the "missing NO_y", *J. Geophys. Res.*, *108*(D16), 4501, doi: 10.1029/2003JD003685, **2003**.

Day, D. A., Farmer, D. K., Goldstein, A. H., Wooldridge, P. J., Minejima, C., and Cohen, R. C.: Observations of NO_x, ΣPNs, ΣANs, and HNO_3 at a rural site in the California Sierra Nevada Mountains: summertime diurnal cycles, *Atmos. Chem. Phys.*, *9*(14), 4879–4896, doi: 10.5194/acp-9-4879-2009, **2009**.

Day, D. A., Wooldridge, P. J., Dillon, M. B., Thornton, J. A., and Cohen, R. C.: A thermal dissociation laser-induced fluorescence instrument for in situ detection of NO_2, peroxy nitrates, alkyl nitrates, and HNO_3, *J. Geophys. Res.*, *107*(D6), 4046, doi: 10.1029/2001JD000779, **2002**.

Deiber, G., George, Ch., Le Calvé, S., Schweitzer, F., and Mirabel, Ph.: Uptake study of $ClONO_2$ and $BrONO_2$ by Halide containing droplets, *Atmos. Chem. Phys.*, *4*(5), 1291–1299, doi: 10.5194/acp-4-1291-2004, **2004**.

Dentener, F. J., Carmichael, G. R., Zhang, Y., Lelieveld, J., and Crutzen, P.: Role of mineral aerosol as a reactive surface in the global troposphere, *J. Geophys. Res. Atmos.*, *101*(D17), 22869–22889, doi: 10.1029/96JD01818, **1996**.

Di Carlo, P., Brune, W. H., Martinez, M., Harder, H., Lesher, R., Ren, X., Thornberry, T., Carroll, M. A., Young, V., Shepson, P. B., Riemer, D., Apel, E., and Campbell, C.: Missing OH Reactivity in a Forest: Evidence for Unknown Reactive Biogenic VOCs, *Science*, *304*(5671), 722–725, doi: 10.1126/science.1094392, **2004**.

Dibb, J. E., Talbot, R. W., Scheuer, E. M., Blake, D. R., Blake, N. J., Gregory, G. L., Sachse, G. W., and Thornton, D. C.: Aerosol chemical composition and distribution during the Pacific Exploratory Mission (PEM) Tropics, *J. Geosphys. Res.*, *104*(D5), 5785–5800, doi: 10.1029/1998JD100001, **1999**.

Dillon, M. B., Lamanna, M. S., Schade, G. W., Goldstein, A. H., and Cohen, R. C.: Chemical evolution of the Sacramento urban plume: Transport and oxidation, *J. Geophys. Res.-Atmos.*, *107*(D5), 4045, doi: 10.1029/2001JD000969, **2003**.

Dulitz, K., Amedro, D., Dillon, T. J., Pozzer, A., and Crowley, J. N.: Temperature-(208–318 K) and pressure-(18–696 Torr) dependent rate coefficients for the reaction between OH and HNO_3, *Atmos. Chem. Phys.*, *18*(4), 2381–2394, doi: 10.5194/acp-18-2381-2018, **2018**.

Durre, I. and Yin, X.: Enhanced Radiosonde Data For Studies of Vertical Structure, *Bull. Amer. Meteor. Soc.*, *89*(9), 1257–1262, doi: 10.1175/2008BAMS2603.1, **2008**.

Ebben, C. J., Sparks, T. L., Wooldridge, P. J., Campos, T. L., Cantrell, C. A., Mauldin, R. L., Weinheimer, A. J., and Cohen, R. C.: Evolution of NO_x in the Denver Urban Plume during the Front Range Air Pollution and Photochemistry Experiment, *Atmos. Chem. Phys. Discuss.*, pages 1–13, doi: 10.5194/acp-2017-671, **2017**.

Edwards, P. M., Aikin, K. C., Dube, W. P., Fry, J. L., Gilman, J. B., de Gouw, J. A., Graus, M. G., Hanisco, T. F., Holloway, J., Hübler, G., Kaiser, J., Keutsch, F. N., Lerner, B. M., Neuman, J. A., Parrish, D. D., Peischl, J., Pollack, I. B., Ravishankara, A. R., Roberts, J. M., Ryerson, T. B., Trainer, M., Veres, P. R., Wolfe, G. M., Warneke, C., and Brown, S. S.: Transition from high- to low-NO_x control of night-time oxidation in the southeastern US, *Nat. Geosci.*, *10*(7), 490–495, doi: 10.1038/ngeo2976, **2017**.

Edwards, P. M., Young, C. J., Aikin, K., de Gouw, J., Dubé, W. P., Geiger, F., Gilman, J., Helmig, D., Holloway, J. S., Kercher, J., Lerner, B., Martin, R., McLaren, R., Parrish, D. D., Peischl, J., Roberts, J. M., Ryerson, T. B., Thornton, J., Warneke, C., Williams, E. J., and Brown, S. S.: Ozone photochemistry in an oil and natural gas extraction region during winter: simulations of a snow-free season in the Uintah Basin, Utah, *Atmos. Chem. Phys.*, *13*(17), 8955–8971, doi: 10.5194/acp-13-8955-2013, **2013**.

Faloona, I. C., Tan, D., Lesher, R. L., Hazen, N. L., Frame, C. L., Simpas, J. B., Harder, H., Martinez, M., Di Carlo, P., Ren, X., and Brune, W. H.: A Laser-induced Fluorescence Instrument for Detecting Tropospheric OH and HO_2: Characteristics and Calibration, *J. Atmos. Chem.*, *47*(2), 139–167, doi: 10.1023/B:JOCH.0000021036.53185.0e, **2004**.

Farmer, D. K. and Cohen, R. C.: Observations of HNO_3, ΣAN, ΣPN and NO_2 fluxes: evidence for rapid HO_x chemistry within a pine forest canopy, *Atmos. Chem. Phys*, *8*(14), 3899–3917, doi: 10.5194/acp-8-3899-2008, **2008**.

Farmer, D. K., Perring, A. E., Wooldridge, P. J., Blake, D. R., Baker, A., Meinardi, S., Huey, L. G., Tanner, D., Vargas, O., and Cohen, R. C.: Impact of organic nitrates on urban ozone production, *Atmos. Chem. Phys.*, *11*(9), 4085–4094, doi: 10.5194/acp-11-4085-2011, **2011**.

Feiner, P. A., Brune, W. H., Miller, D. O., Zhang, L., Cohen, R. C., Romer, P. S., Goldstein, A. H., Keutsch, F. N., Skog, K. M., Wennberg, P. O., Nguyen, T. B., Teng, A. P., DeGouw, J., Koss, A., Wild, R. J., Brown, S. S., Guenther, A., Edgerton, E., Baumann, K., and Fry, J. L.: Testing Atmospheric Oxidation in an Alabama Forest, *J. Atmos. Sci.*, *73*(12), 4699–4710, doi: 10.1175/JAS-D-16-0044.1, **2016**.

Finlayson-Pitts, B. J. and Pitts, J. N., Jr.: *Chemistry of the Upper and Lower Atmosphere: Theory, Experiments, and Applications*, Elsevier Science, San Diego, **1999**, ISBN 9780080529073.

Fisher, J. A., Jacob, D. J., Travis, K. R., Kim, P. S., Marais, E. A., Chan Miller, C., Yu, K., Zhu, L., Yantosca, R. M., Sulprizio, M. P., Mao, J., Wennberg, P. O., Crounse, J. D., Teng, A. P., Nguyen, T. B., St. Clair, J. M., Cohen, R. C., Romer, P., Nault, B. A., Wooldridge, P. J., Jimenez, J. L., Campuzano-Jost, P., Day, D. A., Hu, W., Shepson, P. B., Xiong, F., Blake, D. R., Goldstein, A. H., Misztal, P. K., Hanisco, T. F., Wolfe, G. M., Ryerson, T. B., Wisthaler, A., and Mikoviny, T.: Organic nitrate chemistry and its implications for nitrogen budgets in an isoprene- and monoterpene-rich atmosphere: constraints from aircraft (SEAC^{4}RS) and ground-based (SOAS) observations in the Southeast US, *Atmos. Chem. Phys.*, *16*(9), 5969–5991, doi: 10.5194/acp-16-5969-2016, **2016**.

Forouzanfar, M. H., et al.: Global, regional, and national comparative risk assessment of 79 behavioural, environmental and occupational, and metabolic risks or clusters of risks in 188 countries, 19902013: a systematic analysis for the Global Burden of Disease Study 2013, *Lancet*, *386*(10010), 2287–2323, doi: 10.1016/S0140-6736(15)00128-2, **2015**.

Fowler, D., Coyle, M., Skiba, U., Sutton, M. A., Cape, J. N., Reis, S., Sheppard, L. J., Jenkins, A., Grizzetti, B., Galloway, J. N., Vitousek, P., Leach, A., Bouwman, A. F., Butterbach-Bahl, K., Dentener, F., Stevenson, D., Amann, M., and Voss, M.: The global nitrogen cycle in the twenty-first century, *Philos. T. Roy. Soc. B*, *368*(1621), doi: 10.1098/rstb.2013.0164, **2013**.

Frost, G. J., Trainer, M., Allwine, G., Buhr, M. P., Calvert, J. G., Cantrell, C. A., Fehsenfeld, F. C., Goldan, P. D., Herwehe, J., Hübler, G., Kuster, W. C., Martin, R., McMillen, R. T., Montzka, S. A., Norton, R. B., Parrish, D. D., Ridley, B. A., Shetter, R. E., Walega, J. G., Watkins, B. A., Westberg, H. H., and Williams, E. J.: Photochemical ozone production in the rural southeastern United States during the 1990 Rural Oxidants in the Southern Environment (ROSE) program, *J. Geophys. Res.*, *103*(D17), 22491–22508, doi: 10.1029/98JD00881, **1998**.

Fry, J. L., Draper, D. C., Zarzana, K. J., Campuzano-Jost, P., Day, D. A., Jimenez, J. L., Brown, S. S., Cohen, R. C., Kaser, L., Hansel, A., Cappellin, L., Karl, T., Hodzic Roux, A., Turnipseed, A., Cantrell, C., Lefer, B. L., and Grossberg, N.: Observations of gas- and aerosol-phase organic nitrates at BEACHON-RoMBAS 2011, *Atmos. Chem. Phys.*, *13*(17), 8585–8605, doi: 10.5194/acp-13-8585-2013, **2013**.

Fu, T.-M., Zheng, Y., Paulot, F., Mao, J., and Yantosca, R. M.: Positive but variable sensitivity of August surface ozone to large-scale warming in the southeast United States, *Nat. Clim. Change*, *5*(5), 454–458, doi: 10.1038/nclimate2567, **2015**.

Fuchs, H., Bohn, B., Hofzumahaus, A., Holland, F., Lu, K. D., Nehr, S., Rohrer, F., and Wahner, A.: Detection of HO_2 by laser-induced fluorescence: calibration and interferences from RO_2 radicals, *Atmos. Meas. Tech.*, *4*(6), 1209–1225, doi: 10.5194/amt-4-1209-2011, **2011**.

Fuentes, J. D., Wang, D., Bowling, D. R., Potosnak, M., Monson, R. K., Goliff, W. S., and Stockwell, W. R.: Biogenic Hydrocarbon Chemistry within and Above a Mixed Deciduous Forest, *J. Atmos. Chem.*, *56*(2), 165–185, doi: 10.1007/s10874-006-9048-4, **2007**.

Ganzeveld, L. and Lelieveld, J.: Dry deposition parameterization in a chemistry general circulation model and its influence on the distribution of reactive trace gases, *J. Geophys. Res.*, *100*(D10), 20999–21012, doi: 10.1029/95JD02266, **1995**.

Gao, R. S., Fahey, D. W., Del Negro, L. A., Donnelly, S. G., Keim, E. R., Neuman, J. A., Teverovskaia, E., Wennberg, P. O., Hanisco, T. F., Lanzendorf, E. J., Proffitt, M. H., Margitan, J. J., Wilson, J. C., Elkins, J. W., Stimpfle, R. M., Cohen, R. C., McElroy, C. T., Bui, T. P., Salawitch, R. J., Brown, S. S., Ravishankara, A. R., Portmann, R. W., Ko, M. K. W., Weisenstein, D. K., and Newman, P. A.: A comparison of observations and model simulations of NO_x/NO_y in the lower stratosphere, *Geophys. Res. Lett.*, *26*(8), 1153–1156, doi: 10.1029/1999GL900162, **1999**.

Gaston, C. J., Riedel, T. P., Zhang, Z., Gold, A., Surratt, J. D., and Thornton, J. A.: Reactive Uptake of an Isoprene-Derived Epoxydiol to Submicron Aerosol Particles, *Environ. Sci. Technol.*, *48*(19), 11178–11186, doi: 10.1021/es5034266, **2014**.

Geddes, J. A., Murphy, J. G., and Wang, D. K.: Long term changes in nitrogen oxides and volatile organic compounds in Toronto and the challenges facing local ozone control, *Atmos. Environ.*, *43*(21), 3407–3415, doi: 10.1016/j.atmosenv.2009.03.053, **2009**.

Ghosh, B., Bugarin, A., Connell, B. T., and North, S. W.: Isomer-Selective Study of the OH-Initiated Oxidation of Isoprene in the Presence of O_2 and NO: 2. The Major OH Addition Channel, *J. Phys. Chem. A*, *114*(7), 2553–2560, doi: 10.1021/jp909052t, **2010**.

Giacopelli, P., Ford, K., Espada, C., and Shepson, P. B.: Comparison of the measured and simulated isoprene nitrate distributions above a forest canopy, *J. Geophys. Res. Atmos.*, *110*(D1), D01304, doi: 10.1029/2004JD005123, **2005**.

Gilman, J. B., Burkhart, J. F., Lerner, B. M., Williams, E. J., Kuster, W. C., Goldan, P. D., Murphy, P. C., Warneke, C., Fowler, C., Montzka, S. A., Miller, B. R., Miller, L., Oltmans, S. J., Ryerson, T. B., Cooper, O. R., Stohl, A., and de Gouw, J. A.: Ozone variability and halogen oxidation within the Arctic and sub-Arctic springtime boundary layer, *Atmos. Chem. Phys.*, *10*(21), 10223–10236, doi: 10.5194/acp-10-10223-2010, **2010**.

Goldan, P. D., Kuster, W. C., Williams, E., Murphy, P. C., Fehsenfeld, F. C., and Meagher, J.: Nonmethane hydrocarbon and oxy hydrocarbon measurements during the 2002 New England Air Quality Study, *J. Geophys. Res.*, *109*(D21), D21309, doi: 10.1029/2003JD004455, **2004**.

Goldstein, A. H. and Galbally, I. E.: Known and Unexplored Organic Constituents in the Earth's Atmosphere, *Environ. Sci. Technol.*, *41*(5), 1514–1521, doi: 10.1021/es072476p, **2007**.

Grossenbacher, J. W., Barket, D. J., Jr., Shepson, P. B., Carroll, M. A., Olszyna, K., and Apel, E.: A comparison of isoprene nitrate concentrations at two forest-impacted sites, *J. Geophys. Res.*, *109*(D11), D11311, doi: 10.1029/2003JD003966, **2004**.

Hansen, D. A., Edgerton, E. S., Hartsell, B. E., Jansen, J. J., Kandasamy, N., Hidy, G. M., and Blanchard, C. L.: The Southeastern Aerosol Research and Characterization Study: Part 1—Overview, *J. Air Waste Manage.*, *53*(12), 1460–1471, doi: 10.1080/10473289.2003.10466318, **2003**.

Hanson, D. R., Ravishankara, A. R., and Lovejoy, E. R.: Reaction of $BrONO_2$ with H_2O on submicron sulfuric acid aerosol and the implications for the lower stratosphere, *J. Geophys. Res.*, *101*(D4), 9063–9069, doi: 10.1029/96JD00347, **1996**.

Hauglustaine, D. A., Ridley, B. A., Solomon, S., Hess, P. G., and Madronich, S.: HNO_3/NO_x ratio in the remote troposphere During MLOPEX 2: Evidence for nitric acid reduction on carbonaceous aerosols?, *Geophys. Res. Lett.*, *23*(19), 2609–2612, doi: 10.1029/96GL02474, **1996**.

Heagle, A. S.: Ozone and Crop Yield, *Annu. Rev. Phytopathol.*, *27*(1), 397–423, doi: 10.1146/annurev.py.27.090189.002145, **1989**.

Henderson, B. H., Pinder, R. W., Crooks, J., Cohen, R. C., Carlton, A. G., Pye, H. O. T., and Vizuete, W.: Combining Bayesian methods and aircraft observations to constrain the $HO^{\cdot}$ + NO_2 reaction rate, *Atmos. Chem. Phys.*, *12*(2), 653–667, doi: 10.5194/acp-12-653-2012, **2012**.

Hennigan, C. J., Sullivan, A. P., Fountoukis, C. I., Nenes, A., Hecobian, A., Vargas, O., Peltier, R. E., Case Hanks, A. T., Huey, L. G., Lefer, B. L., Russel, A. G., and Weber, R. J.: On the volatility and production mechanisms of newly formed nitrate and water soluble organic aerosol in Mexico City, *Atmos. Chem. Phys.*, *8*(14), 3761–3768, doi: 10.5194/acp-8-3761-2008, **2008**.

Hickman, J. E., Wu, S., Mickley, L. J., and Lerdau, M. T.: Kudzu (*Pueraria montana*) invasion doubles emissions of nitric oxide and increases ozone pollution, *Proc. Natl. Acad. Sci. USA*, *107*(22), 10115–10119, doi: 10.1073/pnas.0912279107, **2010**.

Hidy, G. M., Blanchard, C. L., Baumann, K., Edgerton, E., Tanenbaum, S., Shaw, S., Knipping, E., Tombach, I., Jansen, J., and Walters, J.: Chemical climatology of the southeastern United States, 1999–2013, *Atmos. Chem. Phys.*, *14*(21), 11893–11914, doi: 10.5194/acp-14-11893-2014, **2014**.

Hirsch, A. I., Munger, J. W., Jacob, D. J., Horowitz, L. W., and Goldstein, A. H.: Seasonal variation of the ozone production efficiency per unit NO_x at Harvard Forest, Massachusetts, *J. Geophys. Res.*, *101*(D7), 12659–12666, doi: 10.1029/96JD00557, **1996**.

Horowitz, L. W., Fiore, A. M., Milly, G. P., Cohen, R. C., Perring, A., Wooldridge, P. J., Hess, P. G., Emmons, L. K., and Lamarque, J.-F.: Observational constraints on the chemistry of isoprene nitrates over the eastern United States, *J. Geophys. Res. Atmos.*, *112*(D12), D12S08, doi: 10.1029/2006JD007747, **2007**.

Hossaini, R., Chipperfield, M. P., Saiz-Lopez, A., Fernandez, R., Monks, S., Feng, W., Brauer, P., and von Glasow, R.: A global model of tropospheric chlorine chemistry: Organic versus inorganic sources and impact on methane oxidation, *J. Geophys. Res. Atmos.*, *121*(23), 14,271–14,297, doi: 10.1002/2016JD025756, **2016**.

Hu, K. S., Darer, A. I., and Elrod, M. J.: Thermodynamics and kinetics of the hydrolysis of atmospherically relevant organonitrates and organosulfates, *Atmos. Chem. Phys.*, *11*(16), 8307–8320, doi: 10.5194/acp-11-8307-2011, **2011**.

Hudman, R. C., Moore, N. E., Mebust, A. K., Martin, R. V., Russell, A. R., Valin, L. C., and Cohen, R. C.: Steps towards a mechanistic model of global soil nitric oxide emissions: implementation and space based-constraints, *Atmos. Chem. Phys.*, *12*(16), 7779–7795, doi: 10.5194/acp-12-7779-2012, **2012**.

Ito, A., Sillman, S., and Penner, J. E.: Effects of additional nonmethane volatile organic compounds, organic nitrates, and direct emissions of oxygenated organic species on global tropospheric chemistry, *J. Geophys. Res.-Atmos.*, *112*(D6), D06309, doi: 10.1029/2005JD006556, **2007**.

Ito, A., Sillman, S., and Penner, J. E.: Global chemical transport model study of ozone response to changes in chemical kinetics and biogenic volatile organic compounds emissions due to increasing temperatures: Sensitivities to isoprene nitrate chemistry and grid resolution, *J. Geophys. Res. Atmos.*, *114*(D9), D09301, doi: 10.1029/2008JD011254, **2009**.

Ito, K., De Leon, S. F., and Lippmann, M.: Associations Between Ozone and Daily Mortality: Analysis and Meta-Analysis, *Epidemiology*, *16*(4), 446–457, doi: 10.1097/01.ede.0000165821.90114.7f, **2005**.

Jacob, D. J., Logan, J. A., Gardner, G. M., Yevich, R. M., Spivakovsky, C. M., Wofsy, S. C., Sillman, S., and Prather, M. J.: Factors regulating ozone over the United States and its export to the global atmosphere, *J. Geophys. Res.*, *98*(D8), 14817–14826, doi: 10.1029/98JD01224, **1993**.

Jacob, D. J. and Winner, D. A.: Effect of climate change on air quality, *Atmos. Environ.*, *43*, 51–63, doi: 10.1016/j.atmosenv.2008.09.051, **2009**.

Jenkin, M. E., Young, J. C., and Rickard, A. R.: The MCM v3.3.1 degradation scheme for isoprene, *Atmos. Chem. Phys.*, *15*(20), 11433–11459, doi: 10.5194/acp-15-11433-2015, **2015**.

Jiang, Z., McDonald, B. C., Worden, H., Worden, J. R., Miyazaki, K., Qu, Z., Henze, D. K., Jones, D. B. A., Arellano, A. F., Fischer, E. V., Zhu, L., and Boersma, K. F.: Unexpected slowdown of US pollutant emission reduction in the past decade, *Proc. Natl. Acad. Sci. USA*, *115*(20), 5099–5104, doi: 10.1073/pnas.1801191115, **2018**.

Kaiser, J., Skog, K. M., Baumann, K., Bertman, S. B., Brown, S. B., Brune, W. H., Crounse, J. D., de Gouw, J. A., Edgerton, E. S., Feiner, P. A., Goldstein, A. H., Koss, A., Misztal, P. K., Nguyen, T. B., Olson, K. F., St. Clair, J. M., Teng, A. P., Toma, S., Wennberg, P. O., Wild, R. J., Zhang, L., and Keutsch, F. N.: Speciation of OH reactivity above the canopy of an isoprene-dominated forest, *Atmos. Chem. Phys*, *16*(14), 9349–9359, doi: 10.5194/acp-16-9349-2016, **2016**.

Kaser, L., Karl, T., Schnitzhofer, R., Graus, M., Herdlinger-Blatt, I. S., DiGangi, J. P., Sive, B., Turnipseed, A., Hornbrook, R. S., Zheng, W., Flocke, F. M., Guenther, A., Keutsch, F. N., Apel, E., and Hansel, A.: Comparison of different real time VOC measurement techniques in a ponderosa pine forest, *Atmos. Chem. Phys.*, *13*(5), 2893–2906, doi: 10.5194/acp-13-2893-2013, **2013**.

Kasibhatla, P., Sherwen, T., Evans, M. J., Carpenter, L. J., Reed, C., Alexander, B., Chen, Q., Sulprizio, M., Lee, J. D., Read, K. A., Bloss, W., Crilley, L. R., Keene, W. C., Pszenny, A. A. P., and Hodzic, A.: Global impact of nitrate photolysis in sea-salt aerosol on NO_x, OH, and O_3 in the marine boundary layer, *Atmos. Chem. Phys. Discuss.*, *2018*, 1–31, doi: 10.5194/acp-2018-303, **2018**.

Kesik, M., Brüggemann, N., Forkel, R., Kiese, R., Knoche, R., Li, C., Seufert, G., Simpson, D., and Butterbach-Bahl, K.: Future scenarios of N_2O and NO emissions from European forest soils, *J. Geophys. Res.*, *111*(G2), G02018, doi: 10.1029/2005JG000115, **2006**.

Kleinman, L., Lee, Y.-N., Springston, S. R., Nunnermacker, L., Zhou, X., Brown, R., Hallock, K., Klotz, P., Leahy, D., Lee, J. H., and Newman, L.: Ozone formation at a rural site in the southeastern United States, *J. Geophys. Res.*, *99*(D2), 3469–3482, doi: 10.1029/93JD02991, **1994**.

Kleinman, L. I., Daum, P. H., Imre, D. G., Lee, J. H., Lee, Y.-N., Nunnermacker, L. J., Springston, S. R., Weinstein-Lloyd, J., and Newman, L.: Ozone production in the New York City urban plume, *J. Geophys. Res.*, *105*(D11), 14495–14511, doi: 10.1029/2000JD900011, **2000**.

LaFranchi, B. W., Wolfe, G. M., Thornton, J. A., Harrold, S. A., Browne, E. C., Min, K. E., Wooldridge, P. J., Gilman, J. B., Kuster, W. C., Goldan, P. D., de Gouw, J. A., McKay, M., Goldstein, A. H., Ren, X., Mao, J., and Cohen, R. C.: Closing the peroxy acetyl nitrate budget: observations of acyl peroxy nitrates (PAN, PPN, and MPAN) during BEARPEX 2007, *Atmos. Chem. Phys.*, *9*(19), 7623–7641, doi: 10.5194/acp-9-7623-2009, **2009**.

Lee, B. H., Mohr, C., Lopez-Hilfiker, F. D., Lutz, A., Hallquist, M., Lee, L., Romer, P., Cohen, R. C., Iyer, S., Kurtén, T., Hu, W., Day, D. A., Campuzano-Jost, P., Jimenez, J. L., Xu, L., Ng, N. L., Guo, H., Weber, R. J., Wild, R. J., Brown, S. S., Koss, A., de Gouw, J., Olson, K., Goldstein, A. H., Seco, R., Kim, S., McAvey, K., Shepson, P. B., Starn, T., Baumann, K., Edgerton, E. S., Liu, J., Shilling, J. E., Miller, D. O., Brune, W., Schobesberger, S., D'Ambro, E. L., and Thornton, J. A.: Highly functionalized organic nitrates in the southeast United States: Contribution to secondary organic aerosol and reactive nitrogen budgets, *Proc. Natl. Acad. Sci. USA*, *113*(6), 1516–1521, doi: 10.1073/pnas.1508108113, **2016**.

Lee, L., Teng, A. P., Wennberg, P. O., Crounse, J. D., and Cohen, R. C.: On Rates and Mechanisms of OH and O_3 Reactions with Isoprene-Derived Hydroxy Nitrates, *J. Phys. Chem. A*, *118*(9), 1622–1637, doi: 10.1021/jp4107603, **2014**a.

Lee, L., Wooldridge, P. J., Gilman, J. B., Warneke, C., de Gouw, J., and Cohen, R. C.: Low temperatures enhance organic nitrate formation: evidence from observations in the 2012 Uintah Basin Winter Ozone Study, *Atmos. Chem. Phys.*, *14*(22), 12441–12454, doi: 10.5194/acp-14-12441-2014, **2014**b.

Liu, S. and Liang, X.-Z.: Observed Diurnal Cycle Climatology of Planetary Boundary Layer Height, *J. Climate*, *23*(21), 5790–5809, doi: 10.1175/2010JCLI3552.1, **2010**.

Liu, S., Shilling, J. E., Song, C., Hiranuma, N., Zaveri, R. A., and Russell, L. M.: Hydrolysis of Organonitrate Functional Groups in Aerosol Particles, *Aerosol Sci. Tech.*, *46*(12), 1359–1369, doi: 10.1080/02786826.2012.716175, **2012**.

Mao, J., Paulot, F., Jacob, D. J., Cohen, R. C., Crounse, J. D., Wennberg, P. O., Keller, C. A., Hudman, R. C., Barkley, M. P., and Horowitz, L. W.: Ozone and organic nitrates over the eastern United States: Sensitivity to isoprene chemistry, *J. Geophys. Res.-Atmos.*, *118*(19), 11256–11268, doi: 10.1002/jgrd.50817, **2013**.

Mao, J., Ren, X., Brune, W. H., Olson, J. R., Crawford, J. H., Fried, A., Huey, L. G., Cohen, R. C., Heikes, B., Singh, H. B., Blake, D. R., Sachse, G. W., Diskin, G. S., Hall, S. R., and Shetter, R. E.: Airborne measurement of OH reactivity during INTEX-B, *Atmos. Chem. Phys.*, *9*(1), 163–173, doi: 10.5194/acp-9-163-2009, **2009**.

Mao, J., Ren, X., Chen, S., Brune, W. H., Chen, Z., Martinez, M., Harder, H., Lefer, B., Rappenglück, B., Flynn, J., and Leuchner, M.: Atmospheric oxidation capacity in the summer of Houston 2006: Comparison with summer measurements in other metropolitan studies, *Atmos. Environ.*, *44*(33), 4107–4115, doi: 10.1016/j.atmosenv.2009.01.013, **2010**.

Mao, J., Ren, X., Zhang, L., Van Duin, D. M., Cohen, R. C., Park, J.-H., Goldstein, A. H., Paulot, F., Beaver, M. R., Crounse, J. D., Wennberg, P. O., DiGangi, J. P., Henry, S. B., Keutsch, F. N., Park, C., Schade, G. W., Wolfe, G. M., Thornton, J. A., and Brune, W. H.: Insights into hydroxyl measurements and atmospheric oxidation in a California forest, *Atmos. Chem. Phys.*, *12*(17), 8009–8020, doi: 10.5194/acp-12-8009-2012, **2012**.

Martinez, M., Harder, H., Kovacs, T. A., Simpas, J. B., Bassis, J., Lesher, R., Brune, W. H., Frost, G. J., Williams, E. J., Stroud, C. A., Jobson, B. T., Roberts, J. M., Hall, S. R., Shetter, R. E., Wert, B., Fried, A., Alicke, B., Stutz, J., Young, V. L., White, A. B., and Zamora, R. J.: OH and HO_2 concentrations, sources, and loss rates during the Southern Oxidants Study in Nashville, Tennessee, summer 1999, *J. Geophys. Res.*, *108*(D19), 4617, doi: 10.1029/2003JD003551, **2003**.

McDuffie, E. E., Fibiger, D. L., Dubé, W. P., Lopez-Hilfiker, F., Lee, B. H., Thornton, J. A., Shah, V., Jaeglé, L., Guo, H., Weber, R. J., Reeves, J. M., Weinheimer, A. J., Schroder, J. C., Campuzano-Jost, P., Jimenez, J. L., Dibb, J. E., Veres, P., Ebben, C., Sparks, T. L., Wooldridge, P. J., Cohen, R. C., Hornbrook, R. S., Apel, E. C., Campos, T., Hall, S. R., Ullmann, K., and Brown, S. S.: Heterogeneous N_2O_5 Uptake During Winter: Aircraft Measurements During the 2015 WINTER Campaign and Critical Evaluation of Current Parameterizations, *J. Geophys. Res. Atmos.*, *123*(8), 4345–4372, doi: 10.1002/2018JD028336, **2018**.

McNaughton, C. S., Clarke, A. D., Kapustin, V., Shinozuka, Y., Howell, S. G., Anderson, B. E., Winstead, E., Dibb, J., Scheuer, E., Cohen, R. C., Wooldridge, P., Perring, A., Huey, L. G., Kim, S., Jimenez, J. L., Dunlea, E. J., DeCarlo, P. F., Wennberg, P. O., Crounse, J. D., Weinheimer, A. J., and Flocke, F.: Observations of heterogeneous reactions between Asian pollution and mineral dust over the Eastern North Pacific during INTEX-B, *Atmos. Chem. Phys.*, *9*(21), 8283–8308, doi: 10.5194/acp-9-8283-2009, **2009**.

Mebust, A. K. and Cohen, R. C.: Space-based observations of fire NO_x emission coefficients: a global biome-scale comparison, *Atmos. Chem. Phys.*, *14*(5), 2509–2524, doi: 10.5194/acp-14-2509-2014, **2014**.

Mickley, L. J., Jacob, D. J., and Rind, D.: Uncertainty in preindustrial abundance of tropospheric ozone: Implications for radiative forcing calculations, *J. Geophys. Res.*, *106*(D4), 3389–3399, doi: 10.1029/2000JD900594, **2001**.

Millet, D. B., Baasandorj, M., Farmer, D. K., Thornton, J. A., Baumann, K., Brophy, P., Chaliyakunnel, S., de Gouw, J. A., Graus, M., Hu, L., Koss, A., Lee, B. H., Lopez-Hilfiker, F. D., Neuman, J. A., Paulot, F., Peischl, J., Pollack, I. B., Ryerson, T. B., Warneke, C., Williams, B. J., and Xu, J.: A large and ubiquitous source of atmospheric formic acid, *Atmos. Chem. Phys.*, *15*(11), 6283–6304, doi: 10.5194/acp-15-6283-2015, **2015**.

Min, K.-E., Pusede, S. E., Browne, E. C., LaFranchi, B. W., and Cohen, R. C.: Eddy covariance fluxes and vertical concentration gradient measurements of NO and NO_2 over a ponderosa pine ecosystem: observational evidence for within-canopy chemical removal of NO_x, *Atmos. Chem. Phys.*, *14*(11), 5495–5512, doi: 10.5194/acp-14-5495-2014, **2014**.

Min, K.-E., Pusede, S. E., Browne, E. C., LaFranchi, B. W., Wooldridge, P. J., Wolfe, G. M., Harrold, S. A., Thornton, J. A., and Cohen, R. C.: Observations of atmosphere-biosphere exchange of total and speciated peroxynitrates: nitrogen fluxes and biogenic sources of peroxynitrates, *Atmos. Chem. Phys.*, *12*(20), 9763–9773, doi: 10.5194/acp-12-9763-2012, **2012**.

Mogensen, D., Gierens, R., Crowley, J. N., Keronen, P., Smolander, S., Sogachev, A., Nölscher, A. C., Zhou, L., Kulmala, M., Tang, M. J., Williams, J., and Boy, M.: Simulations of atmospheric OH, O_3 and NO_3 reactivities within and above the boreal forest, *Atmos. Chem. Phys.*, *15*(7), 3909–3932, doi: 10.5194/acp-15-3909-2015, **2015**.

Mollner, A. K., Valluvadasan, S., Feng, L., Sprague, M. K., Okumura, M., Milligan, D. B., Bloss, W. J., Sander, S. P., Martien, P. T., Harley, R. A., McCoy, A. B., and Carter, W. P. L.: Rate of Gas Phase Association of Hydroxyl Radical and Nitrogen Dioxide, *Science*, *330*(6004), 646–649, doi: 10.1126/science.1193030, **2010**.

Müller, J.-F., Peeters, J., and Stavrakou, T.: Fast photolysis of carbonyl nitrates from isoprene, *Atmos. Chem. Phys.*, *14*(5), 2497–2508, doi: 10.5194/acp-14-2497-2014, **2014**.

Myhre, G. D., Shindell, D. T., Béon, F.-M., Collins, W., Fuglestvedt, J., Huang, J., Koch, D., Lamarque, J.-F., Lee, D., Mendoza, B., Nakajima, T., Robock, A., Stephens, G., Takemura, T., and Zhang, H.: Anthropogenic and Natural Radiative Forcing, in Stocker, T. F., Qin, D., Plattner, G.-K., Tignor, M., Allen, S. K., Boschung, J., Nauels, A., Xia, Y., Bex, V., and Midgley, P. M. (Editors), *Climate Change 2013: The Physical Science Basis. Contribution of Working Group I to the Fifth Assessment Report of the Intergovernmental Panel on Climate Change*, pages 659–740, Cambridge University Press, Cambridge, United Kingdom, **2013**.

Nault, B. A., Garland, C., Wooldridge, P. J., Brune, W. H., Campuzano-Jost, P., Crounse, J. D., Day, D. A., Dibb, J., Hall, S. R., Huey, L. G., Jimenez, J. L., Liu, X., Mao, J., Mikoviny, T., Peischl, J., Pollack, I. B., Ren, X., Ryerson, T. B., Scheuer, E., Ullmann, K., Wennberg, P. O., Wisthaler, A., Zhang, L., and Cohen, R. C.: Observational Constraints on the Oxidation of NO_x in the Upper Troposphere, *J. Phys. Chem. A*, *120*(9), 1468–1478, doi: 10.1021/acs.jpca.5b07824, **2016**.

Nault, B. A., Laughner, J. L., Wooldridge, P. J., Crounse, J. D., Dibb, J., Diskin, G., Peischl, J., Podolske, J. R., Pollack, I. B., Ryerson, T. B., Scheuer, E., Wennberg, P. O., and Cohen, R. C.: Lightning NO_x Emissions: Reconciling Measured and Modeled Estimates With Updated NO_x Chemistry, *Geophys. Res. Lett.*, *44*(18), 9479–9488, doi: 10.1002/2017GL074436, **2017**.

Ndour, M., Conchon, P., D'Anna, B., Ka, O., and George, C.: Photochemistry of mineral dust surface as a potential atmospheric renoxification process, *Geophys. Res. Lett.*, *36*(5), L05816, doi: 10.1029/2008GL036662, **2009**.

Neuman, J. A., Parrish, D. D., Trainer, M., Ryerson, T. B., Holloway, J. S., Nowak, J. B., Swanson, A., Flocke, F., Roberts, J. M., Brown, S. S., Stark, H., Sommariva, R., Stohl, A., Peltier, R., Weber, R., Wollny, A. G., Sueper, D. T., Hubler, G., and Fehsenfeld, F. C.: Reactive nitrogen transport and photochemistry in urban plumes over the North Atlantic Ocean, *J. Geophys. Res. Atmos.*, *111*(D23), D23S54, doi: 10.1029/2005JD007010, **2006**.

Nguyen, T. B., Crounse, J. D., Teng, A. P., St. Clair, J. M., Paulot, F., Wolfe, G. M., and Wennberg, P. O.: Rapid deposition of oxidized biogenic compounds to a temperate forest, *Proc. Natl. Acad. Sci. USA*, *112*(5), E392–E401, doi: 10.1073/pnas.1418702112, **2015**.

Nissenson, P., Dabdub, D., Das, R., Maurino, V., Minero, C., and Vione, D.: Evidence of the water-cage effect on the photolysis of NO_3^- and $FeOH^{2+}$. Implications of this effect and of H_2O_2 surface accumulation on photochemistry at the air-water interface of atmospheric droplets, *Atmos. Environ.*, *44*(38), 4859–4866, doi: 10.1016/j.atmosenv.2010.08.035, **2010**.

Oikawa, P. Y., Ge, C., Wang, J., Eberwein, J. R., Liang, L. L., Allsman, L. A., Grantz, D. A., and Jenerette, G. D.: Unusually high soil nitrogen oxide emissions influence air quality in a

high-temperature agricultural region, *Nat. Commun.*, *6*, 8753, doi: 10.1038/ncomms9753, **2015**.

Orlando, J. J. and Tyndall, G. S.: Laboratory studies of organic peroxy radical chemistry: an overview with emphasis on recent issues of atmospheric significance, *Chem. Soc. Rev.*, *41*(19), 6294–6317, doi: 10.1039/c2cs35166h, **2012**.

Oswald, R., Behrendt, T., Ermel, M., Wu, D., Su, H., Cheng, Y., Breuninger, C., Moravek, A., Mougin, E., Delon, C., Loubet, B., Pommerening-Röser, A., Sörgel, M., Pöschl, U., Hoffmann, T., Andreae, M. O., Meixner, F. X., and Trebs, I.: HONO Emissions from Soil Bacteria as a Major Source of Atmospheric Reactive Nitrogen, *Science*, *341*(6151), 1233–1235, doi: 10.1126/science.1242266, **2013**.

Papale, D., Reichstein, M., Aubinet, M., Canfora, E., Bernhofer, C., Kutsch, W., Longdoz, B., Rambal, S., Valentini, R., Vesala, T., and Yakir, D.: Towards a standardized processing of Net Ecosystem Exchange measured with eddy covariance technique: algorithms and uncertainty estimation, *Biogeosciences*, *3*(4), 571–583, doi: 10.5194/bg-3-571-2006, **2006**.

Paulot, F., Crounse, J. D., Kjaergaard, H. G., Kroll, J. H., Seinfeld, J. H., and Wennberg, P. O.: Isoprene photooxidation: new insights into the production of acids and organic nitrates, *Atmos. Chem. Phys.*, *9*(4), 1479–1501, doi: 10.5194/acp-9-1479-2009, **2009**.

Paulot, F., Henze, D. K., and Wennberg, P. O.: Impact of the isoprene photochemical cascade on tropical ozone, *Atmos. Chem. Phys.*, *12*(3), 1307–1325, doi: 10.5194/acp-12-1307-2012, **2012**.

Peeters, J., Müller, J.-F., Stavrakou, T., and Nguyen, V. S.: Hydroxyl Radical Recycling in Isoprene Oxidation Driven by Hydrogen Bonding and Hydrogen Tunneling: The Upgraded LIM1 Mechanism, *J. Phys. Chem. A*, *118*(38), 8625–8643, doi: 10.1021/jp5033146, **2014**.

Pérez, I. M., LaFranchi, B. W., and Cohen, R. C.: Nitrogen oxide chemistry in an urban plume: investigation of the chemistry of peroxy and multifunctional organic nitrates with a Lagrangian model, *Atmos. Chem. Phys. Discuss.*, *9*(6), 27099–27165, doi: 10.5194/acpd-9-27099-2009, **2009**.

Perkins, K. K., Hanisco, T. F., Cohen, R. C., Koch, L. C., Stimpfle, R. M., Voss, P. B., Bonne, G. P., Lanzendorf, E. J., Anderson, J. G., Wennberg, P. O., Gao, R. S., Del Negro, L. A., Salawitch, R. J., McElroy, C. T., Hintsa, E. J., Loewenstein, M., and Bui, T. P.: The NO_x–HNO_3 System in the Lower Stratosphere: Insights from In Situ Measurements and Implications of the J_{HNO_3}–[OH] Relationship, *J. Phys. Chem. A*, *105*(9), 1521–1534, doi: 10.1021/jp002519n, **2001**.

Perring, A. E., Bertram, T. H., Farmer, D. K., Wooldridge, P. J., Dibb, J., Blake, N. J., Blake, D. R., Singh, H. B., Fuelberg, H., Diskin, G., Sachse, G., and Cohen, R. C.: The production and persistence of $\Sigma RONO_2$ in the Mexico City plume, *Atmos. Chem. Phys.*, *10*(15), 7215–7229, doi: 10.5194/acp-10-7215-2010, **2010**.

Perring, A. E., Bertram, T. H., Wooldridge, P. J., Fried, A., Heikes, B. G., Dibb, J., Crounse, J. D., Wennberg, P. O., Blake, N. J., Blake, D. R., Brune, W. H., Singh, H. B., and Cohen, R. C.: Airborne observations of total $RONO_2$: new constraints on the yield and lifetime of isoprene nitrates, *Atmos. Chem. Phys.*, *9*(4), 1451–1463, doi: 10.5194/acp-9-1451-2009, **2009**.

Perring, A. E., Pusede, S. E., and Cohen, R. C.: An Observational Perspective on the Atmospheric Impacts of Alkyl and Multifunctional Nitrates on Ozone and Secondary Organic Aerosol, *Chem. Rev.*, *113*, 5848–5870, doi: 10.1021/cr300520x, **2013**.

Pilegaard, K.: Processes regulating nitric oxide emissions from soils, *Phil. Trans. R. Soc. B*, *368*(1621), 20130126, doi: 10.1098/rstb.2013.0126, **2013**.

Pilegaard, K., Skiba, U., Ambus, P., Beier, C., Brüggemann, N., Butterbach-Bahl, K., Dick, J., Dorsey, J., Duyzer, J., Gallagher, M., Gasche, R., Horvath, L., Kitzler, B., Leip, A., Pihlatie, M. K., Rosenkranz, P., Seufert, G., Vesala, T., Westrate, H., and Zechmeister-Boltenstern, S.: Factors controlling regional differences in forest soil emission of nitrogen oxides (NO and N_2O), *Biogeosciences*, *3*(4), 651–661, doi: 10.5194/bg-3-651-2006, **2006**.

Pleijel, H., Danielsson, H., Ojanperä, K., De Temmerman, L., Högy, P., Badiani, M., and Karlsson, P. E.: Relationships between ozone exposure and yield loss in European wheat and potato—a comparison of concentration- and flux-based exposure indices, *Atmos. Environ.*, *38*(15), 2259–2269, doi: 10.1016/j.atmosenv.2003.09.076, **2004**.

Pollack, I. B., Ryerson, T. B., Trainer, M., Neuman, J. A., Roberts, J. M., and Parrish, D. D.: Trends in ozone, its precursors, and related secondary oxidation products in Los Angeles, California: A synthesis of measurements from 1960 to 2010, *J. Geophys. Res. Atmos.*, *118*(11), 5893–5911, doi: 10.1002/jgrd.50472, **2013**.

Pope, C. A., Ezzati, M., and Dockery, D. W.: Fine-Particulate Air Pollution and Life Expectancy in the United States, *N. Engl. J. Med.*, *360*(4), 376–386, doi: 10.1056/NEJMsa0805646, **2009**.

Pusede, S. E., Duffey, K. C., Shusterman, A. A., Saleh, A., Laughner, J. L., Wooldridge, P. J., Zhang, Q., Parworth, C. L., Kim, H., Capps, S. L., Valin, L. C., Cappa, C. D., Fried, A., Walega, J., Nowak, J. B., Weinheimer, A. J., Hoff, R. M., Berkoff, T. A., Beyersdorf, A. J., Olson, J., Crawford, J. H., and Cohen, R. C.: On the effectiveness of nitrogen oxide reductions as a control over ammonium nitrate aerosol, *Atmos. Chem. Phys.*, *16*(4), 2575–2596, doi: 10.5194/acp-16-2575-2016, **2016**.

Pusede, S. E., Gentner, D. R., Wooldridge, P. J., Browne, E. C., Rollins, A. W., Min, K.-E., Russell, A. R., Thomas, J., Zhang, L., Brune, W. H., Henry, S. B., DiGangi, J. P., Keutsch, F. N., Harrold, S. A., Thornton, J. A., Beaver, M. R., St. Clair, J. M., Wennberg, P. O., Sanders, J., Ren, X., VandenBoer, T. C., Markovic, M. Z., Guha, A., Weber, R., Goldstein,

A. H., and Cohen, R. C.: On the temperature dependence of organic reactivity, nitrogen oxides, ozone production, and the impact of emission controls in San Joaquin Valley, California, *Atmos. Chem. Phys.*, *14*(7), 3373–3395, doi: 10.5194/acp-14-3373-2014, **2014**.

Pusede, S. E., Steiner, A. L., and Cohen, R. C.: Temperature and Recent Trends in the Chemistry of Continental Surface Ozone, *Chem. Rev.*, *115*(10), 3898–3918, doi: 10.1021/cr5006815, **2015**.

Pye, H. O. T., Luecken, D. J., Xu, L., Boyd, C. M., Ng, N. L., Baker, K. R., Ayres, B. R., Bash, J. O., Baumann, K., Carter, W. P. L., Edgerton, E. S., Fry, J. L., Hutzell, W. T., Schwede, D., and Shepson, P. B.: Modeling the Current and Future Roles of Particulate Organic Nitrates in the Southeastern United States, *Environ. Sci. Technol.*, doi: 10.1021/acs.est.5b03738, **2015**.

Reed, C., Evans, M. J., Crilley, L. R., Bloss, W. J., Sherwen, T., Read, K. A., Lee, J. D., and Carpenter, L. J.: Evidence for renoxification in the tropical marine boundary layer, *Atmos. Chem. Phys.*, *17*(6), 4081–4092, doi: 10.5194/acp-17-4081-2017, **2017**.

Reuter, M., Buchwitz, M., Hilboll, A., Richter, A., Schneising, O., Hilker, M., Heymann, J., Bovensmann, H., and Burrows, J. P.: Decreasing emissions of NO_x relative to CO_2 in East Asia inferred from satellite observations, *Nat. Geosci.*, *7*(11), 792–795, doi: 10.1038/ngeo2257, **2014**.

Richter, D., Weibring, P., Walega, J. G., Fried, A., Spuler, S. M., and Taubman, M. S.: Compact highly sensitive multi-species airborne mid-IR spectrometer, *Appl. Phys. B*, *119*(1), 119–131, doi: 10.1007/s00340-015-6038-8, **2015**.

Rindelaub, J. D., McAvey, K. M., and Shepson, P. B.: The photochemical production of organic nitrates from α-pinene and loss via acid-dependent particle phase hydrolysis, *Atmos. Environ.*, *100*, 193–201, doi: 10.1016/j.atmosenv.2014.11.010, **2015**.

Rivera-Rios, J. C., Nguyen, T. B., Crounse, J. D., Jud, W., St. Clair, J. M., Mikoviny, T., Gilman, J. B., Lerner, B. M., Kaiser, J. B., de Gouw, J., Wisthaler, A., Hansel, A., Wennberg, P. O., Seinfeld, J. H., and Keutsch, F. N.: Conversion of hydroperoxides to carbonyls in field and laboratory instrumentation: Observational bias in diagnosing pristine versus anthropogenically controlled atmospheric chemistry, *Geophys. Res. Lett.*, *41*(23), 8645–8651, doi: 10.1002/2014GL061919, **2014**.

Rohrer, F., Lu, K., Hofzumahaus, A., Bohn, B., Brauers, T., Chang, C.-C., Fuchs, H., Häseler, R., Holland, F., Hu, M., Kita, K., Kondo, Y., Li, X., Lou, S., Oebel, A., Shao, M., Zeng, L., Zhu, T., Zhang, Y., and Wahner, A.: Maximum efficiency in the hydroxyl-radical-based self-cleansing of the troposphere, *Nat. Geosci.*, *7*(8), 559–563, doi: 10.1038/ngeo2199, **2014**.

Rollins, A. W., Browne, E. C., Min, K.-E., Pusede, S. E., Wooldridge, P. J., Gentner, D. R., Goldstein, A. H., Liu, S., Day, D. A., Russell, L. M., and Cohen, R. C.: Evidence for NO_x Control Over Nighttime SOA Formation, *Science*, *337*(6099), 1210–1212, doi: 10.1126/science.1221520, **2012**.

Rollins, A. W., Smith, J. D., Wilson, K. R., and Cohen, R. C.: Real Time In Situ Detection of Organic Nitrates in Atmospheric Aerosols, *Environ. Sci. Technol.*, *44*(14), 5540–5545, doi: 10.1021/es100926x, **2010**.

Romer, P. S., Duffey, K. C., Wooldridge, P. J., Allen, H. M., Ayres, B. R., Brown, S. S., Brune, W. H., Crounse, J. D., de Gouw, J., Draper, D. C., Feiner, P. A., Fry, J. L., Goldstein, A. H., Koss, A., Misztal, P. K., Nguyen, T. B., Olson, K., Teng, A. P., Wennberg, P. O., Wild, R. J., Zhang, L., and Cohen, R. C.: The lifetime of nitrogen oxides in an isoprene-dominated forest, *Atmos. Chem. Phys.*, *16*(12), 7623–7637, doi: 10.5194/acp-16-7623-2016, **2016**.

Romer, P. S., Duffey, K. C., Wooldridge, P. J., Edgerton, E., Baumann, K., Feiner, P. A., Miller, D. O., Brune, W. H., Koss, A. R., de Gouw, J. A., Misztal, P. K., Goldstein, A. H., and Cohen, R. C.: Effects of temperature-dependent NO_x emissions on continental ozone production, *Atmos. Chem. Phys.*, *18*(4), 2601–2614, doi: 10.5194/acp-18-2601-2018, **2018**.

Rosen, R. S., Wood, E. C., Wooldridge, P. J., Thornton, J. A., Day, D. A., Kuster, W., Williams, E. J., Jobson, B. T., and Cohen, R. C.: Observations of total alkyl nitrates during Texas Air Quality Study 2000: Implications for O_3 and alkyl nitrate photochemistry, *J. Geophys. Res.*, *109*(D7), D07303, doi: 10.1029/2003JD004227, **2004**.

Russell, A. R., Perring, A. E., Valin, L. C., Bucsela, E. J., Browne, E. C., Wooldridge, P. J., and Cohen, R. C.: A high spatial resolution retrieval of NO_2 column densities from OMI: method and evaluation, *Atmos. Chem. Phys*, *11*(16), 8543–8554, doi: 10.5194/acp-11-8543-2011, **2011**.

Russell, A. R., Valin, L. C., and Cohen, R. C.: Trends in OMI NO_2 observations over the United States: effects of emission control technology and the economic recession, *Atmos. Chem. Phys.*, *12*(24), 12197–12209, doi: 10.5194/acp-12-12197-2012, **2012**.

Russo, R. S., Zhou, Y., Haase, K. B., Wingenter, O. W., Frinak, E. K., Mao, H., Talbot, R. W., and Sive, B. C.: Temporal variability, sources, and sinks of C_1-C_5 alkyl nitrates in coastal New England, *Atmos. Chem. Phys.*, *10*(4), 1865–1883, doi: 10.5194/acp-10-1865-2010, **2010**.

Ryerson, T. B., Buhr, M. P., Frost, G. J., Goldan, P. D., Holloway, J. S., Hübler, G., Jobson, B. T., Kuster, W. C., McKeen, S. A., Parrish, D. D., Roberts, J. M., Sueper, D. T., Trainer, M., Williams, J., and Fehsenfeld, F. C.: Emissions lifetimes and ozone formation in power plant plumes, *J. Geophys. Res.*, *103*(D17), 22569–22583, doi: 10.1029/98JD01620, **1998**.

Ryerson, T. B., Trainer, M., Angevine, W. M., Brock, C. A., Dissly, R. W., Fehsenfeld, F. C., Frost, G. J., Goldan, P. D., Holloway, J. S., Hübler, G., Jakoubek, R. O., Kuster, W. C., Neuman, J. A., Nicks, D. K., Jr., Parrish, D. D., Roberts, J. M., Sueper, D. T., Atlas, E. L., Donnelly, S. G., Flocke, F., Fried, A., Potter, W. T., Schauffler, S., Stroud, V., Weinheimer, A. J., Wert, B. P., Wiedinmyer, C., Alvarez, R. J., Banta, R. M., Darby, L. S., and Senff, C. J.: Effect of petrochemical industrial emissions of reactive alkenes and NO_x on tropospheric ozone formation in Houston, Texas, *J. Geophys. Res.*, *108*(D8), 4249, doi: 10.1029/2002JD003070, **2003**.

Ryerson, T. B., Williams, E. J., and Fehsenfeld, F. C.: An efficient photolysis system for fast-response NO_2 measurements, *J. Geophys. Res.*, *105*(D21), 26447–26461, doi: 10.1029/2000JD900389, **2000**.

Sachse, G. W., Hill, G. F., Wade, L. O., and Perry, M. G.: Fast-response, high-precision carbon monoxide sensor using a tunable diode laser absorption technique, *J. Geophys. Res. Atmos.*, *92*(D2), 2071–2081, doi: 10.1029/JD092iD02p02071, **1987**.

Saunders, S. M., Jenkin, M. E., Derwent, R. G., and Pilling, M. J.: Protocol for the development of the Master Chemical Mechanism, MCM v3 (Part A): tropospheric degradation of non-aromatic volatile organic compounds, *Atmos. Chem. Phys.*, *3*(1), 161–180, doi: 10.5194/acp-3-161-2003, **2003**.

Scheffe, R. D., Solomon, P. A., Husar, R., Hanley, T., Schmidt, M., Koerber, M., Gilroy, M., Hemby, J., Watkins, N., Papp, M., Rice, J., Tikvart, J., and Valentinetti, R.: The National Ambient Air Monitoring Strategy: Rethinking the Role of National Networks, *J. Air Waste Manage.*, *59*(5), 579–590, doi: 10.3155/1047-3289.59.5.579, **2009**.

Schmidt, J. A., Jacob, D. J., Horowitz, H. M., Hu, L., Sherwen, T., Evans, M. J., Liang, Q., Suleiman, R. M., Oram, D. E., Le Breton, M., Percival, C. J., Wang, S., Dix, B., and Volkamer, R.: Modeling the observed tropospheric BrO background: Importance of multiphase chemistry and implications for ozone, OH, and mercury, *J. Geophys. Res. Atmos.*, *121*(19), 11819–11835, doi: 10.1002/2015JD024229, **2016**.

Schneider, M., Luxenhofer, O., Deissler, A., and Ballschmiter, K.: C_1–C_{15} Alkyl Nitrates, Benzyl Nitrate, and Bifunctional Nitrates: Measurements in California and South Atlantic Air and Global Comparison Using C_2Cl_4 and $CHBr_3$ as Marker Molecules, *Environ. Sci. Technol.*, *32*(20), 3055–3062, doi: 10.1021/es980132g, **1998**.

Seinfeld, J. H. and Pandis, S. N.: *Atmospheric Chemistry and Physics: From Air Pollution to Climate Change*, Wiley-Interscience, Hoboken, N.J, 2nd edition, **2006**, ISBN 978-0-471-72018-8.

Shen, L., Mickley, L. J., and Gilleland, E.: Impact of increasing heat waves on U.S. ozone episodes in the 2050s: Results from a multimodel analysis using extreme value theory, *Geophys. Res. Lett.*, *43*(8), 4017–4025, doi: 10.1002/2016GL068432, **2016**.

Sherwen, T., Schmidt, J. A., Evans, M. J., Carpenter, L. J., Großmann, K., Eastham, S. D., Jacob, D. J., Dix, B., Koenig, T. K., Sinreich, R., Ortega, I., Volkamer, R., Saiz-Lopez, A., Prados-Roman, C., Mahajan, A. S., and Ordóñez, C.: Global impacts of tropospheric halogens (Cl, Br, I) on oxidants and composition in GEOS-Chem, *Atmos. Chem. Phys.*, *16*(18), 12239–12271, doi: 10.5194/acp-16-12239-2016, **2016**.

Shetter, R. E. and Müller, M.: Photolysis frequency measurements using actinic flux spectroradiometry during the PEM-Tropics mission: Instrumentation description and some results, *J. Geophys. Res. Atmos.*, *104*(D5), 5647–5661, doi: 10.1029/98JD01381, **1999**.

Sillman, S. and Samson, P. J.: Impact of temperature on oxidant photochemistry in urban, polluted rural and remote environments, *J. Geophys. Res.*, *100*, 11497–11508, doi: 10.1029/94JD02146, **1995**.

Singh, R. B. and Sloan, J. J.: A high-resolution NO_x emission factor model for North American motor vehicles, *Atmos. Environ.*, *40*(27), 5214–5223, doi: 10.1016/j.atmosenv.2006.04.012, **2006**.

Sobanski, N., Thieser, J., Schuladen, J., Sauvage, C., Song, W., Williams, J., Lelieveld, J., and Crowley, J. N.: Day and night-time formation of organic nitrates at a forested mountain site in south-west Germany, *Atmos. Chem. Phys.*, *17*(6), 4115–4130, doi: 10.5194/acp-17-4115-2017, **2017**.

Sprengnether, M., Demerjian, K. L., Donahue, N. M., and Anderson, J. G.: Product analysis of the OH oxidation of isoprene and 1,3-butadiene in the presence of NO, *J. Geophys. Res.*, *107*(D15), 4268, doi: 10.1029/2001JD000716, **2002**.

Stavrakou, T., Müller, J.-F., Boersma, K. F., van der A, R. J., Kurokawa, J., Ohara, T., and Zhang, Q.: Key chemical NO_x sink uncertainties and how they influence top-down emissions of nitrogen oxides, *Atmos. Chem. Phys.*, *13*(17), 9057–9082, doi: 10.5194/acp-13-9057-2013, **2013**.

Steiner, A. L., Davis, A. J., Sillman, S., Owen, R. C., Michalak, A. M., and Fiore, A. M.: Observed suppression of ozone formation at extremely high temperatures due to chemical and biophysical feedbacks, *Proc. Natl. Acad. Sci. USA*, *107*(46), 19685–19690, doi: 10.1073/pnas.1008336107, **2010**.

Steiner, A. L., Tonse, S., Cohen, R. C., Goldstein, A. H., and Harley, R. A.: Influence of future climate and emissions on regional air quality in California, *J. Geophys. Res.*, *111*(D18), D18303, doi: 10.1029/2005JD006935, **2006**.

Stelson, A. W. and Seinfeld, J. H.: Relative humidity and temperature dependence of the ammonium nitrate dissociation constant, *Atmos. Environ.*, *16*(5), 983–992, doi: 10.1016/0004-6981(82)90184-6, **1982**.

Svoboda, O., Kubelová, L., and Slavíček, P.: Enabling Forbidden Processes: Quantum and Solvation Enhancement of Nitrate Anion UV Absorption, *J. Phys. Chem. A*, *117*(48), 12868–12877, doi: 10.1021/jp4098777, **2013**.

Teng, A. P., Crounse, J. D., Lee, L., St. Clair, J. M., Cohen, R. C., and Wennberg, P. O.: Hydroxy nitrate production in the OH-initiated oxidation of alkenes, *Atmos. Chem. Phys.*, *15*(8), 4297–4316, doi: 10.5194/acp-15-4297-2015, **2015**.

Teng, A. P., Crounse, J. D., and Wennberg, P. O.: Isoprene Peroxy Radical Dynamics, *J. Am. Chem. Soc.*, *139*(15), 5367–5377, doi: 10.1021/jacs.6b12838, **2017**.

Thornton, F. C., Pier, P. A., and Valente, R. J.: NO emissions from soils in the southeastern United States, *J. Geophys. Res.*, *102*(D17), 21189–21195, doi: 10.1029/97JD01567, **1997**.

Thornton, J. A., Wooldridge, P. J., and Cohen, R. C.: Atmospheric NO_2: In Situ Laser-Induced Fluorescence Detection at Parts per Trillion Mixing Ratios, *Anal. Chem.*, *72*(3), 528–539, doi: 10.1021/ac9908905, **2000**.

Thornton, J. A., Wooldridge, P. J., Cohen, R. C., Martinez, M., Harder, H., Brune, W. H., Williams, E. J., Roberts, J. M., Fehsenfeld, F. C., Hall, S. R., Shetter, R. E., Wert, B. P., and Fried, A.: Ozone production rates as a function of NO_x abundances and HO_x production rates in the Nashville urban plume, *J. Geophys. Res.*, *107*(D12), 4146, doi: 10.1029/2001JD000932, **2002**.

Trainer, M., Parrish, D. D., Buhr, M. P., Norton, R. B., Fehsenfeld, F. C., Anlauf, K. G., Bottenheim, J. W., Tang, Y. Z., Wiebe, H. A., Roberts, J. M., Tanner, R. L., Newman, L., Bowersox, V. C., Meagher, J. F., Olszyna, K. J., Rodgers, M. O., Wang, T., Berresheim, H., Demerjian, K. L., and Roychowdhury, U. K.: Correlation of ozone with NO_y in photochemically aged air, *J. Geophys. Res.*, *98*(D2), 2917–2925, doi: 10.1029/92JD01910, **1993**.

Travis, K. R., Jacob, D. J., Fisher, J. A., Kim, P. S., Marais, E. A., Zhu, L., Yu, K., Miller, C. C., Yantosca, R. M., Sulprizio, M. P., Thompson, A. M., Wennberg, P. O., Crounse, J. D., St. Clair, J. M., Cohen, R. C., Laughner, J. L., Dibb, J. E., Hall, S. R., Ullmann, K., Wolfe, G. M., Pollack, I. B., Peischl, J., Neuman, J. A., and Zhou, X.: Why do models overestimate surface ozone in the Southeast United States?, *Atmos. Chem. Phys.*, *16*(21), 13561–13577, doi: 10.5194/acp-16-13561-2016, **2016**.

Trebs, I., Bohn, B., Ammann, C., Rummel, U., Blumthaler, M., Königstedt, R., Meixner, F. X., Fan, S., and Andreae, M. O.: Relationship between the NO_2 photolysis frequency and the solar global irradiance, *Atmos. Meas. Tech.*, *2*(2), 725–739, doi: 10.5194/amt-2-725-2009, **2009**.

United States Environmental Protection Agency: Air Pollutant Emissions Trends Data, `https://www.epa.gov/air-emissions-inventories/air-pollutant-emissions-trends-data`, (Last access 2018-07-05), **2018**.

Valin, L. C., Russell, A. R., and Cohen, R. C.: Variations of OH radical in an urban plume inferred from NO_2 column measurements, *Geophys. Res. Lett.*, *40*(9), 1856–1860, doi: 10.1002/grl.50267, **2013**.

VandenBoer, T. C., Brown, S. S., Murphy, J. G., Keene, W. C., Young, C. J., Pszenny, A. A. P., Kim, S., Warneke, C., de Gouw, J. A., Maben, J. R., Wagner, N. L., Riedel, T. P., Thornton, J. A., Wolfe, D. E., Dubé, W. P., Öztürk, F., Brock, C. A., Grossberg, N., Lefer, B., Lerner, B., Middlebrook, A. M., and Roberts, J. M.: Understanding the role of the ground surface in HONO vertical structure: High resolution vertical profiles during NACHTT-11, *J. Geophys. Res. Atmos.*, *118*(17), 10155–10171, doi: 10.1002/jgrd.50721, **2013**.

Vedal, S., Brauer, M., White, R., and Petkau, J.: Air Pollution and Daily Mortality in a City with Low Levels of Pollution, *Environ. Health Persp.*, *111*(1), 45–51, doi: 10.14288/1.0220733, **2002**.

Walega, J. G., Dye, J. E., Grahek, F. E., and Ridley, B. K.: Compact measurement system for the simultaneous determination of NO, NO_2 , NOy, and O_3 using a small aircraft, in Schiff, H. I. (Editor), *Proc. SPIE 1433, Measurement of Atmospheric Gases*, pages 232–241, **1991**, doi: 10.1117/12.46167.

Warneck, P. and Wurzinger, C.: Product quantum yields for the 305-nm photodecomposition of nitrate in aqueous solution, *J. Phys. Chem.*, *92*(22), 6278–6283, doi: 10.1021/j100333a022, **1988**.

Warneke, C., de Gouw, J. A., Holloway, J. S., Peischl, J., Ryerson, T. B., Atlas, E., Blake, D., Trainer, M., and Parrish, D. D.: Multiyear trends in volatile organic compounds in Los Angeles, California: Five decades of decreasing emissions, *J. Geophys. Res. Atmos.*, *117*(D21), D00V17, doi: 10.1029/2012JD017899, **2012**.

Washenfelder, R. A., Wagner, N. L., Dube, W. P., and Brown, S. S.: Measurement of Atmospheric Ozone by Cavity Ring-down Spectroscopy, *Environ. Sci. Technol.*, *45*(7), 2938–2944, doi: 10.1021/es103340u, **2011**.

Weaver, C. P., et al.: A Preliminary Synthesis of Modeled Climate Change Impacts on U.S. Regional Ozone Concentrations, *Bull. Amer. Meteor. Soc.*, *90*, 1843–1863, doi: 10.1175/2009BAMS2568.1, **2009**.

Wennberg, P. O., Bates, K. H., Crounse, J. D., Dodson, L. G., McVay, R. C., Mertens, L. A., Nguyen, T. B., Praske, E., Schwantes, R. H., Smarte, M. D., St Clair, J. M., Teng, A. P., Zhang, X., and Seinfeld, J. H.: Gas-Phase Reactions of Isoprene and Its Major Oxidation Products, *Chem. Rev.*, *118*(7), 3337–3390, doi: 10.1021/acs.chemrev.7b00439, **2018**.

Williams, E. J. and Fehsenfeld, F. C.: Measurement of soil nitrogen oxide emissions at three North American ecosystems, *J. Geophys. Res.*, *96*(D1), 1033–1042, doi: 10.1029/90JD01903, **1991**.

Wisthaler, A., Hansel, A., Dickerson, R. R., and Crutzen, P. J.: Organic trace gas measurements by PTR-MS during INDOEX 1999, *J. Geophys. Res. Atmos.*, *107*(D19), 8024, doi: 10.1029/2001JD000576, **2002**.

Wolfe, G. M., Marvin, M. R., Roberts, S. J., Travis, K. R., and Liao, J.: The Framework for 0-D Atmospheric Modeling (F0AM) v3.1, *Geosci. Model Dev.*, *9*(9), 3309–3319, doi: 10.5194/gmd-9-3309-2016, **2016**.

Wolfe, G. M., Thornton, J. A., Yatavelli, R. L. N., McKay, M., Goldstein, A. H., LaFranchi, B., Min, K.-E., and Cohen, R. C.: Eddy covariance fluxes of acyl peroxy nitrates (PAN, PPN and MPAN) above a Ponderosa pine forest, *Atmos. Chem. Phys.*, *9*(2), 615–634, doi: 10.5194/acp-9-615-2009, **2009**.

World Health Organization: *Air Quality Guidelines: Global Update 2005, Particulate Matter, Ozone, Nitrogen Dioxide and Sulphur Dioxide*, WHO Regional Office for Europe, Copenhagen, Denmark, **2005**.

Xiong, F., Borca, C. H., Slipchenko, L. V., and Shepson, P. B.: Photochemical degradation of isoprene-derived 4,1-nitrooxy enal, *Atmos. Chem. Phys.*, *16*(9), 5595–5610, doi: 10.5194/acp-16-5595-2016, **2016**.

Xiong, F., McAvey, K. M., Pratt, K. A., Groff, C. J., Hostetler, M. A., Lipton, M. A., Starn, T. K., Seeley, J. V., Bertman, S. B., Teng, A. P., Crounse, J. D., Nguyen, T. B., Wennberg, P. O., Misztal, P. K., Goldstein, A. H., Guenther, A. B., Koss, A. R., Olson, K. F., de Gouw, J. A., Baumann, K., Edgerton, E. S., Feiner, P. A., Zhang, L., Miller, D. O., Brune, W. H., and Shepson, P. B.: Observation of isoprene hydroxynitrates in the southeastern United States and implications for the fate of NO_x, *Atmos. Chem. Phys.*, *15*(19), 11257–11272, doi: 10.5194/acp-15-11257-2015, **2015**.

Xu, L., Guo, H., Boyd, C. M., Klein, M., Bougiatioti, A., Cerully, K. M., Hite, J. R., Isaacman-VanWertz, G., Kreisberg, N. M., Knote, C., Olson, K., Koss, A., Goldstein, A. H., Hering, S. V., de Gouw, J., Baumann, K., Lee, S.-H., Nenes, A., Weber, R. J., and Ng, N. L.: Effects of anthropogenic emissions on aerosol formation from isoprene and monoterpenes in the southeastern United States, *Proc. Natl. Acad. Sci. USA*, *112*(1), 37–42, doi: 10.1073/pnas.1417609112, **2015**a.

Xu, L., Suresh, S., Guo, H., Weber, R. J., and Ng, N. L.: Aerosol characterization over the southeastern United States using high-resolution aerosol mass spectrometry: spatial and seasonal variation of aerosol composition and sources with a focus on organic nitrates, *Atmos. Chem. Phys.*, *15*(13), 7307–7336, doi: 10.5194/acp-15-7307-2015, **2015**b.

Ye, C., Heard, D. E., and Whalley, L. K.: Evaluation of Novel Routes for NO_x Formation in Remote Regions, *Environ. Sci. Technol.*, *51*(13), 7442–7449, doi: 10.1021/acs.est.6b06441, **2017**a.

Ye, C., Zhang, N., Gao, H., and Zhou, X.: Photolysis of Particulate Nitrate as a Source of HONO and NO_x, *Environ. Sci. Technol.*, *51*(12), 6849–6856, doi: 10.1021/acs.est.7b00387, **2017**b.

Ye, C., Zhou, X., Pu, D., Stutz, J., Festa, J., Spolaor, M., Tsai, C., Cantrell, C., Mauldin, R. L., Campos, T., Weinheimer, A., Hornbrook, R. S., Apel, E. C., Guenther, A., Kaser, L., Yuan, B., Karl, T., Haggerty, J., Hall, S., Ullmann, K., Smith, J. N., Ortega, J., and Knote, C.: Rapid cycling of reactive nitrogen in the marine boundary layer, *Nature*, *532*(7600), 489–491, doi: 10.1038/nature17195, **2016**.

Zalakeviciute, R., Alexander, M. L., Allwine, E., Jimenez, J. L., Jobson, B. T., Molina, L. T., Nemitz, E., Pressley, S., VanReken, T. M., Ulbrich, I. M., Velasco, E., and Lamb, B. K.: Chemically-resolved aerosol eddy covariance flux measurements in urban Mexico City during MILAGRO 2006, *Atmos. Chem. Phys.*, *12*(16), 7809–7823, doi: 10.5194/acp-12-7809-2012, **2012**.

Zare, A., Romer, P. S., Nguyen, T., Keutsch, F. N., Skog, K., and Cohen, R. C.: A comprehensive organic nitrate chemistry: insights into the lifetime of atmospheric organic nitrates, *Atmos. Chem. Phys. Discuss.*, *1*, 1–33, doi: 10.5194/acp-2018-530, **2018**.

Zhang, H., Yee, L. D., Lee, B. H., Curtis, M. P., Worton, D. R., Isaacman-VanWertz, G., Offenberg, J. H., Lewandowski, M., Kleindienst, T. E., Beaver, M. R., Holder, A. L., Lonneman, W. A., Docherty, K. S., Jaoui, M., Pye, H. O. T., Hu, W., Day, D. A., Campuzano-Jost, P., Jimenez, J. L., Guo, H., Weber, R. J., de Gouw, J., Koss, A. R., Edgerton, E. S., Brune, W., Mohr, C., Lopez-Hilfiker, F. D., Lutz, A., Kreisberg, N. M., Spielman, S. R., Hering, S. V., Wilson, K. R., Thornton, J. A., and Goldstein, A. H.: Monoterpenes are the largest source of summertime organic aerosol in the southeastern United States, *Proc. Natl. Acad. Sci. USA*, *115*(9), 2038–2043, doi: 10.1073/pnas.1717513115, **2018**.

Zhou, X., Gao, H., He, Y., Huang, G., Bertman, S. B., Civerolo, K., and Schwab, J.: Nitric acid photolysis on surfaces in low-NO_x environments: Significant atmospheric implications, *Geophys. Res. Lett.*, *30*(23), 2217, doi: 10.1029/2003GL018620, **2003**.

Zhou, X., Zhang, N., TerAvest, M., Tang, D., Hou, J., Bertman, S., Alaghmand, M., Shepson, P. B., Carroll, M. A., Griffith, S., Dusanter, S., and Stevens, P. S.: Nitric acid photolysis on forest canopy surface as a source for tropospheric nitrous acid, *Nat. Geosci.*, *4*(7), 440–443, doi: 10.1038/ngeo1164, **2011**.

Zhu, C., Xiang, B., Chu, L. T., and Zhu, L.: 308 nm Photolysis of Nitric Acid in the Gas Phase, on Aluminum Surfaces, and on Ice Films, *J. Phys. Chem. A*, *114*(7), 2561–2568, doi: 10.1021/jp909867a, **2010**.

Zhu, C., Xiang, B., Zhu, L., and Cole, R.: Determination of absorption cross sections of surface-adsorbed HNO_3 in the 290–330 nm region by Brewster angle cavity ring-down spectroscopy, *Chem. Phys. Lett.*, *458*(4), 373–377, doi: 10.1016/j.cplett.2008.04.125, **2008**.